Tropical Cyclone-Induced Waves and Storm Surge at four locations along the Southern African East Coast

by
David James Van Niekerk

Thesis presented in fulfilment of the requirements for the degree of Master of Engineering in the Faculty of Civil Engineering at Stellenbosch University

Supervisor: Prof Koos Schoonees

December 2016

Declaration

By submitting this thesis electronically, I declare that the entirety of the work contained therein is my own, original work, that I am the sole author thereof (save to the extent explicitly otherwise stated), that reproduction and publication thereof by Stellenbosch University will not infringe any third party rights and that I have not previously in its entirety or in part submitted it for obtaining any qualification.

December 2016

Abstract

Tropical cyclones are synoptic scale rotating storms that form over oceans with warm water, producing powerful winds and rainfall. The characteristic low pressure of the system and the extreme winds generate high levels of storm surge, ocean waves and currents, which pose a threat to a coast and its infrastructure. The social and economic consequences of these storms can be devastating, often resulting in human fatalities. Quantification of the risk exposure to these storms is therefore crucial for human safety and the design of infrastructure along the coast of a tropical cyclone-prone region, such as the Southern African East Coast.

Considerable research into the risk presented by tropical cyclones, has been conducted using numerical models, although very little has been done for the South-West Indian Ocean. The present research focusses on the tropical cyclone-induced waves and storm surge, along the Southern African East Coast. The primary results of this thesis are estimates of the 50-, 100-, 200- and 500-year significant wave height and storm surge levels, expected to be produced by tropical cyclones, at four locations along the Southern African East Coast.

Third-generation numerical models were used to generate the wave and storm surge estimates at the four locations, namely; Durban, Maputo, Beira and Pemba. Historical tropical cyclone data from the Best Track data, as well as the results of other studies, were used to develop input parameters for the numerical models. Sensitivity tests of these parameters were conducted in order to see how each parameter influences the model results. The results of the sensitivity tests were used to determine the design storm parameters for the proposed numerical model tests.

The model tests comprised of simulating a tropical cyclone varying in time and space, resulting in estimates of the significant wave height and storm surge levels at the location of interest. A total of four return periods were simulated for each of the four locations, resulting in a total of 16 simulations. The output of the simulations were specified at points along the 20 m contour for the waves and the 10 m contour for storm surge. These depths were chosen in order to determine estimates before certain coastal processes such as refraction and diffraction, have a major influence on the results.

The numerical model was calibrated by simulating Hurricane Ike, which occurred over the Gulf of Mexico in September 2008. The model produced reasonably good results when compared to the measured data, although the model did under-estimate the storm surge. It is advisable to take this into account when using the estimates of the expected storm surge levels.

The results of the model tests indicate that the expected waves produced by tropical cyclones along the Southern African East Coast, do pose a major threat and need to be taken into consideration in the planning and design of coastal infrastructure. The largest waves are expected to occur at Beira and the smallest at Durban. At the 100-year return period, Durban, Maputo, Beira and Pemba are expected to produce significant wave heights of 2.1 m, 4.6 m, 6.3 m and 4.4 m respectively. Estimates of the expected tropical cyclone-induced storm surge indicate that Durban and Pemba are not at risk of flooding, with maximum expected storm surge levels of roughly 0.3 m at the 500-year return period. Beira and Maputo on the other hand, are potentially at risk with maximum storm surge levels of 2.1 m and 1.1 m respectively, at the 500-year return period.

Opsomming

Tropiese siklone is sinoptiese skaal roterende storms wat oor oseane met warm water vorm, wat lei tot kragtige winde en reënval. Die kenmerkende lae druk van die stelsel en die uiterste winde, wek hoë vlakke van stormvloed, see golwe en strome, wat 'n bedreiging vir die kus en sy infrastruktuur inhou. Die sosiale en ekonomiese gevolge van hierdie storms kan verwoestend wees, dikwels lei dit tot menslike sterftes. Kwantifisering van die risiko blootstelling aan hierdie storms is dus noodsaaklik vir menslike veiligheid en die ontwerp van infrastruktuur langs die kus waar tropiese siklone voorkom, soos die Suider-Afrikaanse Ooskus.

Aansienlike navorsing oor tropiese sikloon risiko modellering is gedoen hoewel baie min al gedoen is vir die Suid-Wes Indiese Oseaan. Die huidige navorsing fokus op golwe wat veroorsaak word deur tropiese siklone en die stormvloede langs die Suider-Afrikaanse Ooskus. Die primêre resultate van hierdie tesis is skattings van golfhoogte en stormvloed vlakke vir die 50-, 100-, 200- en 500-jaar herhaal periodes wat na verwagting deur tropiese siklone geskep sal word. Die skattings is vir vier plekke langs die Suider-Afrikaanse Ooskus gedoen.

Derde generasie numeriese modelle is gebruik om die golf en stormvloed skattings op die vier plekke te genereer, naamlik; Durban, Maputo, Beira en Pemba. Historiese tropiese sikloon data van die Best Track data, sowel as die resultate van ander studies, is gebruik om die inset-parameters te ontwikkel vir die numeriese modelle. Sensitiwiteit toetse van hierdie parameters is uitgevoer ten einde te sien hoe elke parameter die model resultate beïnvloed. Die resultate van die sensitiwiteit toetse is gebruik om die invoer parameters te bepaal van die voorgestelde numeriese model toetse.

Die model toetse bestaan uit die simuleering van 'n tropiese sikloon wat varieer in tyd en ruimte, wat lei tot skattings van die golfhoogte en stormvloed vlakke by die plek van belang. 'n Totaal van vier herhaal periodes was gesimuleer vir elk een van die vier plekke, wat lei tot 'n totaal van 16 simulasies. Die uitset van die simulasies is gespesifiseer op punte langs die 20 m kontoer vir die golwe en die 10 m kontoer vir die stormvloed. Hierdie water dieptes was gekies om skattings te bepaal voordat sekere kus prosesse soos breking en diffraksie, ‘n groot invloed op die resultate het.

Die numeriese model is gekalibreer deur die simuleering van Orkaan Ike, wat plaasgevind het oor die Golf van Mexico in September 2008. Die model het redelike goeie resultate gelewer in vergelyking met die gemeet data, alhoewel die model die stormvloed onder-skat het. Dit

word aanbeveel om dit in aanmerking te neem wanneer die skattings van die verwagte stormvloed vlakke gebruik word.

Die resultate van die model toetse dui daarop dat die verwagte golwe wat deur tropiese siklone geskep word langs die Suider-Afrikaanse Ooskus, 'n groot bedreiging is en moet in ag geneem moet word in die beplanning en ontwerp van die kus infrastruktuur. Die grootste branders word verwag om plaas te vind naby Beira en die kleinste naby Durban. By die 100-jaar herhaal periode, kan Durban, Maputo, Beira en Pemba na verwagting beduidende golf hoogtes onderskeidelik verwag van 2.1 m, 4.6 m, 6.3 m en 4.4 m. Die beramings van die verwagte tropiese sikloon wat stormvloede veroorsaak, dui daarop dat Durban en Pemba nie in gevaar van oorstromings is nie, met 'n maksimum verwagte stormvloed vlak van sowat 0.3 m by die 500-jaar herhaal periode. Beira en Maputo aan die ander kant, is moontlik in gevaar met 'n maksimum stormvloed vlak van 2.1 m en 1.1 m onderskeidelik, by die 500-jaar herhaal periode.

Acknowledgements

First and foremost I would like to thank my parents for funding my studies, as well as for the support supplied over the duration of this thesis.

Thank you to my supervisor, Koos Schoonees, for providing valuable guidance and support throughout.

Thank you to Andre Theron for providing guidance when needed.

To my family and friends, thank you for your encouragement and patience.

To Delice Thompson, thank you for your hard work in editing the language of this thesis.

Thank you to WSP – Parsons Brinckerhoff for providing some of the bathymetry data and nautical charts required for this study.

Table of Contents

List of Figures

List of Tables

List of Symbols and Abbreviations

Δf	frequency interval = 1/D
ΔP	central pressure deficit
Δx	surf zone width
γ	breaker index
ρ	density of water
ξ_o	surf similarity parameter
ς	free surface departure from the geoid
ς_{wind}	wind-driven surge
τ_{bx}, τ_{by}	bottom stresses in the x- and y-direction
τ_{sx}, τ_{sy}	imposed surface stresses (wind and waves) in the x- and y-direction
τ_s	wind stress
δ	tropical cyclone track direction
θ	mean wave direction
φ	latitude of tropical cyclone eye
μ	mean
σ	standard deviation
a	amplitude
AHD	Australian Height Datum
β	wind inflow angle
β_{av}	beach slope for non-planar beaches
B_x, B_y	vertically integrated baroclinic pressure gradient in the x- and y-direction
CRM	Coastal Relief Model
c	forward speed of tropical cyclone
c_f	friction coefficient
d	water depth

d_b	depth at breaking
D	duration
$E(f)$	variance density spectrum
$E(f,\theta)$	frequency-direction spectrum
f	Coriolis parameter
g	gravitational acceleration
h	bathymetric depth (measured from the geoid to the bottom)
h_{av}	average water depth
h_s	still water depth
H	wave height
H_b	Wave height at breaking
$H_{0,max}$	deep water wave height
H_{rms_o}	root Mean Square wave height in deep water
H_s	significant wave height
H_{so}	significant wave height in deep water
$H_{1/3}$	significant wave height
ITCZ	Inter-Tropical Convergence Zone
JTWC	Joint Typhoon Warning centre
k	wave number = 2π/L
LAT	Lowest Astronomical Tide
l	shelf width
l_c	overall tropical cyclone track length
l_s	straight line distance from start to end of tropical cyclone track length
L	wave length
L_0	deep water wave length

MFR	Météo France La Réunion
MWL	Mean Water Level
MSL	Mean Sea Level
M_x, M_y	vertically integrated lateral stress gradient in the x- and y-direction
NDBC	National Data Buoy Center
NOAA	National Oceanic and Atmospheric Administration
η	newtonian equilibrium tide potential
η_l	sea level difference
$\bar{\eta}_d$	wave set-down
$\bar{n}_{d_b}$	wave set-down at the point of wave breaking
$\bar{\eta}_s$	shoreline wave set-up
$\bar{\eta}_u$	wave set-up
n	accounts for bottom stress = 1 - $\frac{\tau_b}{\tau_s}$
P_c	atmospheric pressure at the storm centre.
P_o	ambient pressure
P_s	atmospheric pressure at the sea surface
R	radial distance from tropical cyclone eye
RSMC	Regional Specialised Meteorological Centre
S_{100}	100-year storm surge
S_{max}	maximum wave steepness in deep water
SWL	stillwater level
t	time
$tan \propto$	beach slope
TC	Tropical Cyclone
TCWC	Tropical Cyclone Warning Centre
T_p	peak wave period

U	depth-averaged velocity in the x horizontal direction
UKHO	United Kingdom Hydrographic Office
UTC	Coordinated Universal Time
V	depth-averaged velocity in the y horizontal direction
V_{10}	surface wind speed at a 10 m elevation
V_{Fmax}	flight level wind speed
V_g	gradient wind speed
V_{max}	maximum sustained surface (10 m elevation) wind speed
W	wind speed at 10-m elevation
WMO	World Meteorological Organization

1. Introduction

1.1. Background

Tropical cyclones are synoptic scale rotating storms that form over oceans with warm water, producing powerful winds and rainfall. The characteristic low pressure of the system and the extreme winds generate high levels of storm surge, ocean waves and currents, which pose a threat to a coast and its infrastructure. These destructive qualities of tropical cyclones can and have caused many human fatalities. Estimates of expected wave heights and storm surge levels are therefore crucial for human safety and the design of infrastructure along the coast of a tropical cyclone-prone region, such as the Southern African East Coast.

On average, approximately 14 tropical cyclones occur over the South-West Indian Ocean annually. The Mozambique Channel, defined as the area of ocean between Madagascar and Mozambique, experiences 3.5 tropical cyclones per year (Fearon, 2014). There have been numerous tropical cyclone landfalls along the coast of Mozambique. The most intense being Tropical Cyclone Eline, which made landfall 80 km south of Beira on 22 February 2000. Tropical Cyclone Eline was characterised as a Category 4 event according to the Saffir-Simpson scale (discussed in Section 2.1.3) and is shown in Figure 1.1. INGC (2009) estimate a storm surge of over 4 m being generated by the storm. Approximately 2 million people were displaced or left homeless, with about 600 fatalities. An economic impact of over US $167 million was estimated for the event (INGC, 2009).

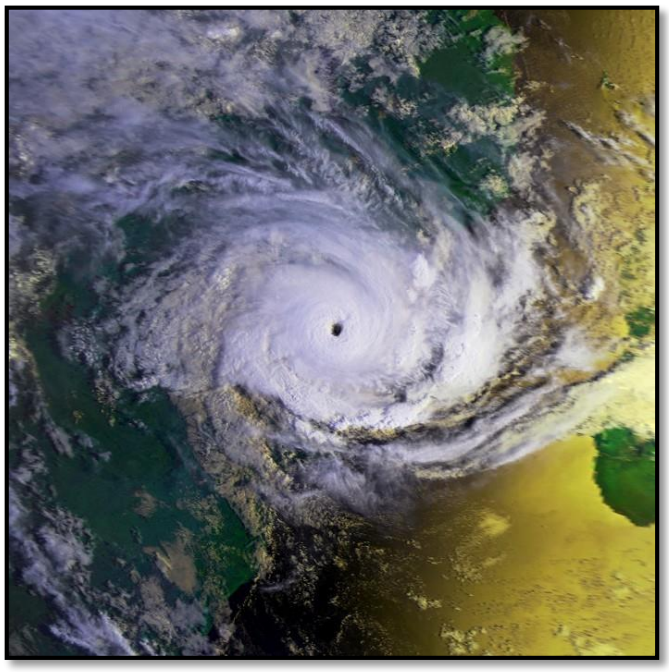

Figure 1.1: Tropical Cyclone Eline making landfall on 22 February 2000 (NOAA, [S.a.]).

Several tropical cyclones have affected the South African coastline over the years. The three most significant tropical cyclones were Domoina in February 2000, Imboa in February 1984 and Eline in February 2000. Domoina resulted in 242 fatalities with an estimated damage of US $199 million.

The social and economic impacts highlight the need for an extensive study into the waves and storm surge generated by tropical cyclones, along the Southern African East Coast. In the past, the expected waves and storm surge levels were estimated using empirical relationships. Today, much more advanced methods are employed using numerical models to simulate the tropical cyclones. The risk of tropical cyclones can be quantified by analysing the expected waves and storm surge, at different return periods.

There has been considerable research into tropical cyclone risk modelling, although these studies have been targeted at more economically advanced areas, such as the North-West Pacific (Yin et al., 2009; Graf & Nishijima, 2009), North Atlantic (Emanuel et al., 2006; Meza-Padilla et al., 2015) and South Pacific (Harper et al., 2004). Fearon (2014) estimated tropical cyclone-induced wind speeds for the South-West Indian Ocean, which the present study builds upon. Although, research into the quantification of tropical cyclone-induced waves and storm surge, is scarce along the Southern African East Coast, highlighting the need for the present study.

1.2. Thesis Objective

The thesis involves the estimation of extreme conditions and impacts generated by tropical cyclones for engineering design. The primary objective of this thesis is to determine best estimates of the 50-, 100-, 200- and 500-year significant wave height and storm surge levels, expected to be produced by tropical cyclones, at four locations along the Southern African East Coast.

1.3. Study Approach

The thesis objective was achieved using third generation numerical models to simulate expected tropical cyclones along the Southern African East Coast. A range of sensitivity tests were conducted, in order to provide input parameters for the numerical model. The model tests consisted of simulating four return periods at each of the four locations, namely; Durban, Maputo, Beira and Pemba. The model was calibrated by simulating Hurricane Ike, which occurred over the Gulf of Mexico in September 2008. The results of this thesis are intended to guide engineers in the planning and design of port and coastal infrastructure.

1.4. Thesis Structure

A study of the literature relevant to the present study is presented in Section 2, while Section 3 provides an overview of the methodology used to achieve the thesis objective. Section 4 presents the sensitivity tests used to obtain input parameters for the model tests, while Section 5 provides an overview of the numerical model tests. The calibration of the numerical model is presented in Section 6, and the results of the model tests are presented in Section 7. Conclusions and recommendations are discussed in Section 8.

2. Literature Study

2.1. Characteristics of Tropical Cyclones

2.1.1. Definition

“A tropical cyclone is the generic term for a non-frontal synoptic scale low-pressure system, over tropical or sub-tropical waters with organized convection (i.e. thunderstorm activity) and a definite cyclonic surface wind circulation” (Holland, 1993).

These weather systems are referred to various names, depending on the region. A “hurricane” is used to describe the above-mentioned system in the North-West Atlantic, Central and North-East Pacific, Caribbean Sea and Gulf of Mexico. In the North-West Pacific they are referred to as “Typhoons”, while in the Bay of Bengal and the Arabian Sea, they are named “Cyclones”. In the South-West Pacific and South-East Indian Ocean, they are termed “severe tropical cyclones”. Lastly, In the South-West Indian Ocean, they are referred to as “tropical cyclones” (WMO, [S.a.]).

2.1.2. Formation and Structure

The formation of a tropical cyclone, also known as tropical cyclone genesis, occurs along the Inter-Tropical Convergence Zone (ITCZ), or monsoon trough, in the South-West Indian Ocean (Rhome & Raman, 2006). Figure 2.1 provides a spatial distribution of tropical cyclone genesis points in the Southern Indian Ocean, during the years 1969 to 2006. These points were defined as the location along the tropical cyclone track where a central pressure of 1000 hPa or lower was achieved (Kuleshov et al., 2009).

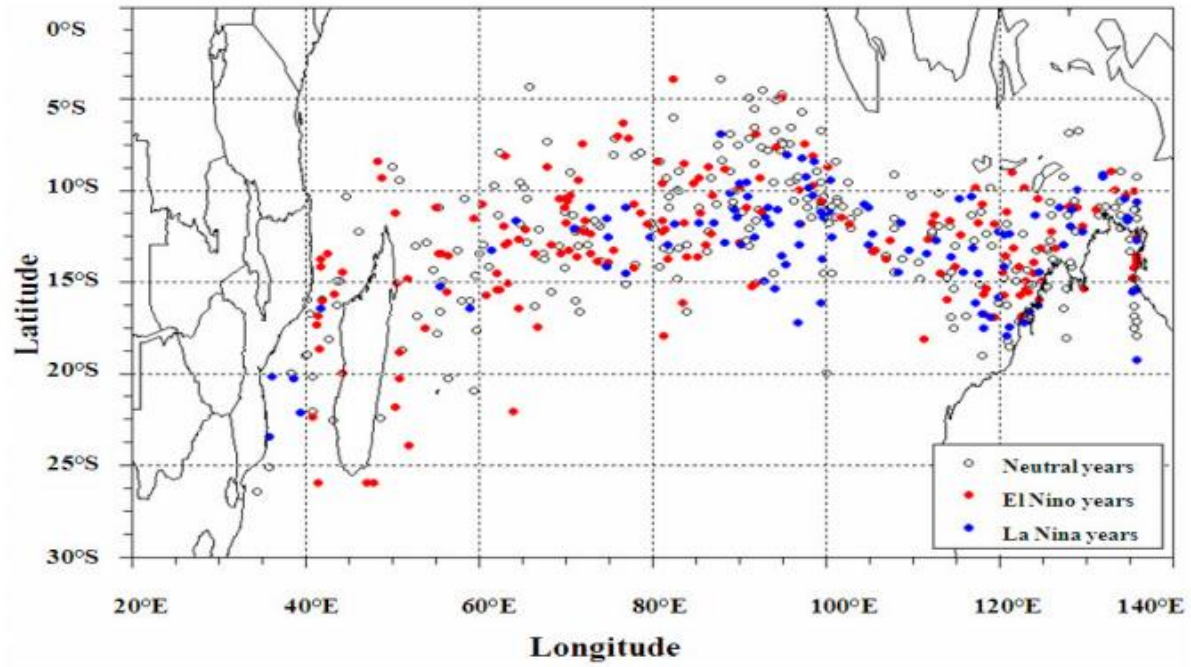

Figure 2.1: Locations of tropical cyclone genesis over the Southern Indian Ocean during the years 1969 to 2006 (Kuleshov et al., 2009).

Several authors have studied the environmental conditions necessary for the formation of a tropical cyclone, these requirements are summarized as follows (Gray 1968, 1979):

- Warm ocean water (minimum 26.5°C) down to a depth of roughly 50 m. Heat is used as fuel to drive the tropical cyclone.
- A rapidly cooling atmosphere with height, which results in an instability to moist convection. The development of a tropical cyclone relies on the heat of the ocean water, which is facilitated by thunderstorm activity.
- A high relative humidity in the mid-troposphere (5 km above sea level). Dry mid-levels are not favourable for facilitating the development of thunderstorm activity.
- A distance of 500 km or greater, north or south of the equator. A threshold amount of the Coriolis force is required for tropical cyclone genesis, as it allows the low pressure of the disturbance to be sustained.
- A pre-existing disturbance near the surface, with adequate spin and convergence.
- A small amount (under 10 m/s) of vertical wind shear between the surface and the upper troposphere. Vertical wind shear is defined as the amount of wind change with height.

If the above-mentioned conditions are met, the transition from a “disturbance” to a mature tropical cyclone can occur. The mechanics of this process is not discussed here however, it

can be found in a study by Rhome and Raman (2006). The main components of a mature tropical cyclone are the eye, eyewall, and rain bands. These components are illustrated in Figure 2.2.

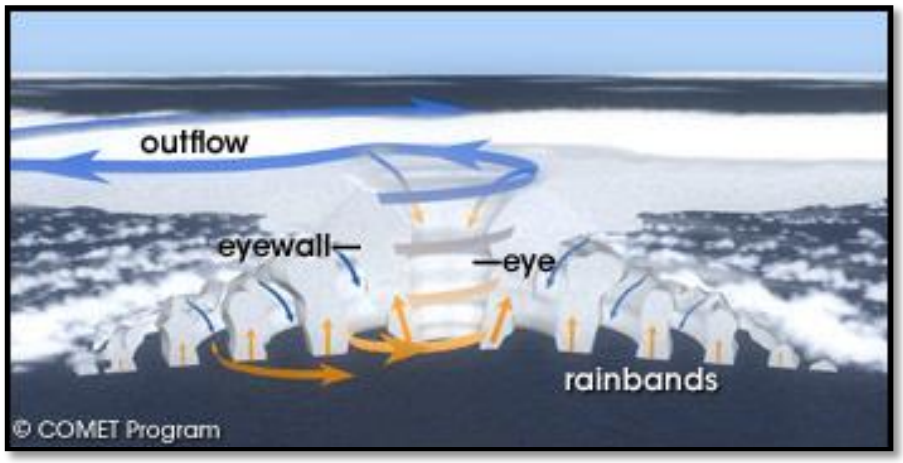

Figure 2.2: Structure of a mature tropical cyclone (Graham & Riebeek, 2006).

The eye is located in the centre of the tropical cyclone and ranges from 10 km to 65 km in diameter. Light winds, clear skies and low surface pressures are observed here. Adjacent to the eye, is the eye wall, a large ring of thunderstorms typically producing the heaviest rains and most intense winds in the system. The eyewall is usually 50 km to 100 km wide. Rain bands surround the eye wall, capable of extending over 1000 km from the eye. These clouds spiral inwards toward the eye. Tropical cyclones rotate clockwise in the southern hemisphere and anticlockwise in the northern hemisphere because of winds deflected by the Coriolis force (Graham & Riebeek, 2006).

2.1.3. Classification

Tropical cyclones occur over seven “basins” as illustrated in Figure 2.3. The South-West Indian Ocean (Basin 5) covers the Indian Ocean from Africa’s coast to 90° east, south of the equator.

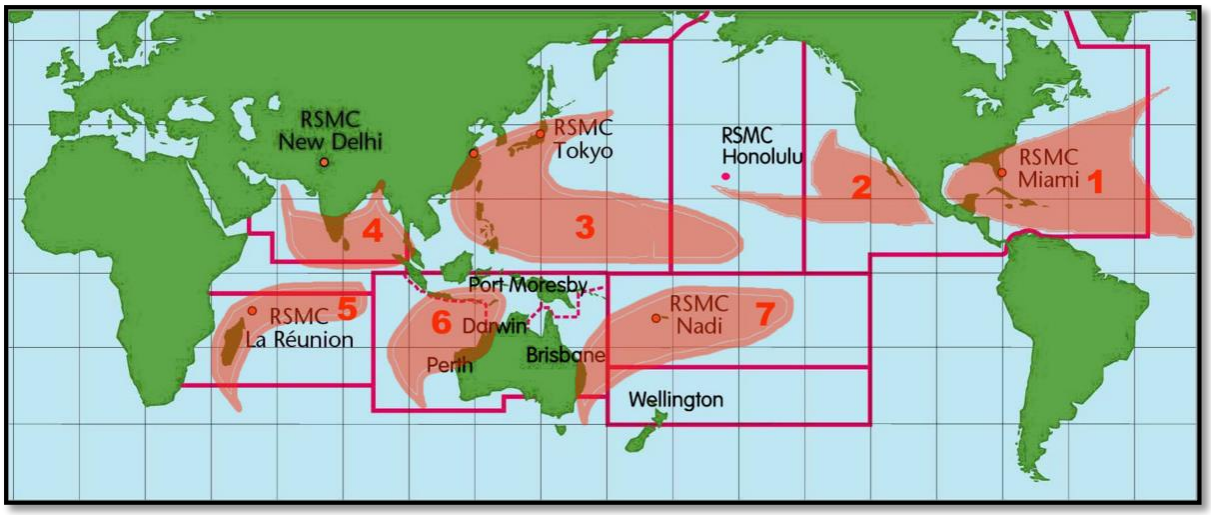

Figure 2.3: The seven tropical cyclone "basins" (Landsea, 2014).

Tropical Cyclone Warning Centres (TCWC) and Regional Specialised Meteorological Centres (RSMC) detect and monitor tropical cyclones for the appropriate region. These centres supply data on the location, movement and intensity of tropical cyclones as well as providing warnings of approaching storms. Météo France La Réunion is the RSMC responsible for the South-West Indian Ocean.

Tropical cyclones are classified in order to quantify the severity and expected damage of the storm. Several classification systems are used, although the most commonly used is the Saffir-Simpson scale. This system uses the wind intensity to classify the tropical cyclone using a 1 – 5 rating. The Saffir-Simpson scale is presented in Table 2.1 along with the expected damage of each category. The V_{max} in Table 2.1 is defined as the maximum sustained surface (10 m elevation) wind speed in the tropical cyclone. The 1-min average V_{max} is defined as the maximum sustained wind speed measured anywhere in the tropical cyclone, averaged over a period of 1 minute.

Table 2.1: The Saffir-Simpson scale

Category	1-min average V_{max} (m/s)	Expected Damage
Tropical Depression	< 17	None or minimal
Tropical Storm	17 - 33	Minimal
1	34 - 42	Minimal
2	43 - 49	Moderate
3	50 - 58	Extensive
4	59 - 69	Extreme
5	> 69	Catastrophic

2.2. Tropical Cyclone-Induced Threats

2.2.1. Introduction

Tropical cyclones are destructive phenomenon, posing a major threat to regions susceptible to these storms. The impacts of tropical cyclones can be human fatalities and destruction of coastal infrastructure. Hurricane Katrina, which occurred in the Gulf of Mexico in 2005, is a good example of the destruction imposed by these storms. About 1200 lives were lost because of Hurricane Katrina with an estimated damage of US $75 billion. Powerful waves and increased storm surge levels damage buildings and other infrastructure along the coast. Currents in conjunction with the waves erode beaches and coastal highways. The combination of storm tides, waves and currents can also damage marinas and boats in harbours. Coastal engineers are responsible for providing protection against these threats.

2.2.2. Waves

2.2.2.1. Wind-Wave Generation

Ocean waves are generated through the interaction of wind blowing over water. The transmission of energy between the ocean and air is complex and involves the near-surface wind profile, wind turbulence, and the wind and wave velocity vector difference (Harper et al., 2001). The growth of wind waves is influenced by three elements namely; wind strength, wind duration and the fetch (distance over which the wind blows).

Waves grow fastest when the wave speed and wind speed are equivalent, and for higher wave frequencies. Waves do not grow infinitely, as they are limited by various conditions. Wave growth can be fetch-limited due to local topography along the coast or the size of the weather system, and duration-limited if the wind does not blow for long enough. If a constant wind blows for long enough over an area that is not limited by the fetch, growth of the waves become self-limited due to wave breaking. Energy is dissipated, preventing the ocean from absorbing more energy and keeping the system in equilibrium. This is termed a “fully developed sea”. The process responsible for this energy dissipation is known as white-capping. In deep water, white-capping (wave breaking) occurs when a certain limit is reached in terms of the wave steepness. Holthuijsen (2007) suggests the maximum wave steepness (S_{max}) is represented by the following:

$$S_{max} = \frac{H_{0,max}}{L_0} \approx 0.14 \qquad (2\text{-}1)$$

where, $H_{0,max}$ = deep water wave height

L_0 = deep water wave length

2.2.2.2. Deep Water Wave Spectra

The most important parameter describing the ocean state is the significant wave height H_s $(or\ H_{1/3})$, defined as the average of the highest one-third of measured wave heights. The sea-surface elevation can be described as the sum of several wave components that differ in height, frequency and direction. Due to the complexity of such a sea state, a more detailed description than the above-mentioned (H_s) is required. The solution is a wave spectrum that accounts for all these wave components.

The one-dimensional wave spectrum is best described by the variance density spectrum. The variance density spectrum describes the sea-surface elevation, by plotting the variance of the waves over different frequencies. Therefore, giving a description of the wave energy as a function of frequency. The variance density spectrum is formulated as follows (Holthuijsen, 2007):

$$E(f) = \lim_{\Delta f \to 0} \frac{1}{\Delta f} E\{\frac{1}{2}\underline{a}^2\} \quad (2\text{-}2)$$

where, $E(f)$ = energy as a function of frequency
a = amplitude
Δf = frequency interval = 1/D
D = duration

The significant wave height estimated from wave spectra (H_{m0}) is calculated using the following equation (Holthuijsen, 2007) :

$$H_{m0} \approx 4\sqrt{m_0} \quad (2\text{-}3)$$

where m_0 is the zeroth-order moment of the variance density spectrum $E(f)$, calculated using the following equation (Holthuijsen, 2007) :

$$m_n = \int_0^\infty f^n E(f) df \quad (2\text{-}4)$$

where, m_n = nth-order moment
n = 0 for zeroth-order moment

Figure 2.4 shows an example of a one-dimensional variance density spectrum. The peak wave period (T_p) is determined from the spectrum by taking the inverse of the frequency, at the peak of spectral energy.

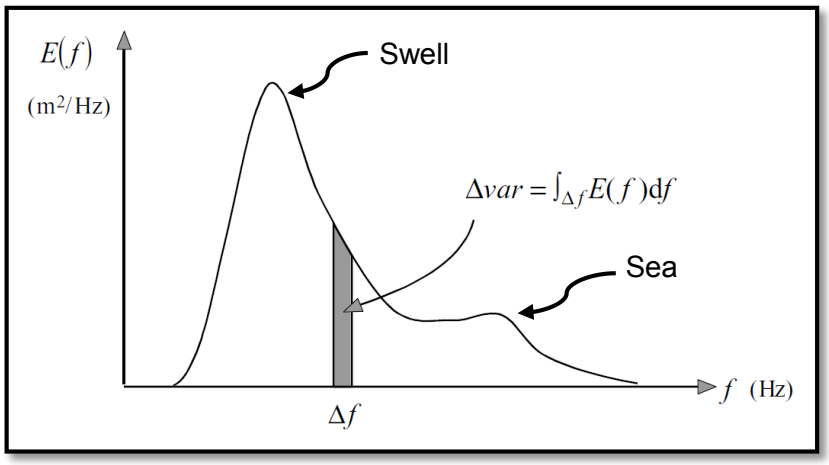

Figure 2.4: A one-dimensional variance density spectrum (After Holthuijsen, 2007)

Due to the wave growth mechanism, waves that are still being generated by the wind have short periods. However, waves that have travelled great distances from the generation area have longer periods because of wave-wave interactions. The shorter period wave is referred to as a "sea" condition and the longer period wave as a "swell" condition. These components can be seen in Figure 2.4. The frequency of a "swell" wave is typically in the range of 0.033 Hz to 0.2 Hz, and a "sea" wave has a frequency in the range of 0.2 to 4 Hz. It is common for the two components to be present together, which can create a mean direction that is different from the two components (Harper et al., 2001).

The one-dimensional spectrum only takes into account the various frequencies of the waves. In order to describe the sea state better, the directions also need to be considered. The two-dimensional frequency-direction spectrum ($E(f,\theta)$) is used, and is formulated as follows (Holthuijsen, 2007):

$$E(f,\theta) = \lim_{\Delta f \to 0} \lim_{\Delta \theta \to 0} \frac{1}{\Delta f \Delta \theta} E\{\frac{1}{2}\underline{a}^2\} \qquad (2\text{-}5)$$

where $E(f,\theta)$ is the frequency-direction spectrum and θ is the direction of wave propagation. Figure 2.5 illustrates the two-dimensional frequency-direction spectrum.

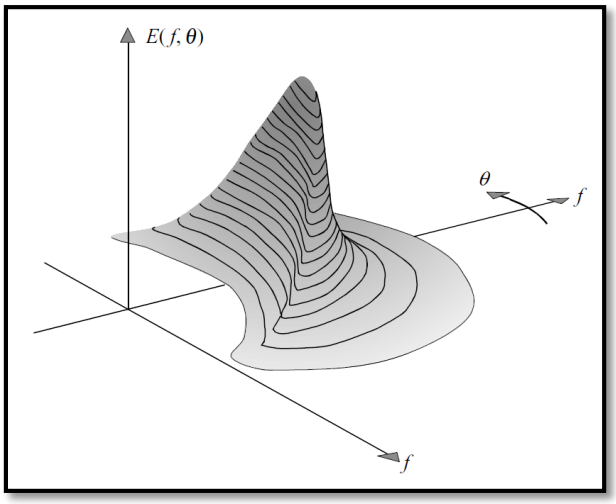

Figure 2.5: The two-dimensional frequency-direction spectrum (Holthuijsen, 2007).

During the propagation towards shallower water, ocean waves are influenced by various coastal processes, which are dealt with in the next section.

2.2.2.3. Nearshore Waves

The erosion generated by coastal processes such as waves, currents and wind, mainly shapes coastlines. As a wave propagates towards the shoreline, its speed, height, direction and wavelength are transformed by different processes resulting a breaking wave (Harper et al., 2001). At a certain point, they reach a depth where the bottom influences the height of the wave. This depth is equal to half the deep-water wavelength (L_0). At depths less than this, bottom friction causes the group velocity of the waves to slow down. The wave energy is then transferred by increasing the wave amplitude as the waves begin to bunch up and increase in height. This process is known as *shoaling*.

Refraction occurs when waves approach depth contours at a certain angle, as illustrated in Figure 2.6. The figure illustrates wave crests approaching a shoreline at an angle where 2 points are located at different points along a wave crest. Point A in the figure is located in shallower water than Point B and therefore will have a slower speed, due to bottom friction. The effect of this, is that the wave crest appears to bend as Point B catches up to Point A and finally approaches the shoreline orthogonally. This process can either concentrate or diffuse wave energy at specific locations along the coastline. Divergence of wave energy occurs in embayments, while convergence occurs along headlands (Harper et al., 2001).

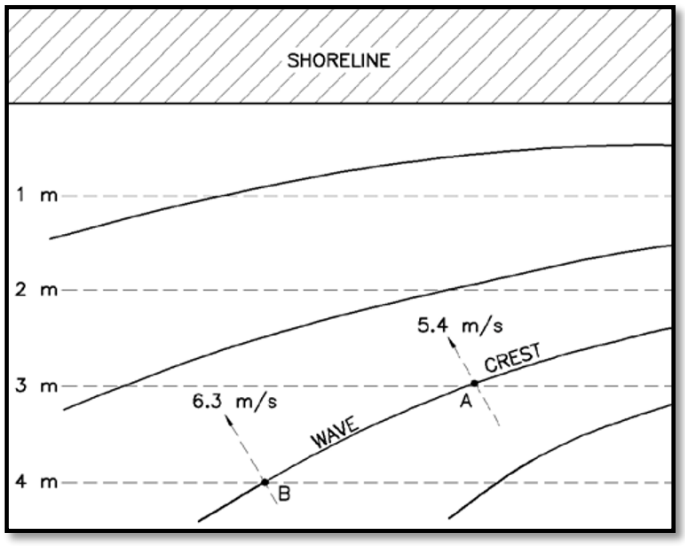

Figure 2.6: Sketch illustrating wave refraction (USACE, 2006)

Diffraction is the lateral transfer of wave energy along a crest, as a wave encounters an obstruction (USACE, 2006). Once a wave hits an obstacle such as a breakwater, the waves will appear to bend around the obstacle. This process is illustrated in Figure 2.7, where wave crests approach a breakwater. Some of the incoming waves are reflected off the breakwater, while behind the breakwater, the waves are diffracted.

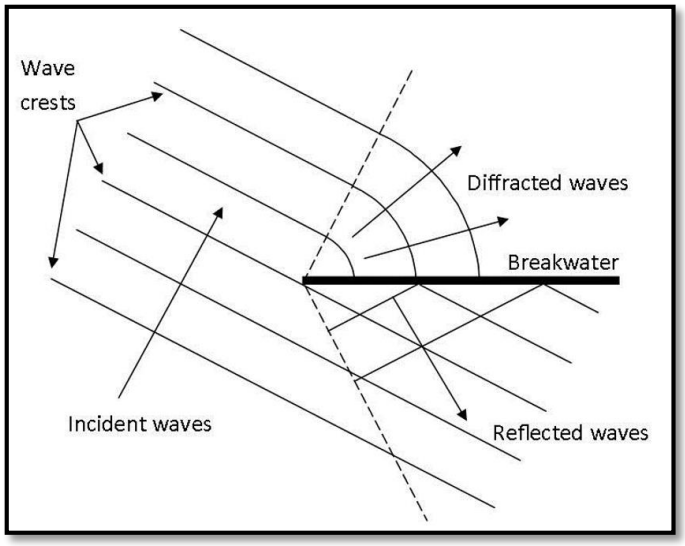

Figure 2.7: Diffraction around a breakwater (After Chadwick et al., 2004)

Waves entering shallow water reach a point where the water particle velocity at the crest of the wave, surpasses that of the wave speed. At this point, wave breaking will occur when a limit of wave height to water depth is reached. This limit is referred to as the breaking index (γ) and is formulated as follows (Chadwick et al., 2004):

$$\gamma = \frac{H_b}{d_b} = 0.78 \quad (2\text{-}6)$$

Where H_b is the wave height at breaking and d_b is the depth at breaking. There are three kinds of wave breaking namely; spilling (gentle slopes), plunging (medium slopes) and surging (steep slopes). The surf zone is the term used to describe the area of breaking waves. Tropical cyclone-generated waves are impacted to these processes, which is why it is important to understand them.

Coastal erosion is the removal of land along the coastline due to waves, currents and winds. The elevated water levels and large waves produced by tropical cyclones can cause large amounts of coastal erosion. Buildings, roads and other infrastructure along the coast are at high risk during a tropical cyclone event.

2.2.3. Wave Set-up

When waves reach the coast, the shoreline stops the transported mass, producing a returning current towards the ocean. The incoming waves and returning current therefore interact, which has lead to much research around this topic. The concept of radiation stress shows that the mean water level falls, below the still water level from deep water, to the point of wave breaking. This is referred to as wave set-down and is illustrated in Figure 2.8. Wave set-down ($\bar{\eta}_d$) can be calculated using the following equation (Horikawa, 1978):

$$\bar{\eta}_d = -\frac{1}{8}\frac{kH^2}{\sinh(2kd)} \quad (2\text{-}7)$$

where H = wave height
k = wave number = 2π/L
d = water depth

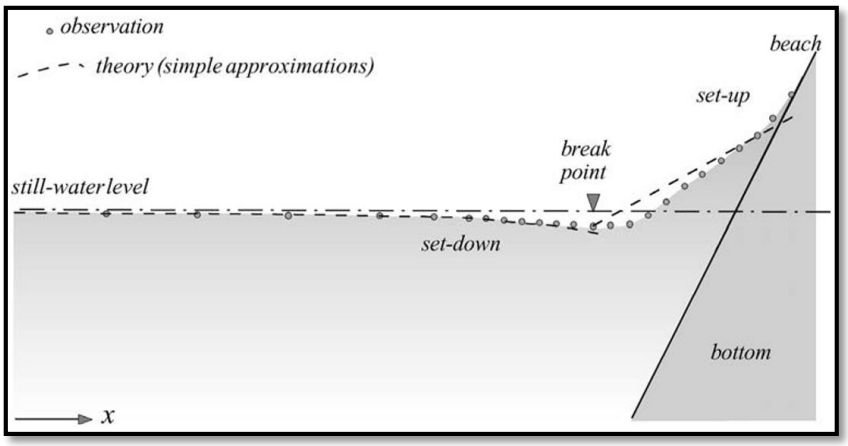

Figure 2.8: Schematic showing wave set-up and set-down (Holthuijsen, 2007)

In the surf zone, the mean water level exceeds the still water level as illustrated in Figure 2.8. This feature is known as the wave set-up ($\bar{\eta}_u$) and can be calculated using the following equation (Horikawa, 1978):

$$\bar{\eta}_u = \left(\frac{1}{1+\frac{8}{3\gamma^2}}\right)(d_b - d) + \bar{n}_{d_b} \qquad (2\text{-}8)$$

where $\bar{n}_{d_b}$ is the wave set-down at the point of breaking.

The shoreline set-up is the wave set-up at a depth equal to zero. Equation 2-8 can be used to calculate the shoreline set-up by substituting *d* = 0. However, Equation 2-8 is a simple model based on regular waves and could lead to the under-estimation of the real shoreline set-up under field conditions. Various authors have studied wave set-up at the shoreline and consequently formulated empirical equations to estimate its magnitude. For more information on these equations, the reader is referred to studies by the following authors: Gourlay (1992), Hanslow and Nielsen (1993) and Raubenheimer et al. (2001).

2.2.4. Storm Surge

Storm surge is a rise in sea level, due to low atmospheric pressure and strong surface winds generated by a storm (Smith, 2013). Storm surge, also known as meteorological tide, is the difference in the measured water level and the predicted tide of a storm. Tropical cyclones have the capability to produce a storm surge of great proportions, affecting in excess of 100 km of coastline. The surge is produced by extreme winds that circle the storm centre, which in turn drive the ocean currents. The lowered atmospheric pressure also contributes to the surge by causing a local rise in water level, which is known as the “inverted barometer” effect (Harper et al., 2001).

The set of equations governing storm surge are the continuity and momentum equations. The depth-integrated continuity equation is formulated as follows (Smith, 2013):

$$\frac{\partial(\varsigma+h)}{\partial t} + \frac{\partial}{\partial x}[U(\varsigma+h)] + \frac{\partial}{\partial y}[V(\varsigma+h)] = 0 \qquad (2\text{-}9)$$

where U, V = depth-averaged velocities in the x, y horizontal directions

h = bathymetric depth (measured from the geoid to the bottom)

ς = free surface departure from the geoid

t = time

and the respective depth-integrated x- and y-momentum equations are (Smith, 2013):

$$\frac{\partial[U(\varsigma+h)]}{\partial t}+\frac{\partial[U^2(\varsigma+h)]}{dx}+\frac{[VU(\varsigma+h)]}{dy}-f[V(\varsigma+h)]=-g(\varsigma+h)\frac{\partial\left[\varsigma+\frac{P_s}{g\rho_o}-\alpha\eta\right]}{\partial x}+\frac{\tau_{sx}}{\rho_o}-\frac{\tau_{bx}}{\rho_o}+M_x-B_x \quad (2\text{-}10)$$

$$\frac{\partial[V(\varsigma+h)]}{\partial t}+\frac{\partial[UV(\varsigma+h)]}{dx}+\frac{[V^2(\varsigma+h)]}{dy}-f[U(\varsigma+h)]=-g(\varsigma+h)\frac{\partial\left[\varsigma+\frac{P_s}{g\rho_o}-\alpha\eta\right]}{\partial y}+\frac{\tau_{sy}}{\rho}-\frac{\tau_{by}}{\rho}+M_y-B_y \quad (2\text{-}11)$$

where
- f = Coriolis parameter
- g = gravitational acceleration
- P_s = atmospheric pressure at the sea surface
- ρ = density of water
- η = Newtonian equilibrium tide potential
- τ_{sx}, τ_{sy} = imposed surface stresses (wind and waves)
- τ_{bx}, τ_{by} = bottom stresses
- M_x, M_y = vertically integrated lateral stress gradient
- B_x, B_y = vertically integrated baroclinic pressure gradient

A tropical cyclone with its characteristic low atmospheric pressure, strong winds and forward motion of the system, generate a transient long-wave flow of the underlying ocean. At first the flow lags behind the system and then slowly decays as it travels along the coast. The generation and propagation of storm surge is therefore greatly affected by the coastal bathymetry. The arrival of a storm surge event is characterized by a gradual increase in water levels, and then a similar decrease, as the system passes. The resulting storm surge due to tropical cyclones, is observed over hundreds of kilometres along the coast but the peak surge levels are located at the point of maximum wind speeds. This can be in the range of 50 to 100 km in diameter with the storm centre as the reference point. The rate at which the water level increases near the peak surge point can be fast, increasing a number of metres over a short period of time (Harper et al., 2001). During Hurricane Ike, the storm surge at Station 8771013 in Galveston Bay, increased by 2 m over a period of 11.5 hours.

The main contributors to storm surge are the tropical cyclone intensity, size and forward speed. In deep water, the inverted barometer effect has the biggest influence on the storm surge. This can be visualized as a mirror image of the tropical cyclone surface pressure profile, underwater. Along islands or coasts with narrow continental shelves, wave set-up is more of a concern rather than storm surge. In shallow waters, the bathymetry and pressure act

together, and can amplify at the coast to surge levels double that of the offshore levels (Harper et al., 2001).

The wind-driven component of storm surge is limited to shallow waters, and is usually the main contributor to the surge levels experienced along the coastline. Dean and Dalrymple (2002) provide a formula to calculate the wind-driven surge by assuming a constant shelf width with a steady, uniform shoreward directed wind. The formula is as follows:

$$\varsigma_{wind} = h\left(\sqrt{1 + \frac{2n\tau_s l}{\rho g h^2}} - 1\right) \qquad (2\text{-}12)$$

where
τ_s = $\rho c_f W^2$ = wind stress
W = wind speed at 10-m elevation
c_f = friction coefficient, typically 1.2 to 3.4 x 10-6
n = 1 - $\frac{\tau_b}{\tau_s}$, which ranges from 1.15 – 1.3
l = shelf width
h = bathymetric depth

Storm surge is more apparent in shallow water with flat continental shelves rather than in deep water. The largest storm surge will occur when a tropical cyclone makes landfall (perpendicular to the coast) , although a system that moves parallel to the coast at a distance near the radius to maximum winds, could generate the same levels of surge. Coastal features such as capes, bays and offshore islands tend to mitigate the impact of the systems that move parallel and increase the impact of the systems that cross landfall perpendicularly. Tropical cyclones that form close to land struggle to generate a big storm surge due to inertial effects in the ocean. Tropical cyclones with a high speed of forward motion tend to increase the peak surge (Harper et al., 2001). As the storm moves faster across the coast, the surge builds up faster and ultimately becomes more powerful (higher peaks). Considering that about half of the forward speed is added to the winds on the left or right of the tropical cyclone, a greater forward speed generates a greater wind speed, and therefore larger peak surge.

2.2.5. Storm Tide

The storm tide is the combination of the storm surge, astronomical tide and wave set-up, at the coast. Wave set-up is often treated as a separate additional component. The storm tide level is referenced to a specific ground contour as in the case for an astronomical tide. Forecasting the storm tide level is of utmost importance to the safety of low-lying areas, subject to tropical cyclones (Harper et al., 2001).

Figure 2.9 illustrates the components of a storm tide using the ground reference contour of the Australian Height Datum (AHD). Currents generated by extreme winds produce a storm surge, which in conjunction with the low pressure of the system, raise the expected tide to make up the stillwater level (SWL). Waves driven by strong winds, consisting of both sea and swell, propagate along the SWL. Due to wave breaking, some of the energy is transferrred to wave setup, producing an increase in the mean water level (MWL). The elevated SWL and further individual waves lead to significant coastal erosion.

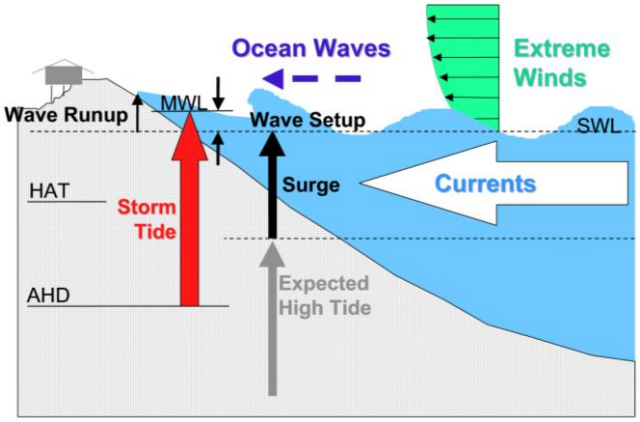

Figure 2.9: Storm tide water levels (Harper et al., 2001).

Storm tide is highly dependent on the tidal phase, as can be seen in Figure 2.10. The peak storm surge arrives during low tide (19 hr on Figure 2.10) and therefore the storm tide level is less. At the point where the MWL exceeds the Highest Astronomical Tide (HAT), erosion of the beach will have taken place because of wave runup effects. Should the water level increase further, flooding of the land behind the dunes will occur, destroying infrastructure and potentially leading to the loss of lives.

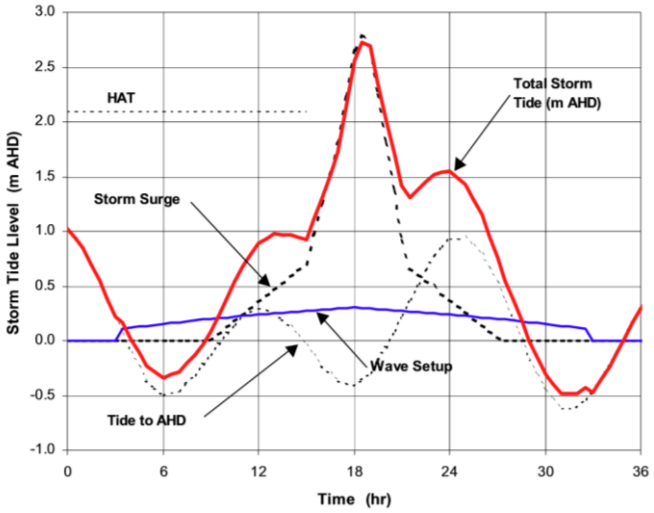

Figure 2.10: Storm tide levels during a storm (Harper et al., 2001).

2.3. Tropical Cyclone Wind Fields

2.3.1. Parametric Wind Field Models

Information describing the spatial arrangement of wind speeds around a tropical cyclone eye is usually not available in historical data. In order to determine this wind field, a simple parametric wind field model can be applied. These simplistic models are based on a few parameters that are used to calculate a wind speed profile such as the one shown in Figure 2.11. An axisymmetric wind field is produced by applying the wind speed profile around the storm eye.

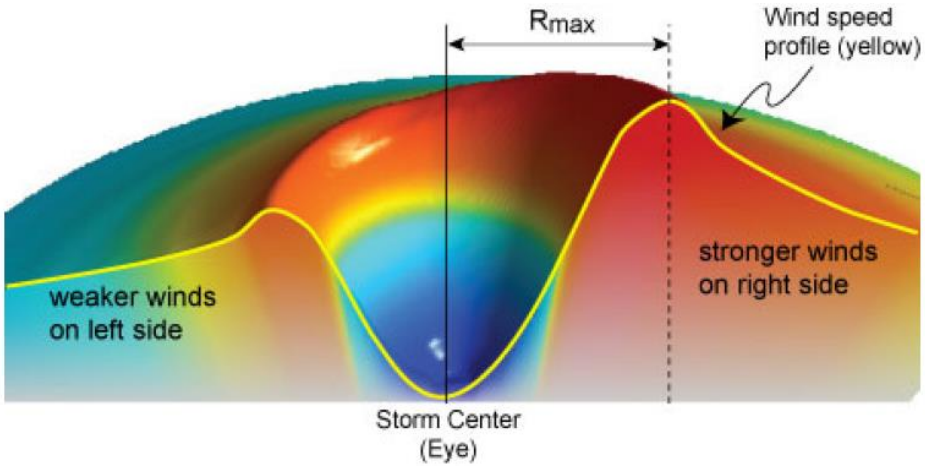

Figure 2.11: Cross section of a tropical cyclone wind field (Dima & Desflots, 2010).

In Figure 2.11, R_{max} is defined as the radial distance from the eye to the point where the strongest winds occur in the tropical cyclone. Stronger winds are observed on the right hand side of forward motion as this example occurs in the northern hemisphere. In the southern hemisphere, stronger winds are observed on the left hand side of forward motion.

Various parametric wind field models have been formulated. Some of the most widely used models are the Modified Rankine Vortex (Depperman, 1947), Holland (1980) model and the Willoughby et al. (2006) model. The Young and Sobey (1981) parametric wind field model used in the present study, is formulated as follows (DHI, 2014d):

$$V_g(r) = V_{max}.\left(\frac{r}{R_{max}}\right)^7.\exp(7\left(1-\frac{r}{R_{max}}\right)) \quad \text{for } r < R_{max} \quad (2\text{-}13)$$

$$V_g(r) = V_{max}.\exp((0.0025R_{max}+0.05)\left(1-\frac{r}{R_{max}}\right)) \quad \text{for } r \geq R_{max} \quad (2\text{-}14)$$

where $V_g(r)$ is the rotational wind gradient speed at a distance r from the cyclone centre. Several wind corrections are typically applied to the wind field models, these include; geostrophic wind corrections, forward motion asymmetry and wind inflow angle corrections. These wind corrections are briefly discussed in the following sections.

2.3.1.1. Geostrophic Wind Correction

The parametric wind field models are often derived from gradient-level winds. Surface winds are therefore calculated, by applying a boundary layer wind speed correction to the gradient wind. The surface wind (10 m elevation) is calculated using the following equation (Harper et al., 2001):

$$V_{10}(R) = K_m . V_g(R) \qquad (2\text{-}15)$$

where $V_{10}(R)$ = surface wind speed at a 10 m elevation

$V_g(R)$ = gradient wind speed

K_m = 0.81 for V_g < 6 m/s

K_m = 0.81 – 2.96 x 10^{-3} (V_g – 6) for 6 ≤ V_g < 19.5 m/s

K_m = 0.77 – 4.31 x 10^{-3} (V_g – 19.5) for 19.5 ≤ V_g < 45 m/s

K_m = 0.66 for V_g > 45 m/s

2.3.1.2. Forward Motion Asymmetry

Due to the clockwise rotation of tropical cyclone winds in the southern hemisphere, stronger winds are observed on the left hand side of the cyclone track as mentioned in Section 2.3.1. The forward movement of the cyclone adds to the wind speed components on the left hand side and reduces the wind speeds on the right hand side. The correction for the asymmetry is formulated as follows (Harper et al., 2001):

$$V_{10}(R, \theta) = K_m . V_g(R) + \delta_{fm} . c . \cos(\theta_{max} - \theta) \qquad (2\text{-}16)$$

where δ_{fm} = proportion of the forward motion added or subtracted from the wind speed (typically 0.5 to 1).

c = forward speed of the tropical cyclone.

θ_{max} = angle to maximum wind speed measured relative to the direction of the system (typically 65° to 115° in the southern hemisphere)

θ = angle measured relative to the cyclone direction

2.3.1.3. Wind Inflow Angle

The parametric wind field models assume a circular wind flow pattern. This is not the case in reality, as frictional effects cause the winds to flow inwards, towards the centre of the system. Sobey et al. (1977) proposed a set of equations to calculate the inflow angle (β) as follows:

$$\begin{aligned} \beta &= 10\frac{R}{R_{max}} && \text{for } 0 \le R < R_{max} \\ \beta &= 10 + 75\left(\frac{R}{R_{max}} - 1\right) && \text{for } R_{max} \le R < 1.2R_{max} \\ \beta &= 25 && \text{for } R \ge 1.2R_{max} \end{aligned} \qquad (2\text{-}17)$$

2.3.2. Radius to Maximum Wind Speeds

The radius to maximum wind speeds (R_{max}) is a very important parameter when representing tropical cyclone wind fields. Research suggests that the intensity of the tropical cyclone winds increase with decreasing values of R_{max}. There is also a relationship between R_{max} and the latitude of the tropical cyclone eye (φ), where R_{max} has been found to increase as the system moves away from the equator. There have been numerous empirical formulas developed to determine R_{max} using other available parameters. These formulas have yielded poor correlation coefficients, and should be used with caution. Some of these formulas are presented below.

Neumann (1987) studied R_{max} values of tropical cyclones over the Atlantic Ocean during the years 1886 through 1987. A total of 852 tropical cyclones were documented. Neumann (1987) assumed R_{max} has a normal distribution with a mean (μ) and standard deviation (σ) as a function of latitude (φ) and storm intensity (V_{max}). The equations are formulated as follows:

$$R_{max}(\mu) = 11.671 + 0.014487 \times \varphi^2 - 0.1660035(10^{-5}) \times {V_{max}}^3 \qquad (2\text{-}18)$$

$$R_{max}(\sigma) = 4.02853 + 0.2822473 \times \varphi - 0.03148963 \times V_{max} \qquad (2\text{-}19)$$

Willoughby and Rahn (2004) formulated an equation for R_{max} using aircraft reconnaissance data measured over the Atlantic and Pacific Oceans from 1977 to 2000. The proposed equation is as follows:

$$R_{max} = 46.29e^{-0.0153V_{Fmax}+0.0166\varphi} \qquad (2\text{-}20)$$

where V_{Fmax} is the flight level wind speed.

Knaff et al. (2007) used a statistical-parametric model to forecast estimates of wind radii. Wind radii estimates from 1988 to 2003, issued by the Joint Typhoon Warning Centre (JTWC) and the National Hurricane Centre (NHC), were used to formulate the following equations for the North Atlantic and East Pacific Oceans:

North Atlantic: $$R_{max} = 36.1 - 0.0492V_{max} + 0.574(\varphi - 25) \quad (2\text{-}21)$$

East Pacific: $$R_{max} = 27.3 - 0.0484V_{max} + 0.033(\varphi - 25) \quad (2\text{-}22)$$

The four relationships presented in this section are considered later in the study. A comparison of the four empirical formulas is presented in Figure 4.1. The formula proposed by Willoughby and Rahn (2004) is the most useful in replicating the measurements.

2.3.3. Wind-Pressure Relationship

The intensity of a tropical cyclone is usually defined by either the maximum sustained surface (10 m elevation) wind speed (V_{max}), or the central pressure deficit ($\Delta P = P_o - P_c$), where P_o is the ambient pressure and P_c is the atmospheric pressure at the storm centre. The following general form is often used to describe the relationship between V_{max} and ΔP:

$$V_{max} = a(\Delta P)^b \quad (2\text{-}23)$$

Where a and b are empirically derived constants, which can be found in the literature for certain regions. Fearon (2014) determined the relationship between V_{max} and P_c for the South-West Indian Ocean using data from the JTWC. The relationship was found to be very good (r^2 = 0.9948) and is presented in Figure 2.12.

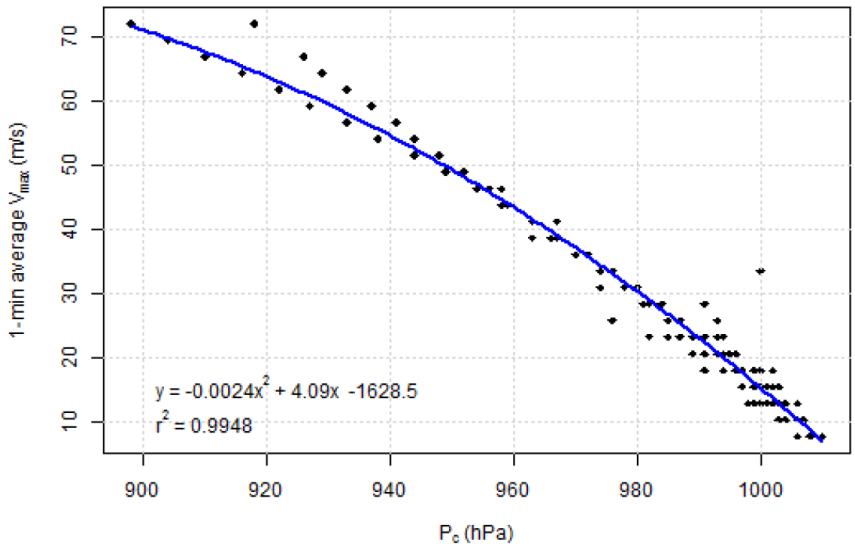

Figure 2.12: Wind-pressure relationship for the South-West Indian Ocean (Fearon, 2014).

2.3.4. Wind Speed Averaging Period

Various meteorological organisations provide wind speed estimates, at different averaging intervals. The 1-min average and 10-min average winds, are typically provided. Ocean response models require wind speed estimates with longer averaging intervals such as the 30-min and 60-min winds. The reason for this is due to the fact that models are formulated on mean wind speeds where wind gusts are averaged out. USACE (2006) provide the following relationship to convert from an averaging period of t seconds to the 1-hour wind speed (V_{3600}):

$$\frac{V_t}{V_{3600}} = 1.277 + 0.296 \tanh[0.9 \log_{10}(\frac{45}{t})] \quad (2\text{-}24)$$

2.4. Tropical Cyclone Studies along the Southern African East Coast

2.4.1. Tropical Cyclone Occurrence and Intensity

Rossouw (1999) studied the occurrence rate and the expected maximum intensity (wind speed) in tropical cyclones, along the Southern African East Coast. Tropical cyclone location and intensity data was retrieved from the Joint Typhoon Warning Centre. The available data only covered a limited period between 1848 and 1999. In order to create a longer series of data, Monte Carlo simulation techniques were used on the available recorded data. The results of the study were estimates of the expected number and maximum intensity of tropical cyclones, occurring within 100 years as a function of latitude. The results are summarized in Table 2.2, which was used to construct an occurrence and intensity map shown in Figure 2.13.

Table 2.2: 100 year occurrence and intensity results (Rossouw, 1999)

Latitude	Average No of Tropical Cyclones in 100 Years	Average Maximum Intensity in 100 years (knots)
2.5	2.2	25.4
5	4.9	54.4
7.5	11.4	80.7
10	28.4	99.6
12.5	72.5	146.2
15	157.2	124.4
17.5	118.5	143.5
20	70.9	117.8
22.5	80.2	136.3
25	34.3	102.6
27.5	11.5	80.6
30	1.5	65.4
32.5	0.0	-

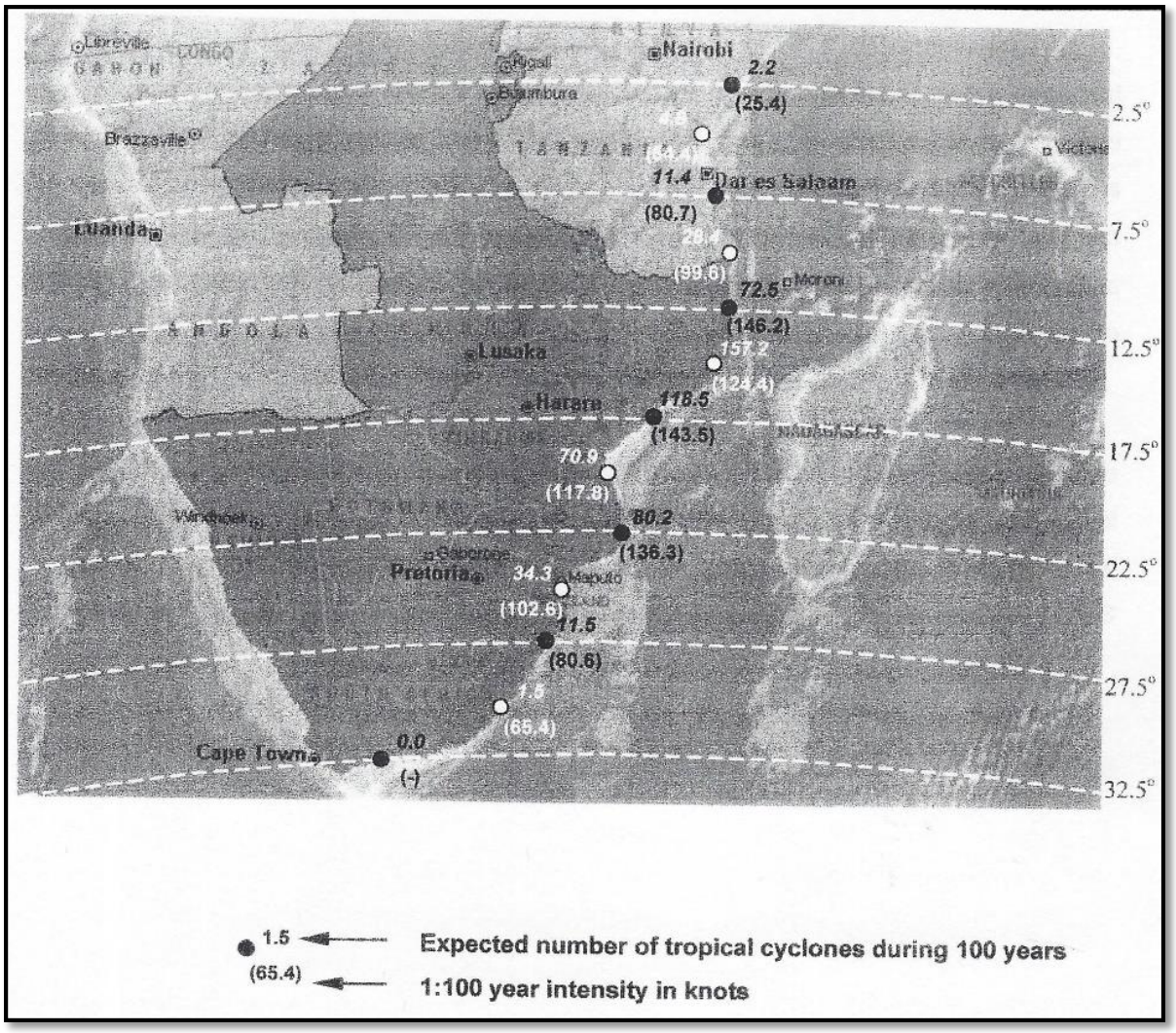

Figure 2.13: Occurrence and intensity map (Rossouw, 1999)

Rossouw (1999) concluded that in a 100-year period, at least one tropical cyclone should occur in the region bordered by the latitudes 2.5°S and 32.5°S, which emphasizes the need to include the impacts of tropical cyclones in the design process at these locations. The maximum number of expected tropical cyclones occurring within 100 years was estimated to be 157.2, located at a latitude of 15°S. The maximum expected intensity (wind speed) of tropical cyclones occurring within 100 years was determined to be 143.5 knots, located at a latitude of 17.5°S.

Rossouw (1999) provides empirical methods to calculate the design wave height, period and water level for a particular location using the tropical cyclone intensities in Table 2.2, forming a parametric model. The empirical formulas for calculating the wave height and period are based on the methods set out in the Shore Protection Manual (USACE, 1984). The storm surge level is obtained using a procedure by Conner et al. (1957). These values serve only as a first approximation, as the methods were developed for other regions, which highlights the

need for an in-depth study of tropical cyclone-induced waves and water levels using advanced numerical models.

2.4.2. Tropical Cyclone-Induced Waves along the Mozambican Coast

Theron et al. (2012) were responsible for a study regarding coastal planning and adaption to mitigate climate change impacts in Mozambique. The study was initiated by the National Institute for Disaster Management (INGC), and aimed to provide protection against the effects of climate change, and to aid in the planning of adaptive measures. As part of the study, the extreme wave conditions generated by tropical cyclones along the Mozambican coast were analysed. This was performed using two procedures. The first involved using empirical methods to calculate the wave height and period using the methods of Rossouw (1999) as described in Section 2.4.1. The second procedure involved the numerical modelling of tropical cyclone-generated waves.

Using the estimated tropical cyclone intensities determined by Rossouw (1999) in Section 2.4.1, Theron et al. (2012) calculated the expected 100-year significant wave height and peak wave period for various locations along the Mozambican coast. The empirical formulas proposed by Rossouw (1999), as discussed in Section 2.4.1, were used. The resulting wave heights and periods are shown in Table 2.3, where the 100-year wave conditions represent offshore locations along the Mozambican coast. These offshore wave conditions are illustrated in Figure 2.14.

Table 2.3: Estimated 100-year wave conditions (Theron et al., 2012)

Onshore City/Town	Latitude (deg)	100-year wave condition		Water depth = 14 m (from 200 m); Slope = 1:50					
				0° (orthogonal)			45° (orthogonal)		
		Hs	Tp	Hs	Dir	L	Hs	Dir	L
Maputo	26.0	**8.2**	**11**	7.8	0.0	122.0	7.0	27.0	122.0
Maxixe	24.0	**8.6**	**12**	8.4	0.0	135.0	7.4	25.0	135.0
Vilanculos	22.0	**9.0**	**12**	8.8	0.0	135.0	7.8	25.0	135.0
Beira	19.8	**8.7**	**12**	8.5	0.0	135.0	7.5	25.0	135.0
Pebane	17.3	**9.3**	**12**	9.1	0.0	135.0	8.0	25.0	135.0
Angoche	16.2	**9.1**	**12**	8.9	0.0	135.0	7.9	25.0	135.0
Memba	14.2	**9.0**	**12**	8.4	0.0	135.0	7.8	25.0	135.0
Ilha Macaloe	12.0	**9.2**	**12**	9.0	0.0	135.0	8.0	25.0	135.0
Mtwara	10.3	**8.4**	**11**	8.0	0.0	122.0	7.2	27.0	122.0

The offshore wave conditions were linearly transformed to produce the wave conditions in shallower water at a depth of 14 m. These wave heights are also presented in Table 2.3 where two wave directions were considered. The first considered waves approaching the shoreline orthogonally, and the second at an angle of 45°.

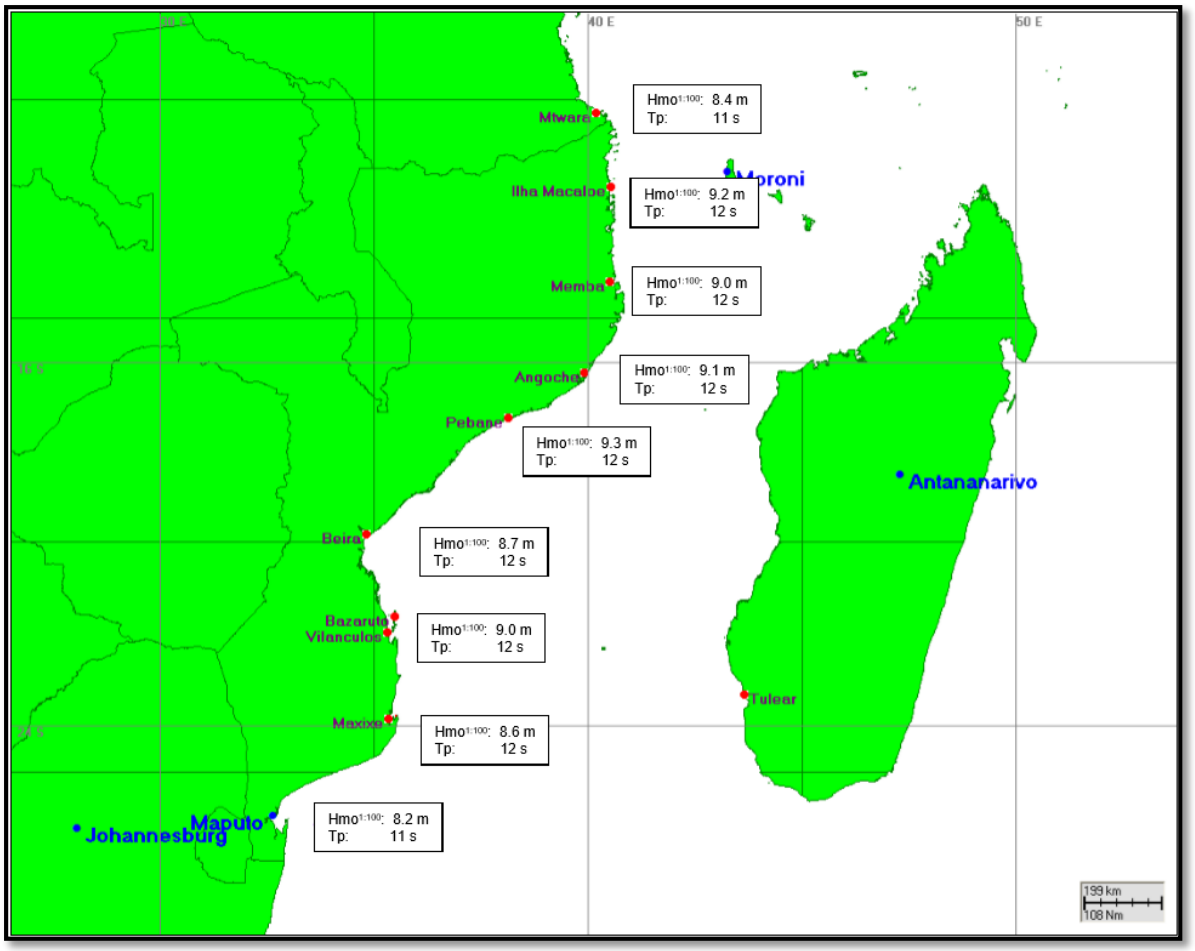

Figure 2.14: Estimated 100-year offshore wave conditions (Theron et al., 2012)

The second procedure used to determine the extreme wave conditions along the Mozambican coast, consisted of numerical modelling. The SWAN model was used to simulate the generation and propagation of waves toward the coast. The 100-year extreme wind intensities, determined by Rossouw (1999) in Section 2.4.1, were used as input for the model. The model was validated by simulating an actual tropical cyclone that occurred in the area. Tropical Cyclone (TC) Lizette occurred off Beira in 1997, while the Council for Scientific and Industrial Research (CSIR) had two wave buoys deployed in the water. The simulated values of TC Lizette and the measured wave data were compared, and it was found that the model produced similar results to the measured data. A peak significant wave height of approximately 4 m was registered during TC Lizette, while the buoy was at a depth of 20 m.

The modelling of waves was restricted to three areas along the coast, namely; Maputo, Beira and Pemba. Several directions of approach were investigated which could be expected along the coast. Table 2.4 summarizes the details of the simulations at the three locations.

Table 2.4: Summary of simulation details (Theron et al., 2012)

Simulation parameter	Location		
	Maputo	Beira	Pemba
Wind speed – hourly average (m/s)	42	48	56
V_f - forward celerity (m/s)	7	7	7
Radius to max wind speed (km)	12	12	12
Approach directions simulated with SWAN	ENE & E	E & SE	NE & E

An example of the resulting wave field at Beira, produced by the SWAN model using the 100-year wind condition, is presented in Figure 2.15. The wave field is represented as wave height contours (colour series) and vectors. The wave vectors represent the mean wave direction, and the vector length represents the wave height. The wave field presented in Figure 2.15 is the result of a tropical cyclone approaching Beira from a south-easterly direction. From the figure, it is evident that the largest waves occur in deeper water and gradually become smaller closer to the shore, where it is shallower.

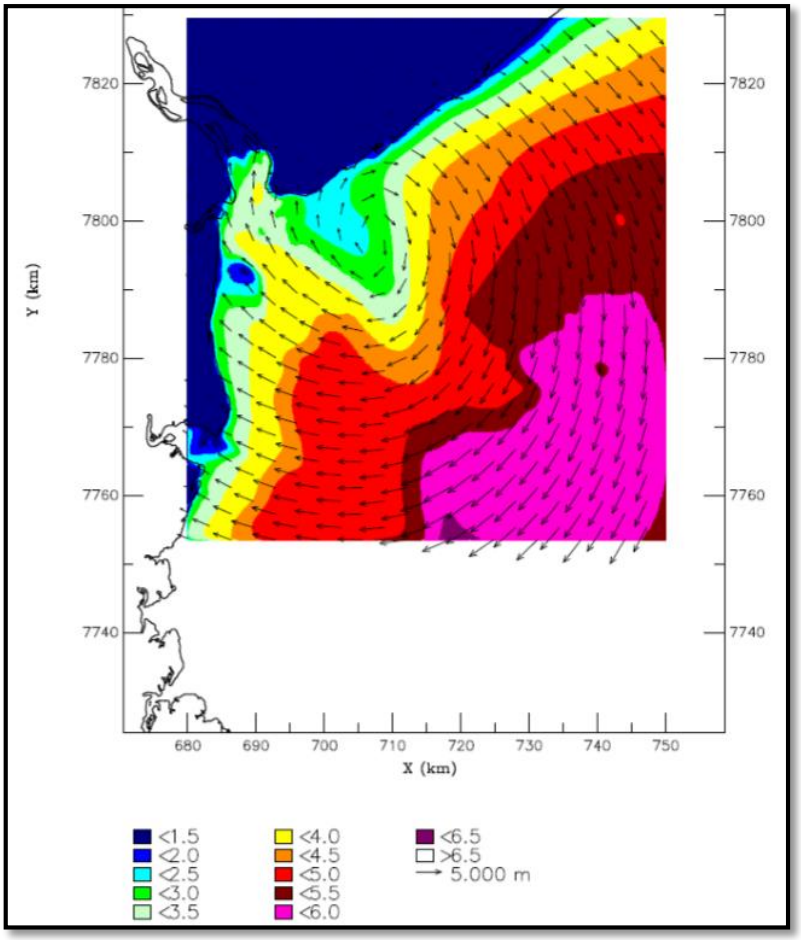

Figure 2.15: Wave model output at Beira for a south-easterly approach (Theron et al., 2012)

2.4.3. Tropical Cyclone-Induced Wind Speeds for the South-West Indian Ocean

Fearon (2014) developed extreme wind speed maps for the South-West Indian Ocean using synthetic tropical cyclone tracks. Best track data consisting of tropical cyclone location and intensity data, from the Joint Typhoon Warning Centre, was used as the primary dataset.

Fearon (2014) used parametric wind field models to produce the tropical cyclone wind fields, using the best track data as input into the models. Two parametric wind field models were considered for the study, namely the Holland (1980) and Willoughby et al. (2006) models. A thorough examination of the ability of the wind field models to generate actual wind fields was performed. The modelled and measured wind speeds were compared at various locations within the South-West Indian Ocean. Both parametric models produced peak wind speeds close to that of the measurements, although it was found that the Willoughby et al. (2006) model produced better results, and was consequently implemented for the remainder of the study.

Due to the small sample size in the historical best track data, a probabilistic methodology was used to estimate the extreme wind speeds caused by tropical cyclones. A synthetic track model was developed with the ability to generate thousands of years of tropical cyclone tracks in the South-West Indian Ocean. The model is solely statistical and is a Markov chain model. The model is based on the best track data where location and wind speed intensities are provided at six hourly intervals. The synthetic track model was validated and reproduced the spatial and temporal occurrence of historical tracks reasonably well. The various track parameters such as the track speed, direction and intensity, were also reproduced reasonably well.

The coupling of the Willoughby et al. (2006) parametric wind field model and the above synthetic track model, made it possible to generate 5000 years of extreme wind speeds caused by tropical cyclones, at any location over the South-West Indian Ocean. Fearon (2014) generated extreme wind speed maps for the South-West Indian Ocean by performing calculations on a 1 degree geographical grid. The maps were generated at return periods of 50, 100, 200 and 500 years. Using these results, estimated 1-min average wind speeds were extracted as a function of latitude, along the Southern African East Coast. These wind speeds are presented in Figure 2.16 for return periods of 50, 100, 200 and 500 years.

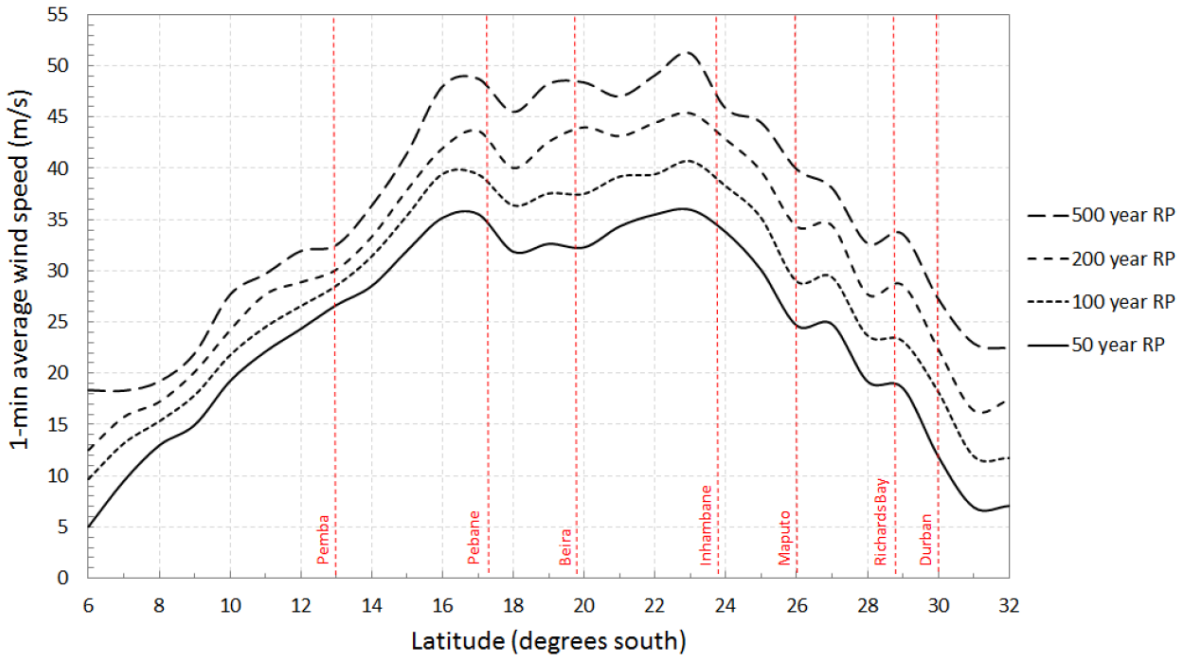

Figure 2.16: Estimates of 1-min average winds speeds expected along the Southern African East Coast at various return periods (Fearon, 2014)

2.4.4. Tropical Cyclone Formation and Motion in the Mozambique Channel

Matyas (2014) studied the formation and motion of tropical cyclones in the Mozambique Channel over the period 1948 to 2010. The storm trajectory and occurrence of landfall was determined using a geographic information system. The NCEP/NCAR reanalysis data was used to detect environmental conditions such as the 500 hPa geopotential heights and precipitable water. The relationship between these conditions, tropical cyclone attributes and four teleconnections were examined, using nonparametric statistical tests. The tropical cyclone's formation latitude and month, trajectory and landfall location were compared to the environmental conditions. The formation frequency, location and storm track were also related to the teleconnections. Results of the study indicate that 94 tropical cyclones formed in the channel, with approximately half reaching land.

3. Study Approach

3.1. General Approach

The study involves the investigation of waves and storm surge, at four locations along the Southern African East Coast, namely; Durban, Maputo, Beira and Pemba as shown in Figure 3.1. These locations were chosen because of their importance and to get an idea of the expected waves and storm surge along the coast, where tropical cyclones typically occur. The results are best estimates of the 50-, 100-, 200- and 500-year significant wave height and storm surge level which are expected to be produced by tropical cyclones at each of the four locations.

Figure 3.1: Study area showing locations of investigation (After Google Earth, 1970a)

At each of the four locations, a study of the waves and storm surge levels generated by tropical cyclones is investigated by applying a third-generation numerical model. The MIKE 21/3 Coupled Model FM by the Danish Hydraulic Institute (DHI) is used.

The waves and storm surge levels are modelled using space and time-varying tropical cyclone wind fields. A deterministic approach is used to determine the wave heights and storm surge levels. In this approach, extreme wind speed estimates (V_{max}) are used from Figure 2.16 in Section 2.4.3. A constant design wind speed is used throughout the simulations. The wind speed estimates are then used to determine other required parameters such as the minimum central pressure (P_c), which can be determined from Figure 2.12 in Section 2.3.3. The other required parameters cannot be determined using the wind speed estimates. These parameters are determined by doing sensitivity tests, to see how the individual parameters influence the model results. Various methods were employed to determine these input parameters. These methods are discussed in the following sections. Using the results of the sensitivity tests, design storm parameters were chosen for input into the numerical model tests.

A total of four return periods are simulated for each of the four locations, resulting in a total of 16 simulations. The output of the simulations are specified at points along the 20 m contour for the waves and the 10 m contour for storm surge. In each simulation, the maximum significant wave height and storm surge level reached, considering all the points, is taken as the design estimate.

In order to see if the proposed model provides reliable estimates of the waves and storm surge, the model was calibrated. The calibration of the model involves the simulation of Hurricane Ike, which occurred over the Gulf of Mexico in September 2008. Hurricane Ike was chosen because of its size, quantity and quality of wave and water level measurements taken during the storm.

3.2. Numerical Modelling Software

The third generation numerical model known as MIKE 21/3 Coupled Model FM by DHI, is used for all numerical modelling. The coupled model allows the interaction of waves and currents between the different modules. The Hydrodynamic module is used to simulate the storm surge/water elevations and the spectral wave module is used to simulate the waves. The coupling of the two models is important as increased storm surge (produced by lowered atmospheric pressure and wind set-up created by onshore winds) creates reduced depth-induced wave breaking, resulting in larger wave heights at the point of interest. The larger wave heights result in higher water levels and wave set-up (Fearon, 2014).

The hydrodynamic module can be used in two-dimension (2D) or three-dimension (3D). For the proposed tests, the 2D model is used, which is based on the incompressible Reynolds

averaged Navier-Stokes equations (shallow water equations). The module simulates water level variations and flows, including the following features and effects (DHI, 2014a):

- Flooding and drying
- Momentum dispersion
- Bottom shear stress
- Coriolis force
- Wind shear stress
- Barometric pressure gradients
- Ice exposure
- Tide effects
- Precipitation/evaporation
- Wave radiation stresses
- Sources and sinks

The spectral wave module uses a fully spectral formulation based on the wave action conservation equation, where the directional-frequency wave action spectrum is the dependent variable. The spectral wave module simulates the growth, transformation and decay of wind-generated waves and swell, including the following phenomena (DHI, 2014a):

- Wind-generated wave growth
- Non-linear wave-wave interaction
- Dissipation caused by white-capping
- Dissipation caused by bottom friction
- Dissipation caused by depth-induced wave breaking
- Refraction and shoaling caused by depth variations
- Wave-current interaction
- Effect of time-varying water depth and flooding and drying

3.3. Numerical Model Input

Tropical cyclones are highly erratic, which makes predicting their characteristics an extremely challenging task. In order to model these storms, several input parameters describing the storm are required. The main input parameters include the tropical cyclone wind speed, pressure, storm size, forward speed and direction. The task of determining typical values of these parameters for tropical cyclones along the Southern African East Coast is complex.

Figure 3.2 illustrates the complexity of the problem, which covers 33 years of historical tropical cyclone tracks over the South-West Indian Ocean. It is a challenging task choosing one direction to model in the proposed tests, out of all of these tracks. The tracks are highly unpredictable and the intensity at any particular point along the track can vary for each tropical cyclone event. The same can be said for the pressure, storm size and forward speed of the storm, highlighting the intricacy of the problem. Fearon (2014) adopted a probabilistic approach to overcome this problem. The shortcoming of this approach is the large number of simulations that would be required, which is why a deterministic approach was adopted for the present study.

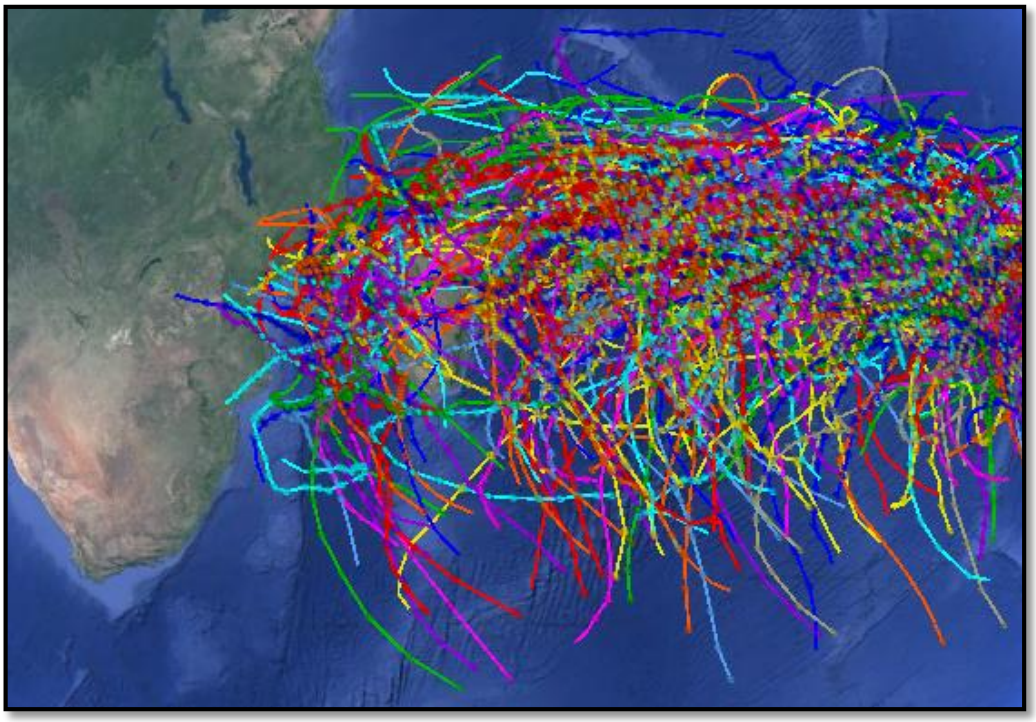

Figure 3.2: Historical tropical cyclone tracks over the South-West Indian Ocean for the years 1982 to 2014 (After Google Earth, 1970a)

This problem is further complicated since the present study focuses on both the waves and storm surge generated by tropical cyclones. A change in the input parameters can result in larger waves on the one hand, but the storm surge could be less on the other hand, and vice versa. The complexity of the problem is addressed by using historical tropical cyclone data to generate typical parameters that can be expected at the location of interest. The parameters for the model tests are then determined by doing sensitivity tests of the variables, to see how the individual parameters influence the model results.

4. Sensitivity Tests of Input Parameters

As discussed in Section 3, various tests are required to determine the design storm input parameters for the proposed numerical model tests. This section provides an overview of these tests and the results obtained.

4.1. Design Storm Parameters

Table 4.1 summarizes the proposed sensitivity test parameters. A constant wind speed of 29 m/s and minimum central pressure of 982 hPa, obtained from Figure 2.16 and Figure 2.12 respectively, is simulated for a 100-year return period. The remaining parameters are tested for their sensitivity in the model using three values. The methods describing how these three values were determined for each parameter, is discussed in Sections 4.1.1 – 4.1.5.

Table 4.1: Sensitivity test parameters

Parameter	Value	Unit
100 - year maximum sustained 1-min average wind speed (V_{max})	29	m/s
Minimum central pressure (P_c)	982	hPa
Radius to maximum wind speeds (R_{max})	13, 31, 109	km
Forward speed (c)	1, 4, 9	m/s
Track direction (δ)	194, 263, 332	°
Sinuosity	1, 1.76, 3.51	(-)
Cyclone Duration	18, 30, 42	hours

4.1.1. Radius to Maximum Wind Speeds

Météo France La Réunion (MFR) provide R_{max} estimates of tropical cyclones over the South-West Indian Ocean during the years 2004 to 2014. Using this data, a comparison of the historically measured values to empirically formulated values of R_{max} found in the literature (Section 2.3.2, Equations 2-18 to 2-22) was made. Only R_{max} values of tropical cyclones that entered the Mozambique Channel (defined as area of ocean between Mozambique and 45°E line of longitude) were taken into consideration, as this is the area of interest for the present study. A list of these tropical cyclones can be found in Appendix A, Table A-1. The results of the comparison are presented in Figure 4.1, where measured and modelled R_{max} values are compared for each of the four empirical formulas.

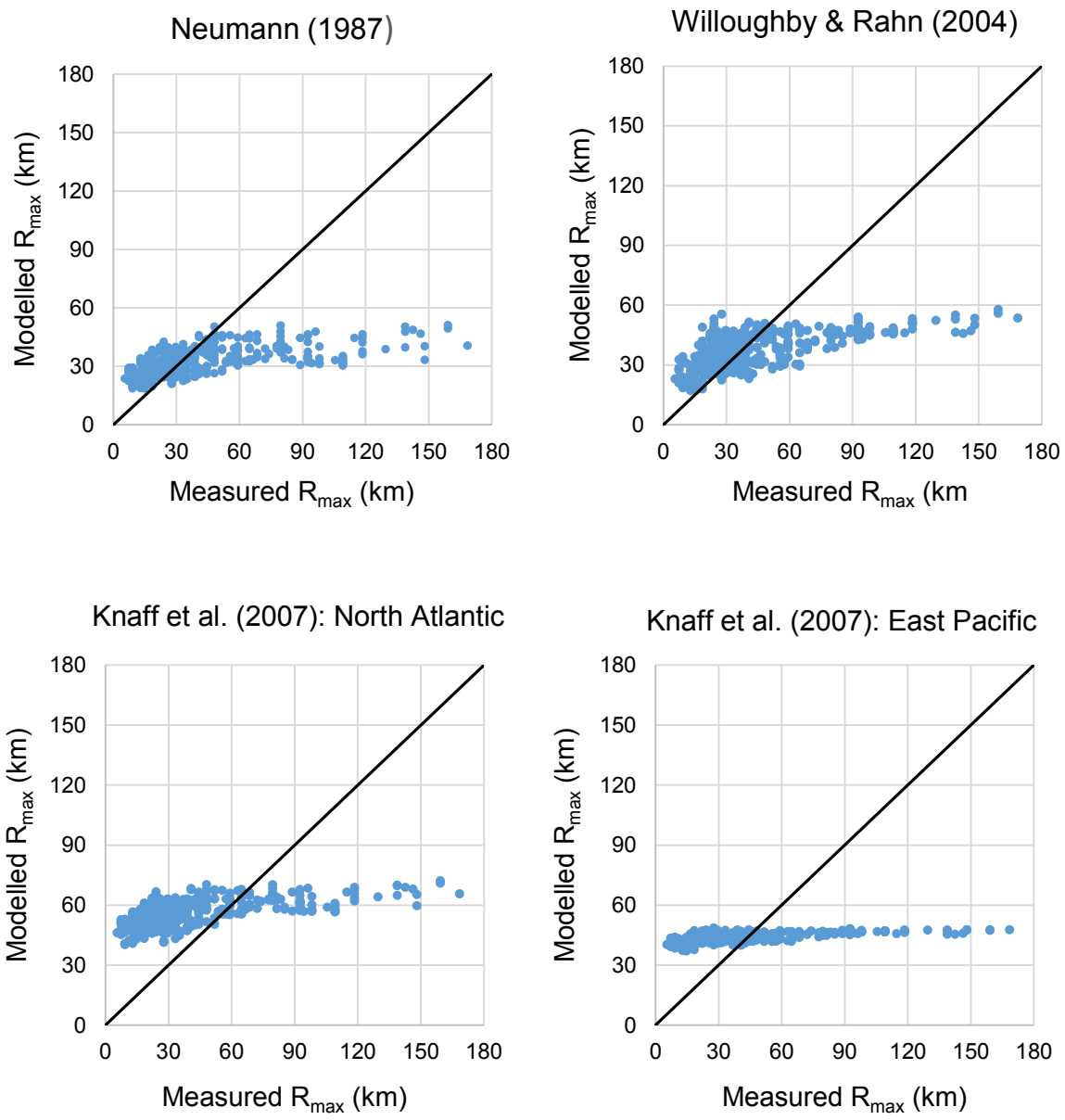

Figure 4.1: Comparison of measured and empirically formulated values of R_{max}

From Figure 4.1, it is evident that none of the empirical formulas represent the measured values well. The reason for this is that these formulas were developed for other regions. The empirical formula proposed by Willoughby and Rahn (2004) appears to fit the measurements the best, considering the four formulas, although it is a poor fit. Based on these results, it was decided that it would be best to use the available historical measured values to determine values of R_{max} for the proposed tests. Using the 487 measured values of R_{max}, a histogram was plotted in Figure 4.2, showing the distribution of the R_{max} values.

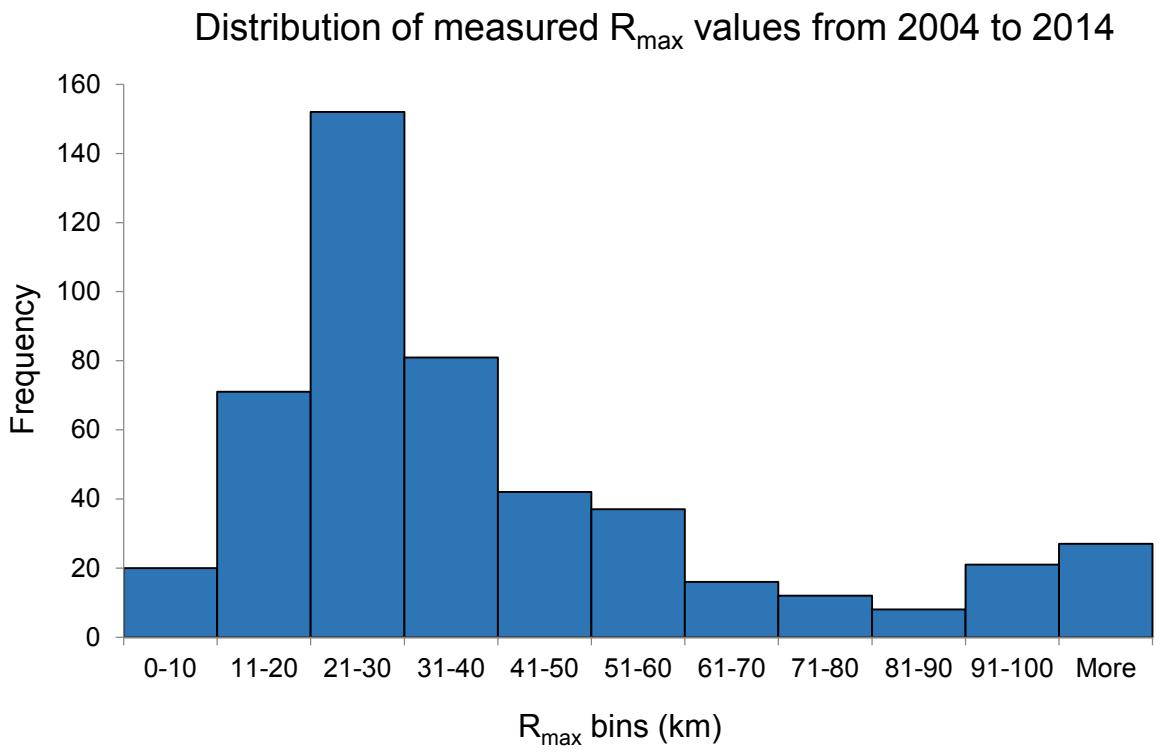

Figure 4.2: Histogram showing distribution of measured R_{max} values from 2004 - 2014

From Figure 4.2, it is evident that the most commonly occurring R_{max} value is in the range of 21 to 30 km. The data cannot be described as a normal distribution and therefore the median provides a better representation of the centre of the data instead of the mean. A summary of the measured values of R_{max} for the 10-year period is presented in Table 4.2.

Table 4.2: Summary of the measured R_{max} values

Parameter	Measured R_{max} (km)
Minimum	5.56
Maximum	168.53
Mean	41.49
Standard Deviation	29.37
Median	31.48
5^{th} Percentile	12.96
95^{th} Percentile	109.27

From Table 4.2, it was decided to use the 5^{th} percentile, median and 95^{th} percentile to get a broad distribution of the historical values. The R_{max} values to be used in the sensitivity tests are therefore 13 km, 31 km and 109 km for the respective 5^{th} percentile, median, and 95^{th} percentile.

4.1.2. Forward Speed

As discussed in Section 2.4.1, Rossouw (1999) studied the occurrence rate and the expected maximum intensity (wind speed) of tropical cyclones along the Southern African East Coast. As part of the study, the distribution of tropical cyclone forward speeds along the coast, was investigated. Figure 4.3 illustrates the findings of the distribution of tropical cyclone forward speeds as a function of latitude (5°S to 30°S).

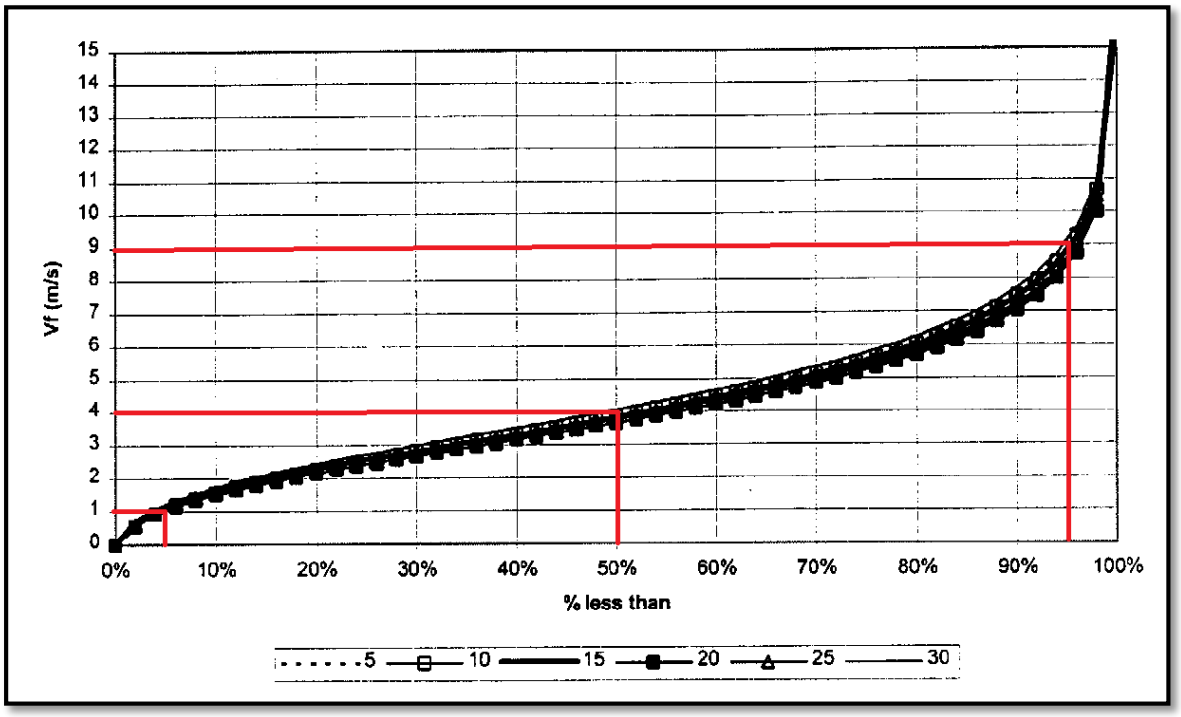

Figure 4.3: Variation of forward speed with latitude (after Rossouw, 1999)

From Figure 4.3, it is evident that there is limited variation of forward speed at the different latitudes. The forward speed input into the model tests will therefore be the same at the four proposed study locations. Using the 5th percentile, median and 95th percentile in Figure 4.3 (red lines), it is possible to get the respective forward speeds of 1 m/s, 4 m/s and 9 m/s to be used in the sensitivity tests.

4.1.3. Track Direction

The Joint Typhoon Warning Centre (JTWC) provides information on historical tropical cyclones. The JTWC also provides historical tropical cyclone tracks that can be viewed in Google Earth, from 1982 to 2014. These tracks were used with Google Earth to determine three track directions to be used in the sensitivity tests. A typical scenario is illustrated in Figure 4.4 where δ is the track direction measured clockwise from north. The directions were

determined by looking at two points in the cyclone track, one before landfall (Point 1 in Figure 4.4) and one after landfall (Point 2 in Figure 4.4). The time between two consecutive points is 6 hours and the angle between these two points was taken as the track direction.

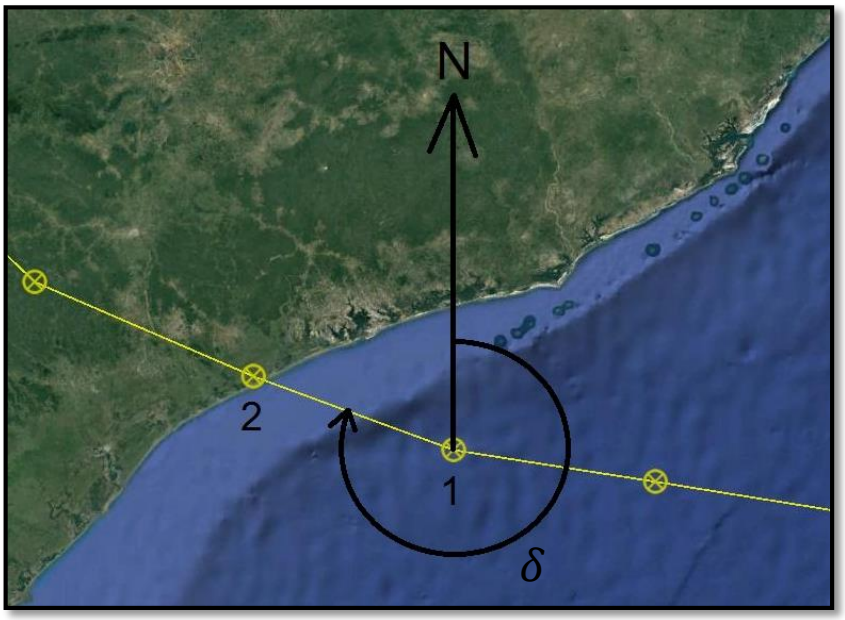

Figure 4.4: Schematic defining track direction (yellow line is the cyclone track)

From the 33 years of historical tracks, only the tropical cyclones making landfall on the Southern African East Coast were taken into consideration. A list of the 21 tropical cyclones and their calculated track directions can be found in Table A-2 of Appendix A. A summary of the results of the study is presented in Table 4.3.

Table 4.3: Summary of historical track directions

Parameter	Track Direction (°)
Minimum	26
Maximum	353
Mean	263
Standard Deviation	69
Median	282
5th Percentile	180
95th Percentile	345

The mean was calculated by averaging all the track directions. Using the 21 track directions, a histogram was plotted in Figure 4.5, showing the distribution of the directions.

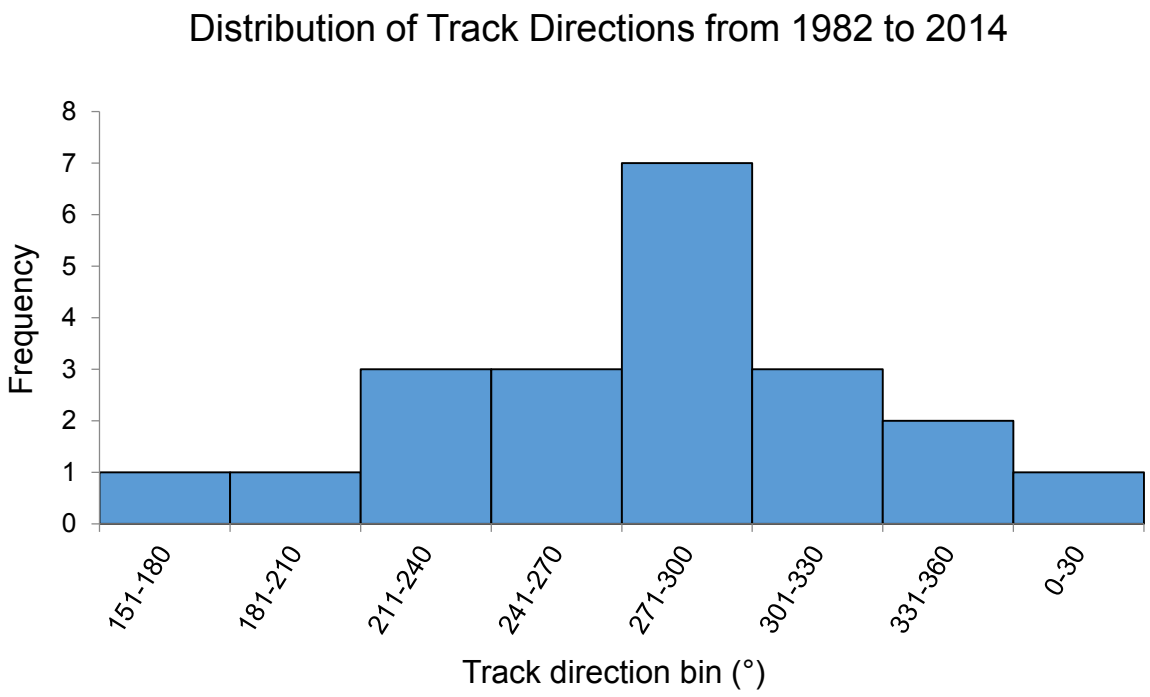

Figure 4.5: Histogram showing distribution of track directions from 1982 to 2014

From Figure 4.5, it is evident that the data is distributed relatively evenly about the mean track direction of 263°. The mean and one standard deviation appears to provide a good representation of the distribution of directions for the sensitivity tests. Based on these results, the three directions to be used in the sensitivity tests are presented in Table 4.4.

Table 4.4: Track directions to be used in the sensitivity tests

Parameter	Track Direction (°)
Mean - Standard Deviation	194
Mean	263
Mean + Standard Deviation	332

4.1.4. Sinuosity

Matyas (2014) studied the formation and motion of tropical cyclones in the Mozambique Channel over the period 1948 to 2010. In order to measure the amount of curvature tropical cyclones experience in the Mozambique Channel, the sinuosity of the tropical cyclone tracks was studied. The sinuosity is defined as the overall tropical cyclone track length (l_c) divided by the straight line distance from start to end (l_s). Sinuosity values greater than 1 are therefore more curved. Figure 4.6 is a schematic showing the sinuosity of a track. The sinuosity was applied in the model, by specifying coordinates that follow the required sinuosity.

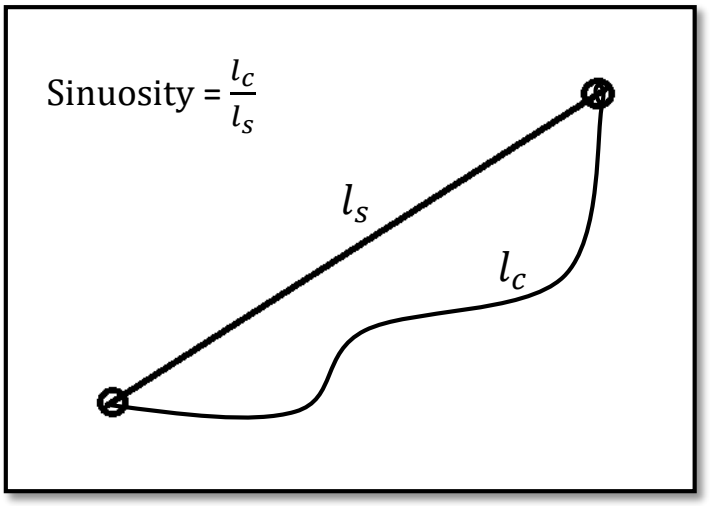

Figure 4.6: Schematic illustrating sinuosity

Using the 94 tropical cyclones that formed in the channel during the study period, a histogram depicting the distribution of the sinuosity values was generated which is presented in Figure 4.7.

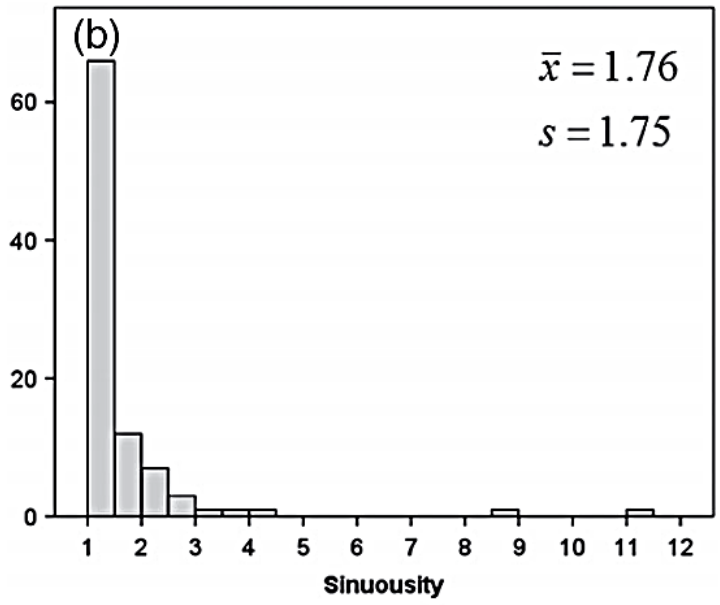

Figure 4.7 Histogram depicting the distribution of sinuosity values of tropical cyclones in the Mozambique Channel from 1948 to 2010 (Matyas, 2014)

From Figure 4.7, it is evident that the majority of tropical cyclones in the Mozambique Channel have sinuosity values between 1 and 1.5. The mean sinuosity of the tracks was determined as 1.76 with a standard deviation of 1.75. Using these values, three sinuosity values were determined for the sensitivity tests as presented in Table 4.5. A sinuosity of less than 1 cannot be achieved, therefore a value of 1 was used for the mean – standard deviation value.

Table 4.5: Sinuosity values to be used in the sensitivity tests.

Parameter	Sinuosity (-)
Mean - Standard Deviation	1
Mean	1.76
Mean + Standard Deviation	3.51

4.1.5. Duration

The duration of the sensitivity tests were based on initial tests, where values of storm surge and wave height reached maximum values in under 18 hour simulations. In order to get a good distribution, durations of 18, 30 and 42 hours were selected. These durations include the simulation of the tropical cyclone 6 hours after making landfall. The origin of the tropical cyclone was determined using the durations, track directions and forward speed of the storm. An example of the determination of the point of origin is illustrated in Figure 4.8, where the track direction is 263°, the forward speed is 4 m/s and the duration is 18 hours. All tropical cyclones made landfall at the location of interest, the origin was therefore determined by working backwards from this point using the duration and forward speed to calculate the distance to the origin. This distance was applied along the specified track direction to obtain the point of origin.

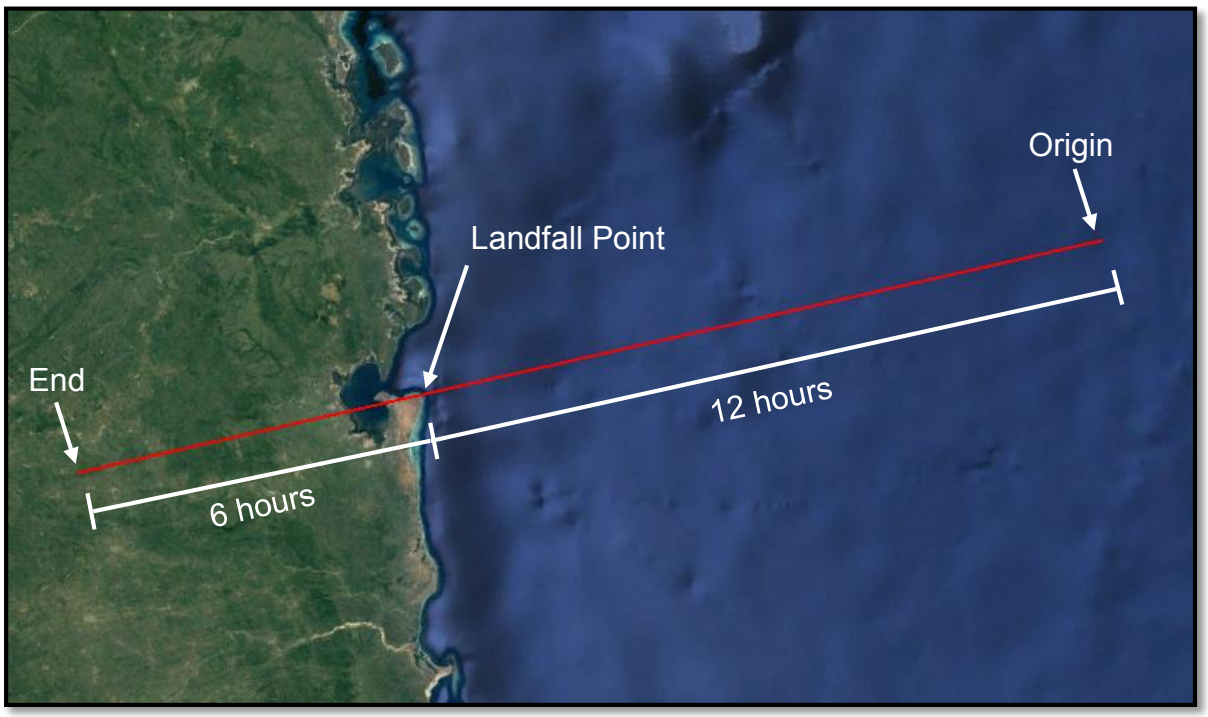

Figure 4.8: Schematic illustrating the determination of the tropical cyclone track origin (red line is the cyclone track)

4.2. Model Set-up

Sensitivity tests were conducted for the region surrounding Pemba. The bathymetry data for Pemba was obtained first, which is why Pemba was chosen as the location for the sensitivity tests. Additional maps were required at the other locations, which were only obtained at a later stage. The purpose of the sensitivity tests is to determine how the different input parameters influence the model results. The focus is therefore not on the values of storm surge and wave heights, but rather how the values change for each input. For this reason, a brief overview of the model set-up is presented in the following sections.

4.2.1. Mesh and Bathymetry

The bathymetry used for the model domain consisted of digitised admiralty charts for the shallow water, and the GEBCO (2014) Grid for the deeper water. The GEBCO (2014) Grid is a 30 arc-second global grid of elevations, produced by using quality-controlled ship depth soundings, with interpolation between sounding points, guided by satellite-derived gravity data.

The model domain with its mesh and bathymetry is presented in Figure 4.9. The mesh consists of three sections, all flexible meshes with triangular elements. Mesh A is a coarse mesh with a grid resolution of 5 km while Mesh B has a finer grid resolution of 1.5 km. An even finer mesh is located at Mesh C, where the grid resolution is 500 m. A close-up of Mesh C is shown in Figure 4.10. Meshes B and C were chosen based on the locations of expected maximum respective waves and storm surge.

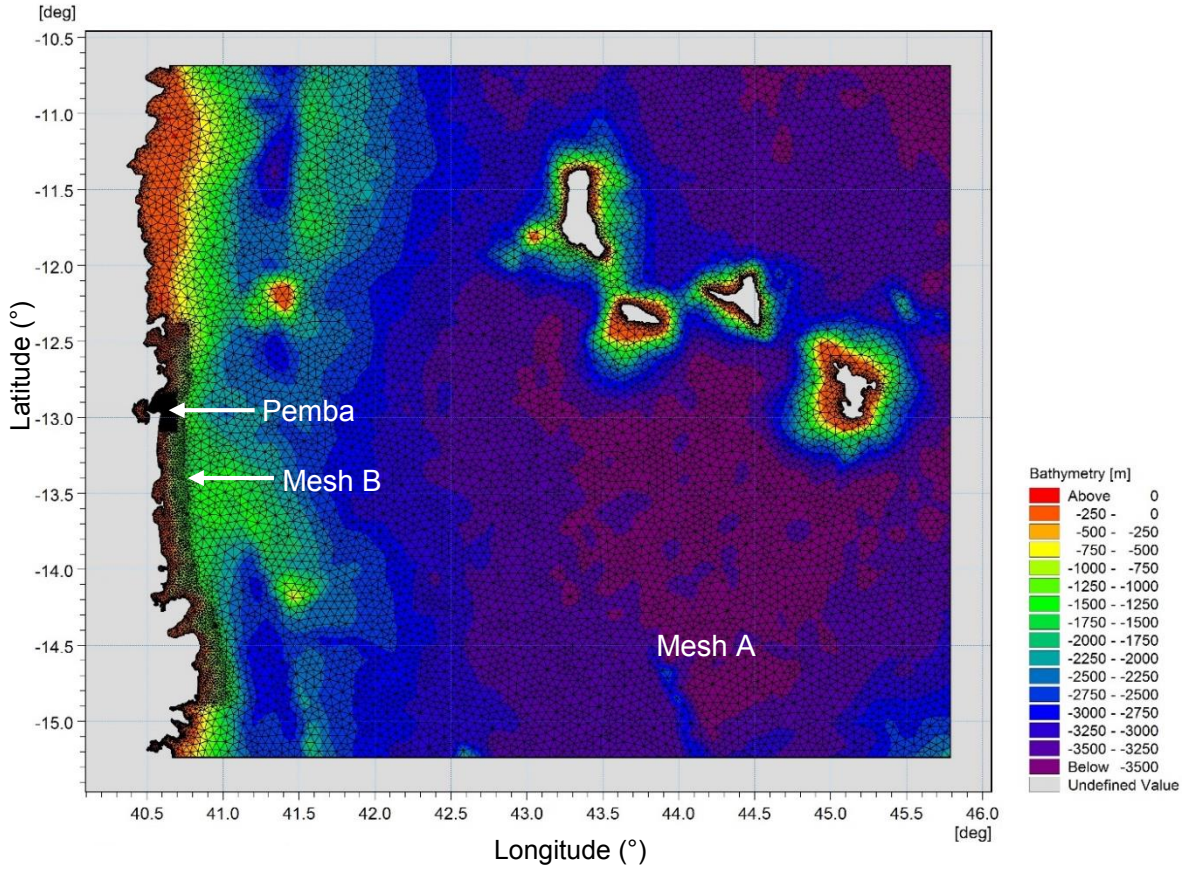

Figure 4.9: Mesh and bathymetry for Pemba sensitivity tests

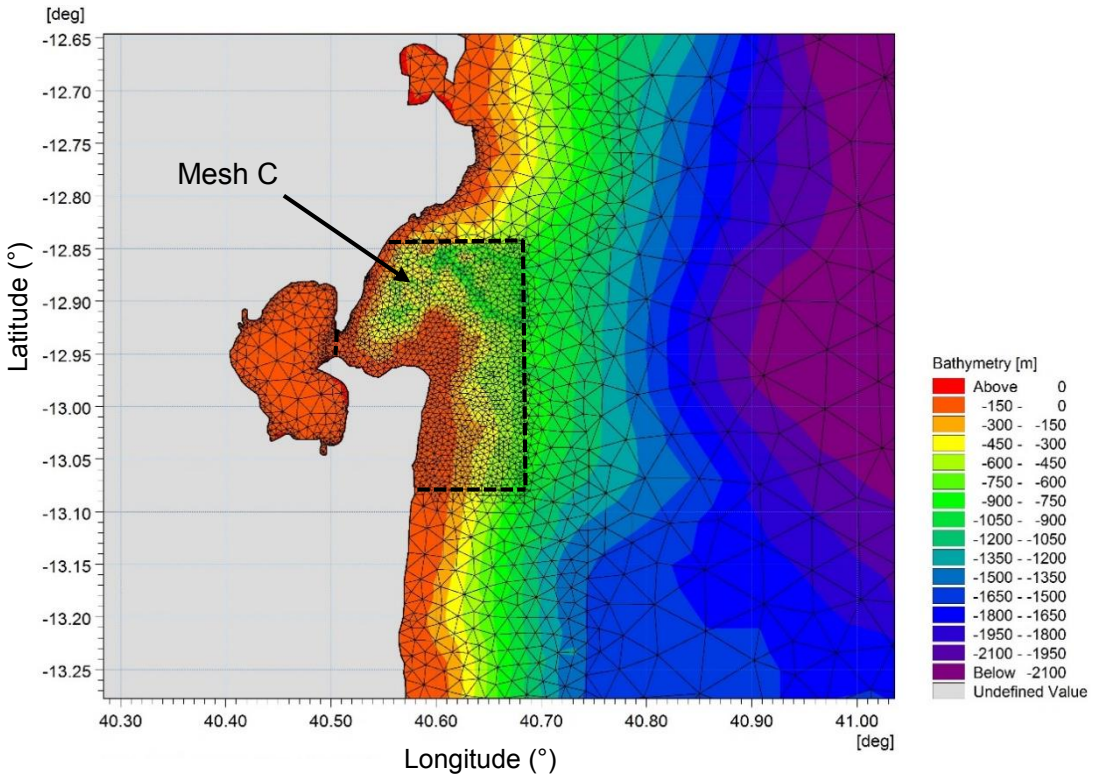

Figure 4.10: Mesh C for Pemba sensitivity tests

4.2.2. Tropical Cyclone Wind Field

The cyclone wind generation tool of Mike 21 was used to generate the wind field of the tropical cyclone in the numerical models. The tool applies a parametric wind field model to compute wind and pressure data produced by the storm. The Young and Sobey (1981) parametric model (refer to Section 2.3.1) was used to generate the tropical cyclone's wind field. The Young and Sobey (1981) model was chosen over the Holland (1980) model due to the simplicity of the input parameters required. As a result, more emphasis was placed on the wind speed estimates produced by Fearon (2014). Although the Young and Sobey (1981) model is simplistic, it is still relevant today.

Several wind corrections (refer to Sections 2.3.1.1 – 2.3.1.3) were applied in the model. No geostrophic wind correction was applied. The forward motion asymmetry of the tropical cyclone was taken into account by specifying δ_{fm} = 0.5 and the angle to maximum wind speed (θ_{max}) was specified as 65°. Inflow angle was specified in the model using the equations proposed by Sobey et al. (1977). The wind field was generated on a 500 x 500 grid.

4.2.3. Hydrodynamic Module

This section provides the technical components of the numerical model parameters used in the tests, for the hydrodynamic module. The purpose is therefore to provide the reader with these values to evaluate the model set-up, and as a reference for future modelling. For this reason, definitions of these parameters are not discussed here. The reader is referred to the hydrodynamic module of the Mike 21 Flow Model FM user guide for these definitions (DHI, 2014b).

Using the hydrodynamic module, the water surface elevation was modelled for each simulation. The shallow water equations were solved using a time integration and space discretization of low-order fast algorithm, with a critical Courant–Friedrichs–Levy (CFL) number of 0.8. The time step was specified as a minimum of 0.01 seconds and a maximum of 300 seconds. The transport equations were also solved using a minimum time step of 0.01 seconds and a maximum of 300 seconds, with a critical CFL number of 0.8. Depth correction, ice coverage, precipitation, evaporation and wave radiation were not included in the simulations. Tides were also not included in order to account only for the tropical cyclone-induced storm surge and waves.

Flooding and drying was included in the simulations, where a respective drying, flooding and wetting depth of 0.005 m, 0.05 m, and 0.1 m was specified. A barotropic density as well as a varying Coriolis force was also simulated in the domain. A constant eddy viscosity of 0.28

was specified under the Smagorinsky formulation, with a minimum and maximum eddy viscosity of 1.8 x 10^{-6} m^2/s and 1 x 10^{10} m^2/s respectively. The bed resistance was specified using a constant Manning number of 32 $m^{1/3}/s$.

A varying wind in time and domain was specified where the tropical cyclone wind field, as discussed in Section 4.2.2, was used as input. A varying wind friction was specified using a drag coefficient between 0.001255 and 0.002425. A neutral pressure of 1013 hPa with a soft start interval of 3600 seconds was used. The initial conditions consisted of a constant 0 m surface elevation as well as a constant velocity of 0 m/s. The model boundaries were considered closed.

4.2.4. Spectral Wave Module

This section provides the technical components of the numerical model parameters used in the tests, for the spectral wave module. As with the hydrodynamic module, definitions of these parameters are not discussed here. The reader is referred to the spectral wave module of the Mike 21 SW FM user guide for these definitions (DHI, 2014c).

Using the spectral wave module, the significant wave height (H_s), peak wave period (T_p) and mean wave direction (θ) were modelled for each simulation. The fully spectral and instationary time formulation was used in the simulations. A logarithmic spectral discretization was specified with 26 frequencies using a minimum frequency of 0.04 Hz (25 s period) and a frequency factor of 1.1. A wide range of frequencies were used to simulate the generation of the wind-waves. A directional discretization using a 360 degree rose was used with 36 directions required for the wider directional distribution of the energy of the wind-waves. There was no separation of wind sea and swell. A low order, fast algorithm solution technique was specified with a minimum and maximum time step of 0.01 seconds and 600 seconds respectively. The maximum number of levels in the transport calculation was set to 32 and the number of steps in the source calculation was specified as 1.

The water level and current conditions were set to vary according to the output of the hydrodynamic simulations. A varying wind in time and domain was specified where the tropical cyclone wind field, as discussed in Section 4.2.2, was used as input. A soft start interval of 3600 seconds was used. A coupled air-sea interaction was specified using a background Charnock parameter of 0.01. Ice coverage and diffraction were not included in the simulations.

The energy transfer includes quadruplet-wave interaction and the wave breaking was specified using a constant gamma value of 0.8 and alpha value of 1. Bottom friction was simulated using a constant Nikuradse roughness of 0.04 m and current friction was set to zero.

Constant values for white capping were used with C_{dis} and Δ_{dis} dissipation coefficients equal to 2.1 and 0.6 respectively. The power for the mean angular frequency and mean wave number was set to 1. The initial conditions were specified as spectra from the JONSWAP fetch growth expression, using a peakness parameter of 3.3 and σ_a= 0.07 and σ_b= 0.09. The wave conditions were specified using a maximum fetch length of 100 km, a maximum peak frequency of 0.4 Hz and a maximum Phillips constant of 0.0081. All model boundaries were considered closed, therefore no waves enter the model domain through the boundary and the outgoing waves were fully absorbed.

4.3. Test Procedures

A total of 11 tests were conducted at a constant Mean Sea Level. The 11 tests were selected with the intention to simulate 3 values of each of the input parameters being investigated. The results of these tests are significant wave heights and storm surge levels. For each simulation, 46 output locations for wave heights and 45 output locations for storm surge were specified in the model. The wave heights were collected at a depth of 20 m and the storm surge at a 10 m depth. These depths were chosen in order to determine estimates before certain coastal features and processes such as refraction and diffraction, have a major influence on the results. The 46 wave output locations were specified in 0.05° latitude intervals ranging from -12.45° to -14.6° (refer to Figure 4.9). The 45 storm surge output locations were specified in 0.005° latitude intervals ranging from -12.870° to -13.075° (refer to Figure 4.10).

For each of the 11 simulations, the maximum significant wave height and maximum storm surge at each of the respective 46 and 45 output points were computed. The largest of these values was taken as the maximum significant wave height and storm surge level of the simulation. Since the largest waves occur south of the storm centre, it was assumed that these waves could be experienced further north at Pemba, since the tropical cyclone can make landfall further north, and was consequently taken as the design wave height. It was also assumed that all the tropical cyclones make landfall at Pemba with co-ordinates of 40.584° E and 12.967°S.

Table 4.6 presents a summary of the different simulations. Simulation 2 served as the baseline test to which the other simulations were compared.

Table 4.6: Summary of sensitivity tests

	V_{max} = 29 m/s and P_c = 982 hPa				
Simulation	R_{max} (km)	Forward Speed (m/s)	Track Direction (°)	Sinuosity (-)	Duration (hours)
1	13	4	263	1	18
2	31	4	263	1	18
3	109	4	263	1	18
4	31	1	263	1	18
5	31	9	263	1	18
6	31	4	194	1	18
7	31	4	332	1	18
8	31	4	263	1.76	18
9	31	4	263	3.51	18
10	31	4	263	1	30
11	31	4	263	1	42

4.4. Results of Sensitivity Tests

The sensitivity results of each design storm parameter is presented in the following sections. The storm surge and significant wave height of each simulation is compared to the baseline test (Simulation 2). The design storm parameters were chosen based on mean values. It was decided that choosing the worst-case scenario for each parameter would lead to an overly conservative design storm.

4.4.1. Radius to Maximum Wind Speeds

The results of the tests for sensitivity of R_{max} are presented in Table 4.7. S_{100} is the maximum storm surge expected to occur over a period of 100 years. Similarly, $H_{s,100}$ is the maximum significant wave height expected to occur over a period of 100 years. The percentage change column is the increase/decrease compared to the baseline test (Simulation 2).

Table 4.7: R_{max} sensitivity test results

Simulation	R_{max} (km)	S_{100} (m)	S_{100} Change (%)	$H_{s,100}$ (m)	$H_{s,100}$ Change (%)
1	13	0.309	5.73	8.01	-7.93
2	31	0.292	-	8.70	-
3	109	0.263	-9.97	10.22	17.38

From Table 4.7, it is evident that the storm surge significantly decreases with increasing R_{max} values. The opposite is observed for the waves, where a larger wave height is produced with

increasing values of $R_{max.}$ The median R_{max} value of 31 km was therefore used in the proposed tests.

From the results, it became apparent that the largest waves occurred at a distance approximately equal to the R_{max} value, south of the point of tropical cyclone landfall. This is illustrated in Figure 4.11, where the R_{max} value is 109 km for Simulation 3.

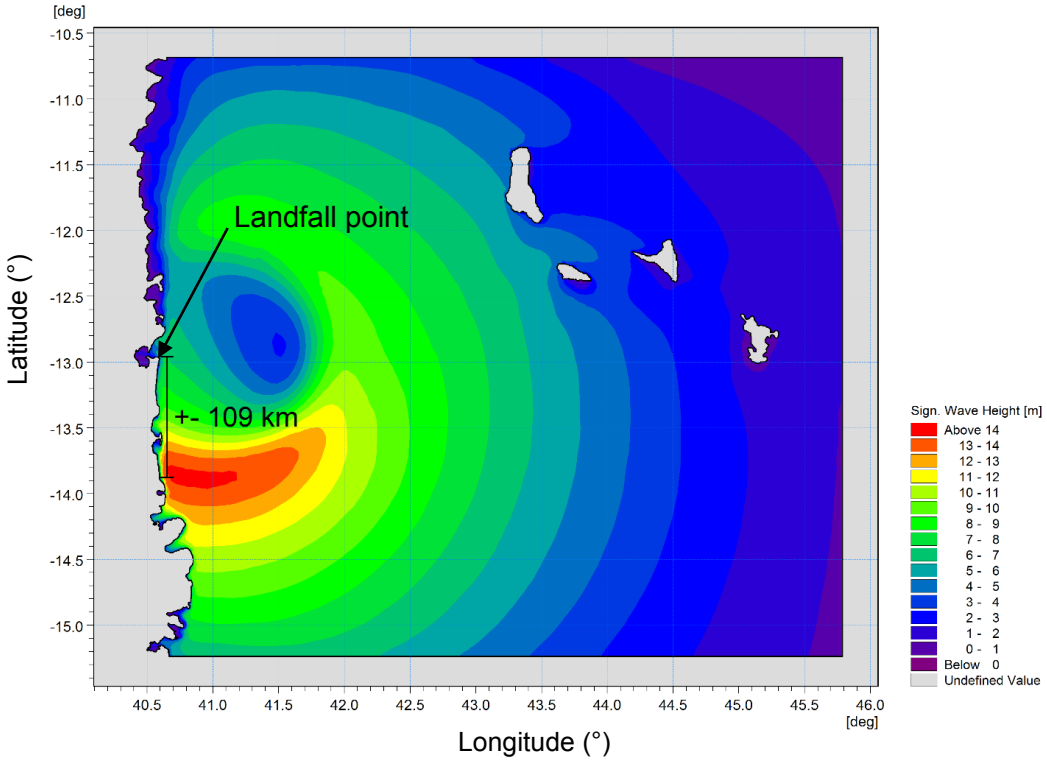

Figure 4.11: Map of Significant wave height for Simulation 3

Figure 4.12 further verifies this occurrence. Significant wave heights are plotted at all 46 points along the coastline, at distances from the point where the tropical cyclone made landfall. Negative values represent distances south of the point of landfall and positive values indicate northwards distances from the landfall point. The dashed line represents the line of latitude where landfall occurs. From Figure 4.12, it is evident that the largest H_s value is observed at approximately 109 km south of the landfall point, which is also the R_{max} value.

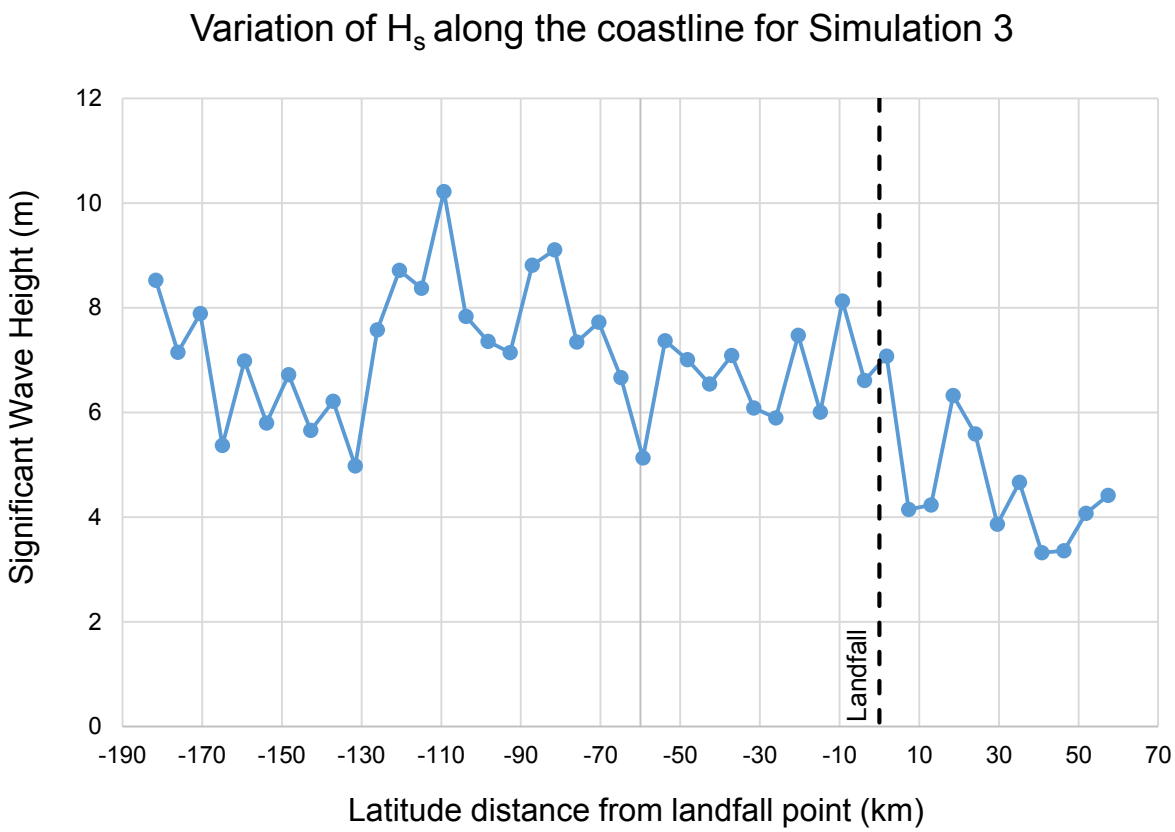

Figure 4.12: Variation of H_s along the coastline for Simulation 3

4.4.2. Forward Speed

The results of the tests for sensitivity of tropical cyclone forward speed (c) are presented in Table 4.8.

Table 4.8: Forward speed sensitivity test results

Simulation	c (m/s)	S_{100} (m)	S_{100} Change (%)	$H_{s,100}$ (m)	$H_{s,100}$ Change (%)
4	1	0.306	4.548	7.310	-16.017
2	4	0.292	-	8.704	-
5	9	0.317	8.437	9.633	10.679

The results in terms of the storm surge are inconclusive. However, from the findings of Harper et al. (2001), storm surge generally tends to increase with increasing forward speed. The results of the waves increase significantly with an increase in the forward speed. Based on these findings, a median forward speed of 4 m/s was used in the proposed tests.

4.4.3. Track Direction

The results of the tests for sensitivity of tropical cyclone track direction (δ) are presented in Table 4.9.

Table 4.9: Track direction sensitivity test results

Simulation	δ (°)	S_{100} (m)	S_{100} Change (%)	$H_{s,100}$ (m)	$H_{s,100}$ Change (%)
6	194	0.298	1.981	9.417	8.195
2	263	0.292	-	8.704	-
7	332	0.294	0.643	7.656	-12.039

The storm surge does not appear to be greatly affected by the track direction. The biggest change in storm surge is 1.98% which is small. There is a strong relationship between the track direction and waves. Storms approaching Pemba from a more northerly direction tend to produce larger waves. Keeping in mind that choosing the worst-case scenario ($\delta = 194°$), which could happen, would lead to an overly conservative design storm if all the other input parameters were chosen based on the worst-case-scenario, a mean track direction of 263° was used for the proposed tests.

4.4.4. Sinuosity

The results of the tests for sensitivity of tropical cyclone track sinuosity are presented in Table 4.10.

Table 4.10: Sinuosity sensitivity test results

Simulation	Sinuosity (-)	S_{100} (m)	S_{100} Change (%)	$H_{s,100}$ (m)	$H_{s,100}$ Change (%)
2	1	0.292	-	8.704	-
8	1.76	0.304	3.967	7.965	-8.489
9	3.51	0.302	3.399	8.379	-3.731

From Table 4.10, it is evident that the sinuosity mostly does not have a large impact on the storm surge or waves. In comparison to Simulation 2, the storm surge increased with more curved trajectories. The opposite is observed for the waves where wave heights decreased with more curved trajectories. As a result, a sinuosity of 1 will be used for the proposed tests.

4.4.5. Duration

The results of the tests for sensitivity of tropical cyclone duration are presented in Table 4.11.

Table 4.11: Duration sensitivity test results

Simulation	Duration (hr)	S_{100} (m)	S_{100} Change (%)	$H_{s,100}$ (m)	$H_{s,100}$ Change (%)
2	18	0.292	-	8.704	-
10	30	0.304	4.042	8.695	-0.103
11	42	0.305	4.140	8.682	-0.247

The storm surge in Simulations 10 and 11 increases by approximately 4% which is small, but significant. There is no change in storm surge after 30 hours. As for the waves, there is no significant change for both simulations. A possible reason for this could be that a fully developed sea state was achieved in the simulations, and the waves became self-limited due to white-capping. Since there is a change in storm surge between durations 18 and 30 hours, a duration of 30 hours is used in the proposed tests.

4.4.6. Summary of Results

A summary of the design storm parameters for input into the proposed model tests, as described in Section 5, is presented in Table 4.12.

Table 4.12: Input values for the proposed model tests.

Parameter	Value	Unit
Radius to maximum wind speed (R_{max})	31	km
Forward speed (c)	4	m/s
Track direction (δ)	263	°
Sinuosity	1	(-)
Cyclone Duration	30	hours

The parameters in Table 4.12 are to be used as input for the proposed numerical model tests along the Southern African East Coast. These parameters remain constant throughout the simulations, and are applied at all four locations along the coast. However, the wind speeds and pressures change based on the simulated return period. These parameters are some the required input parameters for the cyclone wind generation tool used in the model tests.

5. Numerical Model Tests

In order to determine the expected estimates of tropical cyclone-induced waves and storm surge along the Southern African East Coast, detailed numerical modelling was required at the proposed locations. Four locations have been investigated, namely; Durban, Maputo, Beira and Pemba. The following sections describe the numerical model tests used to obtain the wave and storm surge estimates.

5.1. Model Set-up

5.1.1. Mesh and Bathymetry

The bathymetry used for all four model domains consisted of two data sets. For the deeper water, the GEBCO (2014) grid was used. The GEBCO (2014) grid is a 30 arc-second (roughly 900 m) global grid of elevations, produced by using quality-controlled ship depth soundings with interpolation between sounding points, guided by satellite-derived gravity data.

For the shallower water, the bathymetry was produced by digitizing seabed depths from admiralty charts. The charts were purchased from the United Kingdom Hydrographic Office (UKHO). The mesh and bathymetry of the four model domains are discussed in the following sections.

5.1.1.1. Durban

The SAN 131, 132 and 135 admiralty charts were used to construct the bathymetry surrounding Durban. Durban's model domain and bathymetry is presented in Figure 5.1. The mesh consists of three sections, all flexible meshes with triangular elements, as shown in Figure 5.2. Mesh A is a coarse mesh with a grid resolution of 2 km while Mesh B has a finer grid resolution of 500 m. A very fine mesh is located at Mesh C, where the grid resolution is 100 m. Mesh B is used to capture the maximum tropical cyclone-induced waves and storm surge along the coast, while Mesh C captures the immediate area surrounding Durban.

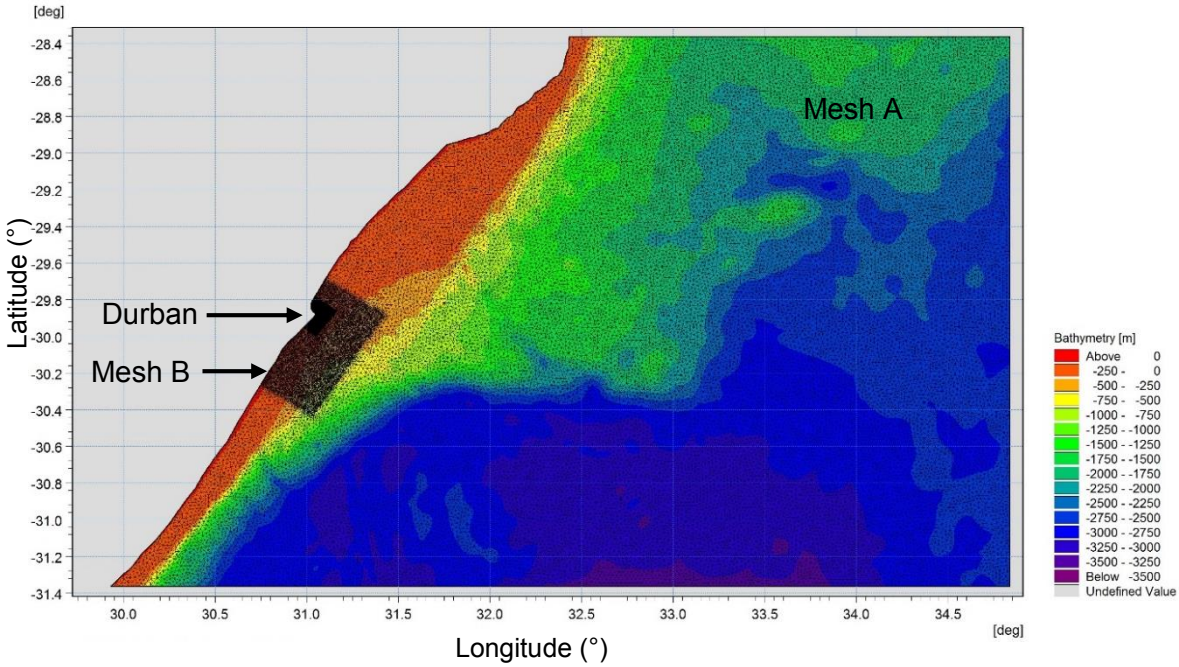

Figure 5.1: Mesh and bathymetry of Durban's model domain

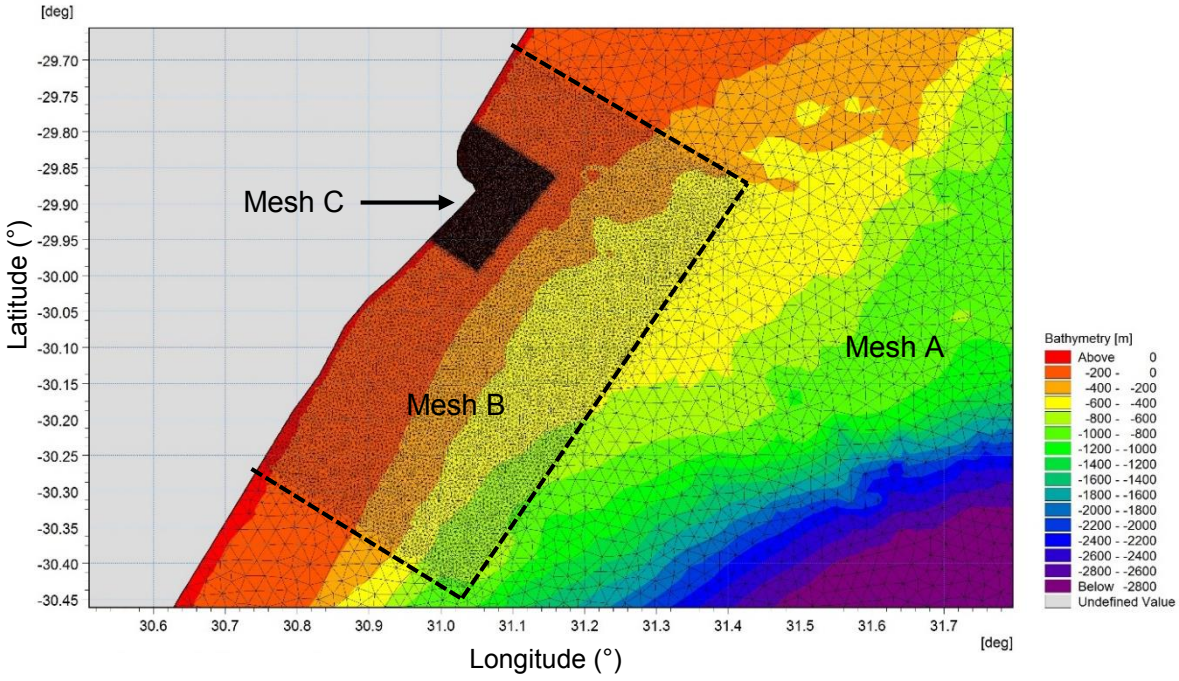

Figure 5.2: Meshes A, B and C of Durban's model domain

5.1.1.2. Maputo

The SAN 61 and UKHO 644 admiralty charts were used to construct the bathymetry surrounding Maputo. Maputo's model domain and bathymetry is presented in Figure 5.3. The mesh consists of two sections, both flexible meshes with triangular elements. Mesh A is a coarse mesh with a grid resolution of 2 km while Mesh B has a finer grid resolution of 200 m. A third mesh was not necessary as Maputo has a much broader (shallower) continental shelf compared to Durban and Pemba, and therefore could be resolved in Mesh B.

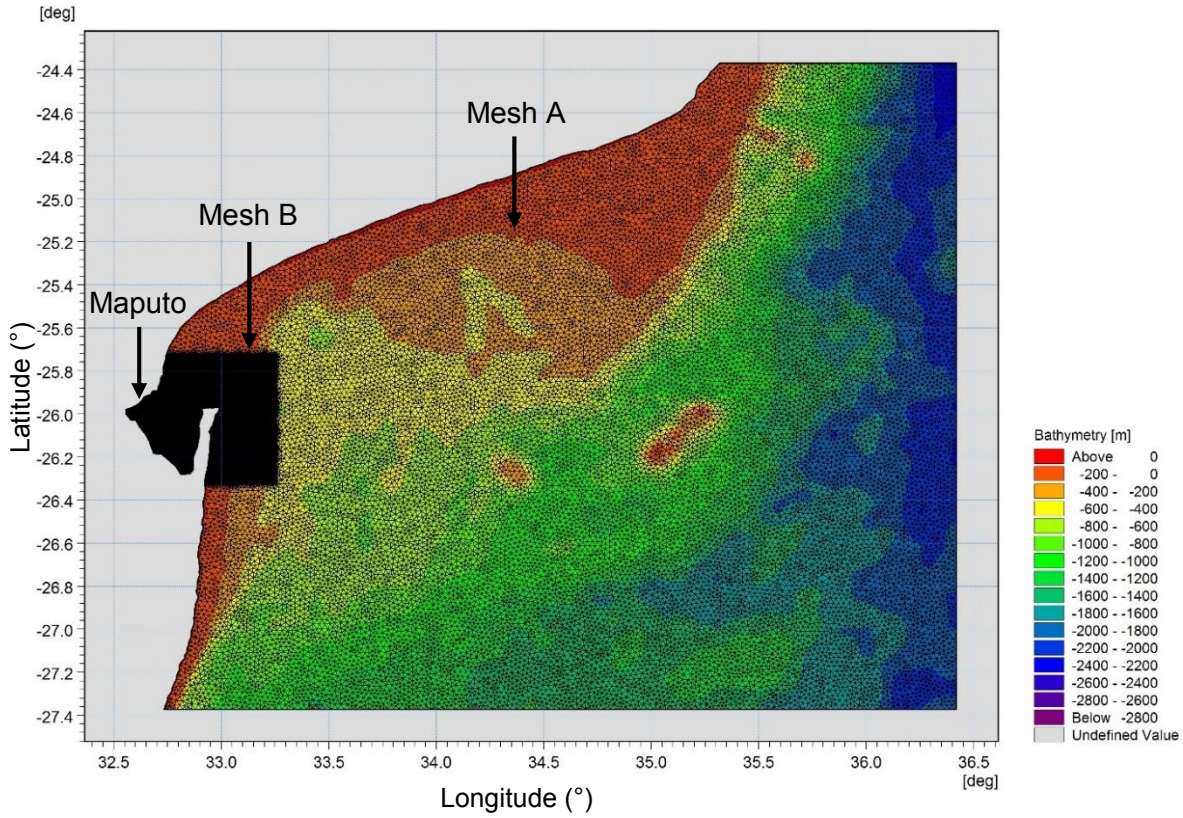

Figure 5.3: Mesh and bathymetry of Maputo's model domain

5.1.1.3. Beira

The UKHO 2932 admiralty chart was used to construct the bathymetry surrounding Beira. Beira's model domain and bathymetry is presented in Figure 5.4. The mesh consists of two sections, both flexible meshes with triangular elements. Mesh A is a coarse mesh with a grid resolution of 2 km while Mesh B has a finer grid resolution of 200 m. A third mesh was not necessary as Beira has a much broader (shallower) continental shelf compared to Durban and Pemba, and therefore could be resolved in Mesh B.

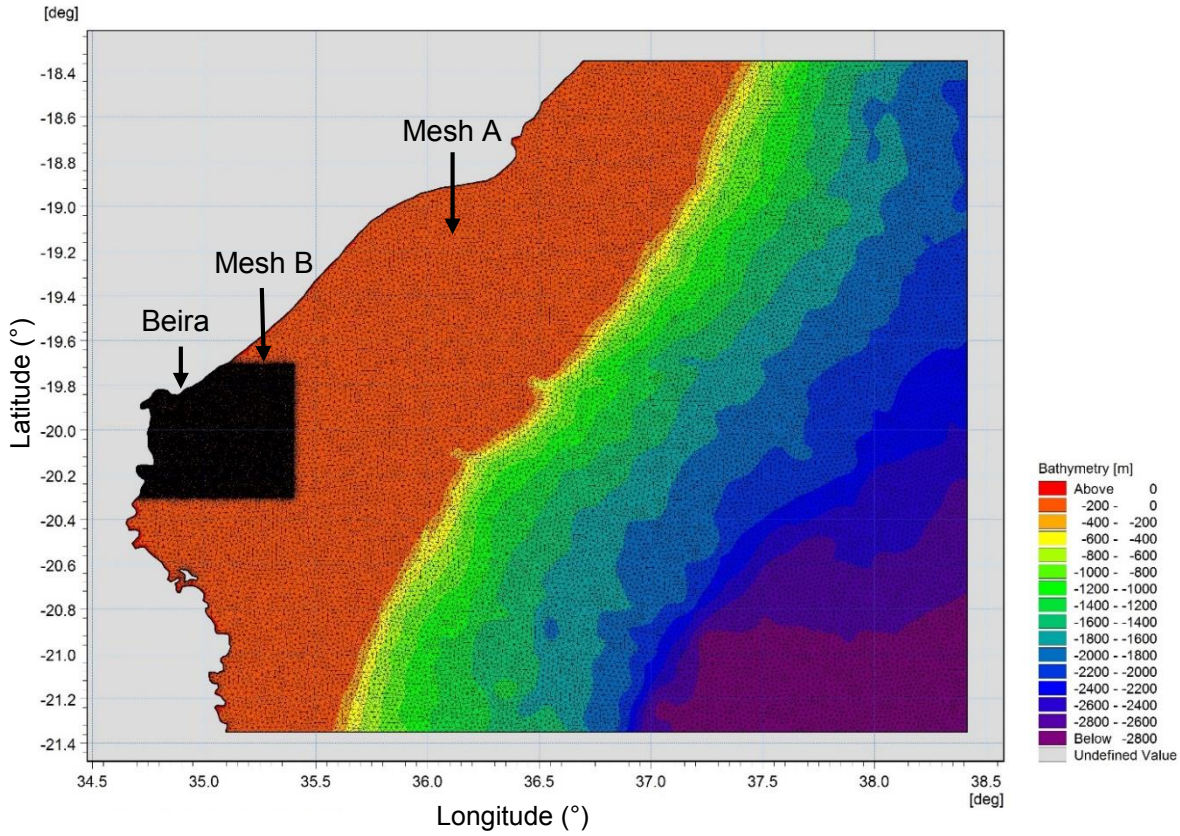

Figure 5.4: Mesh and bathymetry of Beira's model domain

5.1.1.4. Pemba

The UKHO 647 and 2926 admiralty charts were used to construct the bathymetry surrounding Pemba. Pemba's model domain and bathymetry is presented in Figure 5.5. The mesh consists of three sections, all flexible meshes with triangular elements, as shown in Figure 5.6. Mesh A is a coarse mesh with a grid resolution of 2 km while Mesh B has a finer grid resolution of 500 m. A very fine mesh is located at Mesh C, where the grid resolution is 100 m. Mesh B is used to capture the maximum tropical cyclone-induced waves and storm surge along the coast, while mesh C captures the area surrounding Pemba. The bay inside Pemba was not taken into consideration as this study is more focused on the open water conditions before refraction and other processes occur.

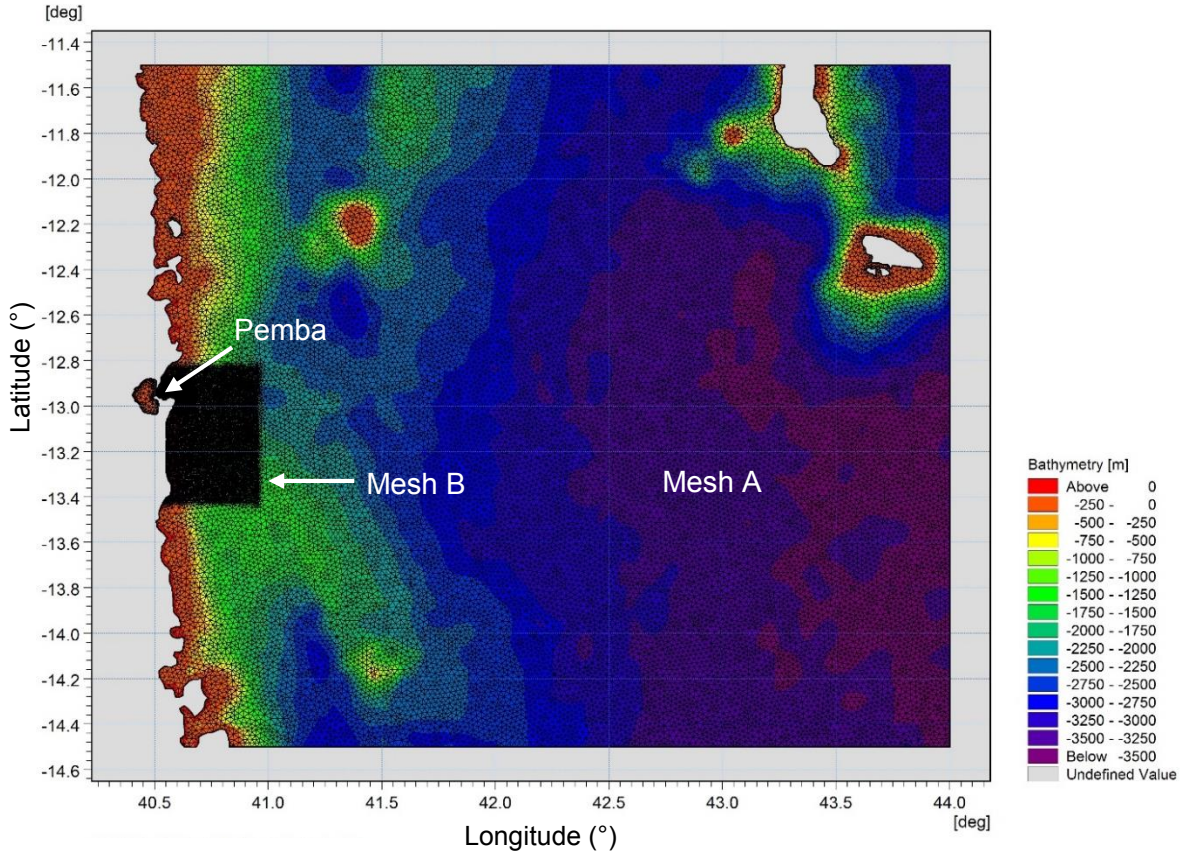

Figure 5.5: Mesh and bathymetry of Pemba's model domain

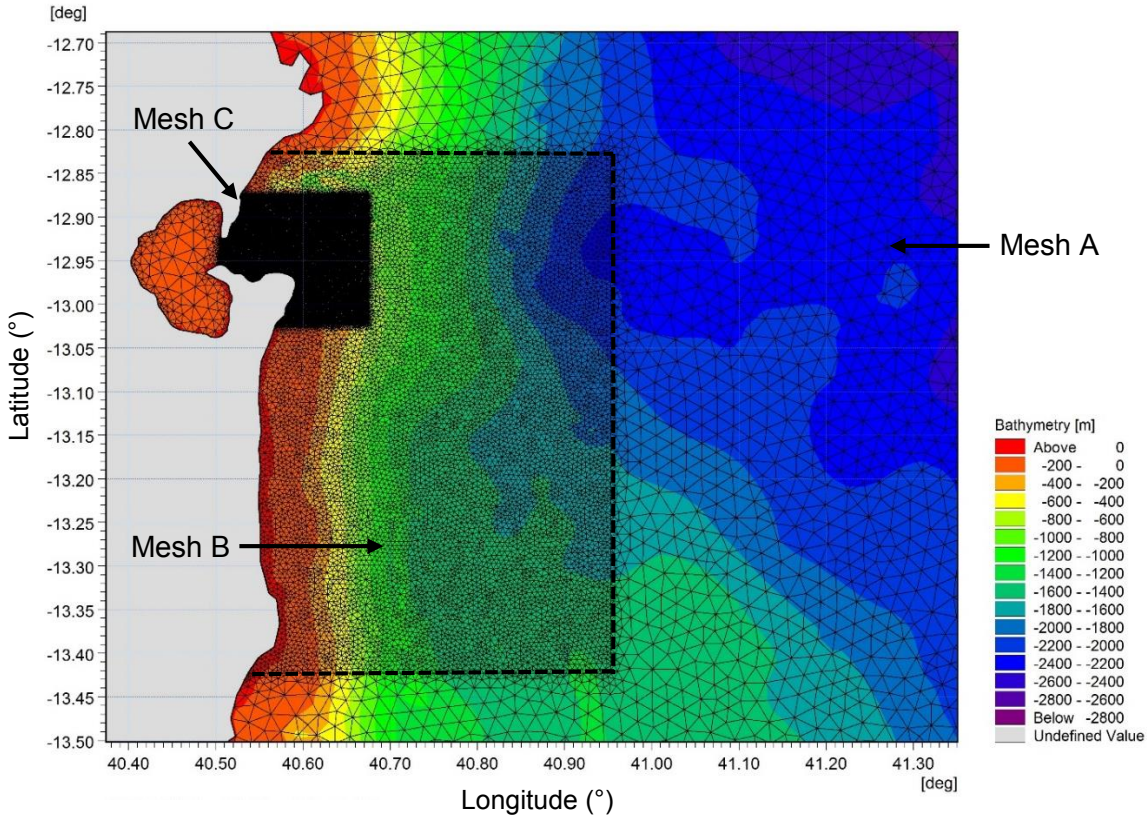

Figure 5.6: Meshes A, B and C of Pemba's model domain

5.1.2. Tropical Cyclone Wind Field

The cyclone wind generation tool of Mike 21 was used to generate the wind field of the tropical cyclone in the numerical models. The tool applies a parametric wind field model to compute wind and pressure data produced by the storm. The Young and Sobey (1981) parametric model (refer to Section 2.3.1) was used to generate the tropical cyclone's wind field. Input into the model consists of several parameters which are discussed in Section 5.2.

Several wind corrections (refer to Sections 2.3.1.1 – 2.3.1.3) were applied in the model. To convert the gradient-level winds produced by the parametric model, to surface winds (10 m elevation), a constant boundary layer wind speed correction (K_m = 0.8) was applied. The forward motion asymmetry of the tropical cyclone was taken into account by subtracting half (δ_{fm} = 0.5) of the cyclone forward speed from the V_{max} data of each simulation. The angle to maximum wind speed (θ_{max}) was specified as 115°, based on recommendations provided by Mike 21. In the Southern Hemisphere, θ_{max} is commonly taken as 115° (DHI, 2014d). Inflow angle was specified in the model using the equations proposed by Sobey et al. (1977). The wind field was generated on a 500 x 500 grid.

5.1.3. Hydrodynamic Module

Using the hydrodynamic module, the water surface elevation was modelled for each simulation. The shallow water equations were solved using a time integration and space discretization of low-order fast algorithm, with a critical Courant–Friedrichs–Levy (CFL) number of 0.8. The time step was specified as a minimum of 0.01 seconds and a maximum of 600 seconds. The transport equations were also solved using a minimum time step of 0.01 seconds and a maximum of 600 seconds, with a critical CFL number of 0.8. Depth correction, ice coverage, precipitation, evaporation and wave radiation were not included in the simulations. Tides were also not included in order to only account for the tropical cyclone-induced storm surge and waves.

Flooding and drying was included in the simulations, where a respective drying, flooding and wetting depth of 0.005 m, 0.05 m, and 0.1 m was specified. A barotropic density as well as a varying Coriolis force was also simulated in the domain. A constant eddy viscosity of 0.28 was specified under the Smagorinsky formulation, with a minimum and maximum eddy viscosity of 1.8 x 10^{-6} m^2/s and 1 x 10^{10} m^2/s respectively. The bed resistance was specified using a constant Manning number of 55 $m^{1/3}/s$, constant for all areas. This value was obtained from the results of the calibration tests in Section 6.2.

A varying wind in time and domain was specified where the tropical cyclone wind field, as discussed in Section 5.1.2, was used as input. A constant wind friction was specified using a drag coefficient of 0.0034. A neutral pressure of 1013 hPa with a soft start interval of 3600 seconds was used. The initial conditions consist of a constant 0 m surface elevation as well as a constant velocity of 0 m/s. The model boundaries were considered closed.

5.1.4. Spectral Wave Module

Using the spectral wave module, the significant wave height (H_s), peak wave period (T_p) and mean wave direction (θ) were modelled for each simulation. The fully spectral and instationary time formulation was used in the simulations. A logarithmic spectral discretization was specified with 26 frequencies using a minimum frequency of 0.04 Hz and a frequency factor of 1.1. A directional discretization using a 360 degree rose was used with 36 directions. There was no separation of wind sea and swell. A low order, fast algorithm solution technique was specified with a minimum and maximum time step of 0.01 seconds and 600 seconds respectively. The maximum number of levels in the transport calculation was set to 32 and the number of steps in the source calculation was specified as 1.

The water level and current conditions were set to vary according to the output of the hydrodynamic simulations. A varying wind in time and domain was specified where the tropical cyclone wind field, as discussed in Section 5.1.2, was used as input. A soft start interval of 3600 seconds was used. A coupled air-sea interaction was specified using a background Charnock parameter of 0.01. Ice coverage and diffraction were not included in the simulations.

The energy transfer included quadruplet-wave interaction and the wave breaking was specified using a constant gamma value of 0.8 and alpha value of 1. Bottom friction was simulated using a constant Nikuradse roughness of 0.06 m and current friction was set to zero. Constant values for white capping were used with C_{dis} and Δ_{dis} dissipation coefficients equal to 4 and 0.3 respectively. The power for the mean angular frequency and mean wave number was set to -1. The initial conditions were specified as spectra from the JONSWAP fetch growth expression, using a peakness parameter of 3.3 and σ_a= 0.07 and σ_b= 0.09. The wave conditions were specified using a maximum fetch length of 100 km, a maximum peak frequency of 0.4 Hz and a maximum Phillips constant of 0.0081. All model boundaries were considered closed, therefore no waves entered the model domain through this boundary and the outgoing waves are fully absorbed.

5.2. Test Procedures

5.2.1. General

At each of the four locations, namely; Durban, Maputo, Beira and Pemba, the 50-, 100-, 200- and 500-year tropical cyclone wind speeds were simulated (see Figure 2.16). A total of 16 simulations were therefore conducted. The simulation time, obtained from the sensitivity test results, was 30 hours. This consisted of 180 time steps with a 600 second time step interval. The tests simulated the tropical cyclone moving towards land over a period of 24 hours and then continued for another 6 hours after landfall. In the tests, it was assumed that all the tropical cyclones made direct landfall at the location of interest. All the tests were simulated on a constant Mean Sea Level (MSL). The MSL was computed as the average between the Mean Low Water Springs (MLWS) and Mean High Water Springs (MHWS) tide level.

A summary of the input parameters to the proposed model tests (determined from the sensitivity test results) are presented in Table 5.1. The wind (V_{max}) and pressure (P_c) values were different for each simulation, although the other parameters remained constant. The V_{max} values from Figure 2.16 were converted to the 1-hour average winds for input into the simulations. Only one direction is modelled to estimate the extreme wave conditions, which is not ideal, but care has been taken (see Section 4.1.3) to decide on a direction that produces both extreme waves and storm surge levels.

Table 5.1: Input values for the model tests.

Parameter	Value	Unit
Maximum sustained 1-min average wind speed (V_{max})	From Figure 2.16	m/s
Minimum central pressure (P_c)	From Figure 2.12	hPa
Radius to maximum wind speed (R_{max})	31	km
Forward speed (c)	4	m/s
Track direction (δ)	263	°
Sinuosity	1	(-)
Cyclone Duration	30	hours

The results of the tests are estimates of the expected significant wave height and storm surge levels. For each simulation, estimates of these parameters were specified along the 10 m depth contour for storm surge and the 20 m depth contour for the waves. These output points were specified in 0.005° latitude intervals. Two areas were investigated along the coast. The first was the immediate area surrounding the four proposed locations, and the second was the area where the maximum waves and storm surge could be expected to occur along the coast.

For each area, the maximum significant wave height and maximum storm surge at each of the specified points was computed. The largest of these values was taken as the maximum significant wave height and storm surge level of that area. Since the largest waves occur south of the storm centre, it was assumed that these waves could be experienced at the proposed location if the tropical cyclone made landfall further north, and was consequently taken as the design wave height. In the following sections, the input parameters are presented for each location.

5.2.2. Durban

Durban's simulated water level (MSL) is presented in Table 5.2. Chart Datum for Durban is 3.703 m below Benchmark.

Table 5.2: Tidal levels for Durban model simulations

Heights in metres above datum		
MHWS (m)	MLWS (m)	Calculated MSL (m)
1.83	0.03	0.93

As explained in Section 5.1.2, the forward motion asymmetry of the tropical cyclone is taken into account by subtracting half (δ_{fm} = 0.5) of the cyclone forward speed from the V_{max} data of each simulation. Table 5.3 presents the calculation of the 1-hour V_{max} values used in the model simulations. The 1-min V_{max} values are determined from Figure 2.16.

Table 5.3: Calculation of V_{max} values for the Durban model simulations (based on Figure 2.16)

Return Period	1-min V_{max} (m/s)	1-hr V_{max} (m/s)	Forward Speed (m/s)	Model V_{max} (m/s)
50	12	9.647	4	**7.647**
100	18.5	14.873	4	**12.873**
200	22.5	18.089	4	**16.089**
500	28	22.511	4	**20.511**

An example of the input into the cyclone wind generation tool for the 50-year simulation at Durban is shown in Table 5.4. The 100-, 200- and 500-year simulation wind field input for Durban can be found in the respective Tables B-1, B-2 and B-3 in Appendix B.

Table 5.4: Durban's 50-year simulation wind field input

Time (hours)	Longitude (°)	Latitude (°)	R_{max} (km)	V_{max} (m/s)	P_c (hPa)	P_n (hPa)
0	34.5811	-29.4389	31	7.6474	1004	1013
24	31.0447	-29.8641	31	7.6474	1004	1013
30	30.1562	-29.9556	31	7.6474	1004	1013

Durban's output points range from a latitude of 29.705° S to 30.255° S with a total of 111 points for the significant wave height and 111 points for the storm surge. These points are illustrated in Figures C-1 and C-2 of Appendix C, for the respective waves and storm surge. The model coordinates of these points are presented in Table D-1 of Appendix D.

5.2.3. Maputo

Maputo's simulated water level (MSL) is presented in Table 5.5. Chart Datum for Maputo is Lowest Astronomical Tide (LAT).

Table 5.5: Tidal levels for Maputo model simulations

Heights in metres above datum		
MHWS (m)	MLWS (m)	Calculated MSL (m)
3.5	0.5	2

Table 5.6 presents the calculation of the 1-hour V_{max} values used in the Maputo model simulations.

Table 5.6: Calculation of V_{max} values for the Maputo model simulations (based on Figure 2.16)

Return Period	1-min V_{max} (m/s)	1-hr V_{max} (m/s)	Forward Speed (m/s)	Model V_{max} (m/s)
50	24.5	19.697	4	**17.697**
100	29	23.315	4	**21.315**
200	34	27.334	4	**25.334**
500	40	32.158	4	**30.158**

An example of the input into the cyclone wind generation tool for the 50-year simulation at Maputo is shown in Table 5.7. The 100-, 200- and 500-year simulation wind field input for Maputo can be found in the respective Tables B-4, B-5 and B-6 in Appendix B.

Table 5.7: Maputo's 50-year simulation wind field input

Time (hours)	Longitude (°)	Latitude (°)	R_{max} (km)	V_{max} (m/s)	P_c (hPa)	P_n (hPa)
0	36.1630	-25.4541	31	17.6968	987	1013
24	32.7517	-25.8721	31	17.6968	987	1013
30	31.8953	-25.9642	31	17.6968	987	1013

Maputo's output points range from a latitude of 25.74° S to 26.315° S with a total of 116 points for the significant wave height and 161 points for the storm surge. These points are illustrated in Figures C-3 and C-4 of Appendix C, for the respective waves and storm surge. The model coordinates of these points are presented in Table D-2 of Appendix D.

5.2.4. Beira

Beira's simulated water level (MSL) is presented in Table 5.8. Chart Datum for Beira is LAT.

Table 5.8: Tidal levels for Beira model simulations

Heights in metres above datum		
MHWS (m)	MLWS (m)	Calculated MSL (m)
6.5	0.9	3.7

Table 5.9 presents the calculation of the 1-hour V_{max} values used in the Beira model simulations.

Table 5.9: Calculation of V_{max} values for the Beira model simulations (based on Figure 2.16)

Return Period	1-min V_{max} (m/s)	1-hr V_{max} (m/s)	Forward Speed (m/s)	Model V_{max} (m/s)
50	32	25.726	4	**23.726**
100	37.5	30.148	4	**28.148**
200	44	35.374	4	**33.374**
500	48.5	38.992	4	**36.992**

An example of the input into the cyclone wind generation tool for the 50-year simulation at Beira is shown in Table 5.10. The 100-, 200- and 500-year simulation wind field input for Beira can be found in the respective Tables B-7, B-8 and B-9 in Appendix B.

Table 5.10: Beira's 50-year simulation wind field input

Time (hours)	Longitude (°)	Latitude (°)	R_{max} (km)	V_{max} (m/s)	P_c (hPa)	P_n (hPa)
0	38.1560	-19.4380	31	23.7265	977	1013
24	34.8905	-19.8497	31	23.7265	977	1013
30	34.0712	-19.9424	31	23.7265	977	1013

Beira's output points range from a latitude of 19.72° S to 20.29° S with a total of 113 points for the significant wave height and 115 points for the storm surge. These points are illustrated in Figures C-5 and C-6 of Appendix C, for the respective waves and storm surge. The model coordinates of these points are presented in Table D-3 of Appendix D.

5.2.5. Pemba

Pemba's simulated water level (MSL) is presented in Table 5.11. Chart Datum for Pemba is LAT.

Table 5.11: Tidal levels for Pemba model simulations

Heights in metres above datum		
MHWS (m)	MLWS (m)	Calculated MSL (m)
4.1	0.5	2.3

Table 5.12 presents the calculation of the 1-hour V_{max} values used in the Pemba model simulations.

Table 5.12: Calculation of V_{max} values for the Pemba model simulations (based on Figure 2.16)

Return Period	1-min V_{max} (m/s)	1-hr V_{max} (m/s)	Forward Speed (m/s)	Model V_{max} (m/s)
50	26.5	21.305	4	**19.305**
100	28.5	22.913	4	**20.913**
200	30	24.119	4	**22.119**
500	32.5	26.128	4	**24.128**

An example of the input into the cyclone wind generation tool for the 50-year simulation at Pemba is shown in Table 5.13. The 100-, 200- and 500-year simulation wind field input for Pemba can be found in the respective Tables B-10, B-11 and B-12 in Appendix B.

Table 5.13: Pemba's 50-year simulation wind field input

Time (hours)	Longitude (°)	Latitude (°)	R_{max} (km)	V_{max} (m/s)	P_c (hPa)	P_n (hPa)
0	43.7423	-12.5689	31	19.3047	985	1013
24	40.5848	-12.9666	31	19.3047	985	1013
36	39.0027	-13.1508	31	19.3047	985	1013

Pemba's output points range from a latitude of 12.85° S to 13.4° S with a total of 112 points for the significant wave height and 116 points for the storm surge. These points are illustrated in Figures C-7 and C-8 of Appendix C, for the respective waves and storm surge. The model coordinates of these points are presented in Table D-4 of Appendix D.

6. Model Calibration

6.1. Introduction

In order to validate that the proposed model provides reliable estimates of waves and storm surge, the model has to be calibrated. This is typically done by simulating a historical tropical cyclone event, and comparing the measured data, to the data produced by the model. It is always best to calibrate against a tropical cyclone that occurred in the area of investigation. Tropical Cyclone Lizette occurred off Beira in the Mozambique Channel in 1997, while two wave buoys were deployed in the water. These measurements would have been well suited for the calibration, but it was not possible to gain access to this data. Due to a lack of historically recorded tropical cyclone data in Mozambique, an alternative location had to be used. Hurricane Ike, which occurred in the Gulf of Mexico, was chosen because of its size, quantity and quality of wave and water level measurements taken during the storm.

Hurricane Ike was classified as a Category 4 major hurricane on the Saffir-Simpson Scale at its peak intensity, and is considered the third costliest Atlantic hurricane of all time after Hurricane Katrina and Sandy. Figures 6.1 and 6.2 provide a summary of the characteristics and movement of Ike's formation to termination. Hurricane Ike entered the Gulf of Mexico at 20:30 UTC (Coordinated Universal Time) on 9 September 2008 and tracked north-west making landfall near Galveston, Texas on 13 September 2008 at 07:00 UTC. 31 hours prior to landfall at Galveston, Ike experienced tropical storm force winds, extending 400 km from the storm centre. During this time, significant wave heights of over 8 m were experienced in the centre of the Gulf (Hope et al., 2013). Ike produced a maximum measured surge at landfall of 5.3 m in Chambers County, Texas (Hope et al., 2013).

The storm surge in Galveston Bay and surrounding regions was caused by a geostrophically driven surge forerunner paired with a shore-perpendicular wind-driven surge. Water levels increased to 2-2.5 m, 12 hours before Ike made landfall, while the wind direction was offshore. The time frame of the forerunner caused the surge to reach inland areas and penetrate connected bodies of water as well as low lying coastal flood plains. The forerunner spread as a free continental shelf wave from Galveston, Texas, southwards on the LATEX shelf with an amplitude of 1.5m. The continental shelf wave arrived at Corpus Christi, a town 300km south of Galveston, coinciding with Ike's landfall at Galveston. The forerunner continued to increase water levels within the Galveston Bay throughout the storm. The increase in water levels was mainly caused by a combination of the forerunner and the strong storm winds of Ike that resulted in the surge being further amplified in and around the Galveston Bay (Hope et al., 2013).

Hours Relative to Landfall	UTC Time	UTC Date (2008)	Latitude	Longitude	Max Wind Velocity (m/s)	Radius to Maximum Winds (km)	Minimum Central Pressure (mb)	Saffir-Simpson Category	Notes
−289	0600	1 Sep.	17.2	37	13	167	1006	Trop. Depression	Formation
−217	0600	4 Sep.	22.4	55.0	54	28	935	4	Maximum Intensity
−194.5	0430	5 Sep.	23.6	60.4	50	28	945	4	Enters SL18+TX33 Domain
−187	1200	5 Sep.	23.4	62.0	46	28	954	3	OWI winds start
−138	1300	7 Sep.	21.0	73.2	49		947	3	Landfall on Great Inagua Island, Bahamas
−124.75	0215	8 Sep.	21.1	75.7	50		945	4	Landfall in Holguin, Cuba
−89	1400	9 Sep.	22.6	82.9	30	-	965	1	Landfall in Pinar del Rio, Cuba
−82.5	2030	9 Sep.							Enters Gulf of Mexico
−31	0000	12 Sep.	26.1	90.0	37	148	954	2	
−19	1200	12 Sep.	26.9	92.2	39	93	954	2	Peak in South Plaquemines
−13	1800	12 Sep.	27.4	93.0	39	93	955	2	Shift in track, WSE peak in NOLA
−7	0000	13 Sep.	28.3	94.1	41	74	952	2	WSE peak in Lake Pontchartrain
0	0700	13 Sep.	29.3	94.7	41		950	2	Landfall at Galveston, Texas
5	1200	13 Sep.	30.3	95.2	37	56	959	1	
11	1800	13 Sep.	31.7	95.3	22	74	974	Trop. Storm	
23	0600	14 Sep.	35.5	93.7	15	93	986	Trop. Depression	OWI winds end
53	1200	15 Sep.							End of simulation

Figure 6.1: Summary of Hurricane Ike with 10-min average winds (Hope et al., 2013)

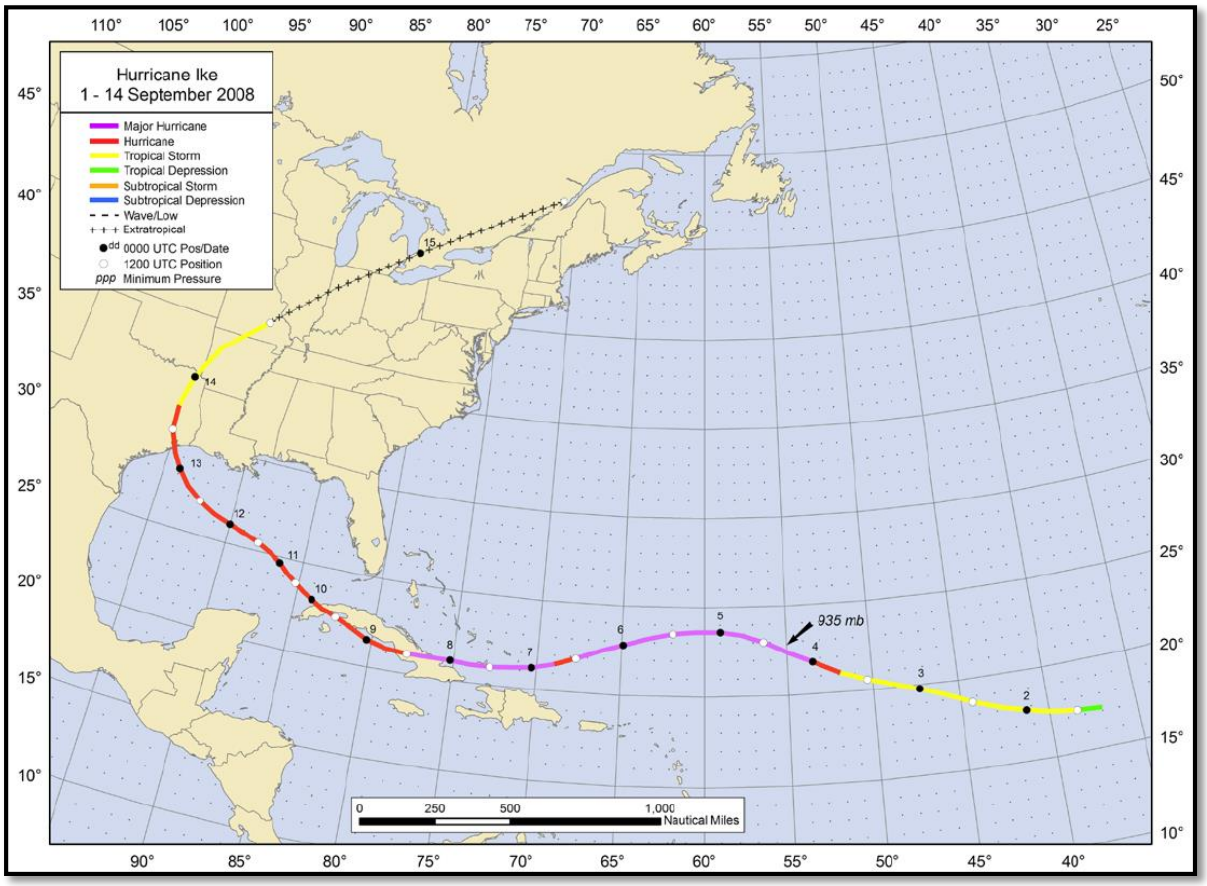

Figure 6.2: Movement of Hurricane Ike (Berg, 2009)

An extremely large quantity of water was pushed up against the coasts of Florida, Mississippi and Texas. A large amount of erosion occurred in the area surrounding Galveston Bay. The storm surge had washed out underneath the houses, exposing the pilings. This often led to the houses being swept away. Wind damage was also a big issue, where roofs were torn off houses.

6.2. Model Set-up

The MIKE 21/3 Coupled Model FM was used to simulate Hurricane Ike. The simulation period ran from 00:00 UTC on 9 September 2008 to 00:00 UTC on 15 September 2008. The hydrodynamic and spectral wave module used to simulate Hurricane Ike, is the same as the modules used in the proposed tests, as described in Section 5.1. The simulation was also run on a constant Mean Sea Level as in the proposed tests.

The calibration parameters used in the hydrodynamic module were the bed resistance and the wind friction. The model under-predicted the storm surge. The bed resistance was therefore lowered by increasing the Manning number to a constant value of 55 $m^{1/3}/s$, based on a Manning's roughness coefficient (n) of 0.018. The wind friction was also increased to produce larger storm surge (produced by increased wind set-up) by increasing the drag coefficient to a constant value of 0.0034.

For the spectral wave module, bottom friction and white capping values were used as calibration parameters. Initially, the model over-predicted the wave heights in shallow water. The bottom friction was therefore increased, by increasing the Nikuradse roughness height to a constant value of 0.06 m. In deeper water, wave heights were being under-predicted by the model. The C_{dis} dissipation coefficient was therefore reduced to 4 to produce larger waves. A Δ_{dis} dissipation coefficient of 0.3 was used to decrease the wave periods slightly.

6.2.1. Mesh and Bathymetry

The bathymetry used for the model domain consisted of two data sets. For the deeper water, the GEBCO (2014) grid was used. The GEBCO (2014) grid is a 30 arc-second (roughly 900 m) global grid of elevations, produced by using quality-controlled ship depth soundings with interpolation between sounding points, guided by satellite-derived gravity data.For the shallower water, the NGDC (2001) Coastal Relief Model (CRM) was used. The NGDC (2001) CRM is a 3 arc-second (roughly 90 m) grid spanning the northern coast of the Gulf of Mexico. Data sources for the CRM include: NGDC's NOS hydrographic surveys, trackline and multibeam bathymetry; the U.S. Geological Survey (USGS); and other federal government agencies and academic institutions. Bathymetric contours from the International Bathymetric

Chart of the Caribbean Sea and the Gulf of Mexico project were also used. The bathymetry for the model domain is shown in Figure 6.3.

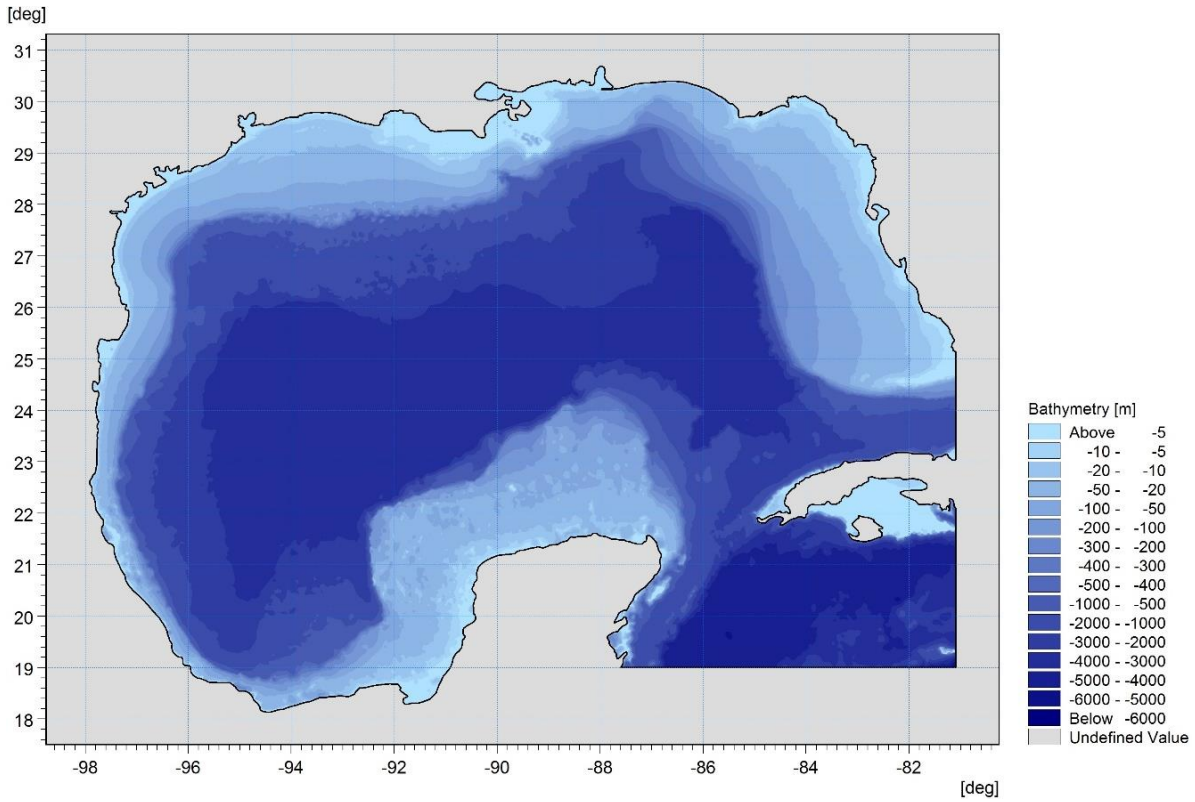

Figure 6.3: Bathymetry for the Gulf of Mexico model domain

The mesh consisted of three sections, all flexible meshes with triangular elements, as shown in Figure 6.4. Due to limitations of the computer, the mesh had to be a lot coarser than the required resolution. Mesh A has a grid resolution of 6 km while Mesh B has a grid resolution of 4 km. A finer mesh is located at Mesh C, where the grid resolution is 500 m.

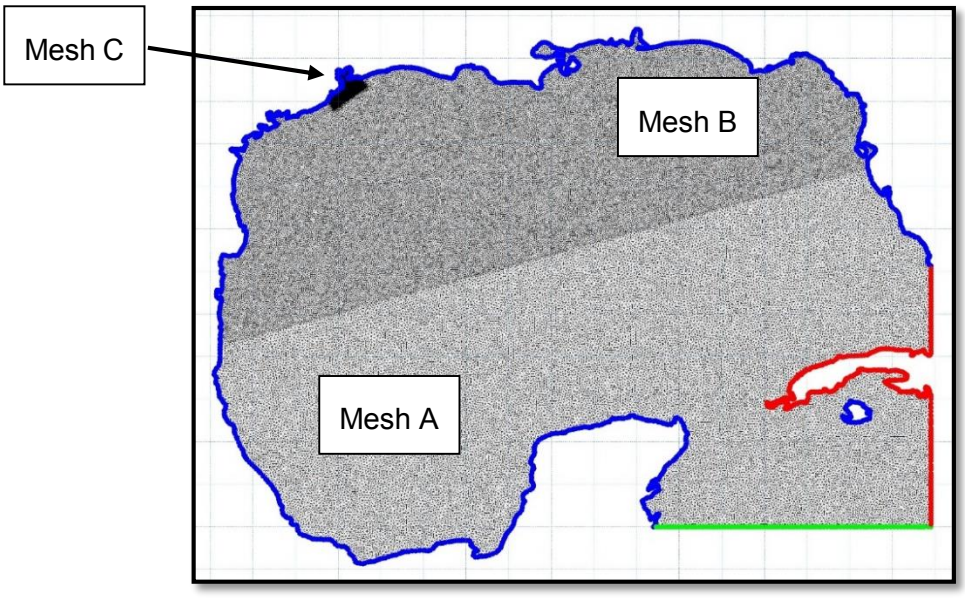

Figure 6.4: Mesh used for the Gulf of Mexico model domain

Mesh C covers a 95 km strech of coastline and extends 25 km offshore as shown in Figure 6.5. The mesh covers the Galveston Bay area.

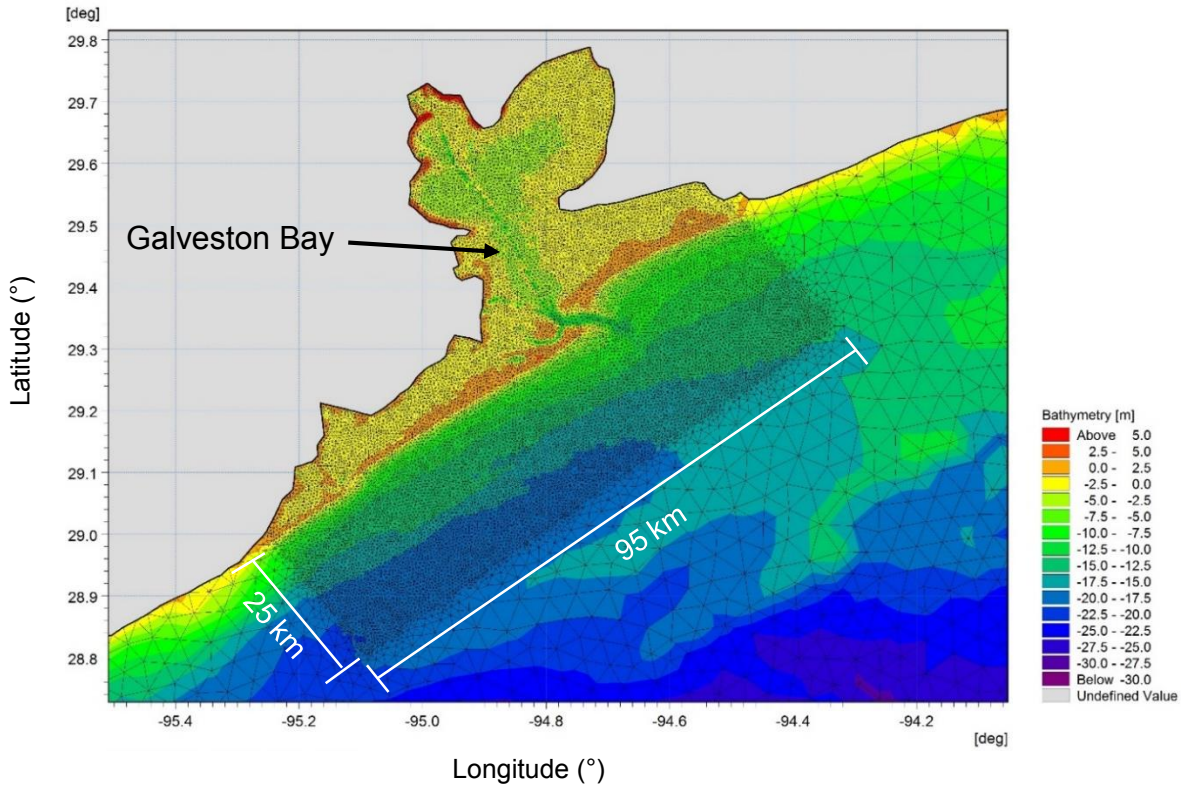

Figure 6.5: Mesh C for the Gulf of Mexico model domain

6.2.2. Hurricane Ike Wind field

Various authors have successfully simulated hurricane Ike's wind field. Hope et al. (2013) used the National Oceanic and Atmospheric Administration's (NOAA's) Hurricane Research Division Wind Analysis System (H*WIND) to generate Ike's wind field. The wind field was produced by obtaining data from buoys and wind towers, remote sensing from satellites and from aircraft measurements. The author obtained positive results in replicating the wind field.

The cyclone wind generation tool of Mike 21 was used to generate the wind field of Hurricane Ike. The tool applies a parametric wind field model to compute wind and pressure data produced by the storm. The Young and Sobey (1981) parametric model (refer to Section 2.3.1) was used to generate Hurricane Ike's wind field. Input into the model consists of several parameter's that can be found in the best track data.

Best track data from the revised Atlantic hurricane database (HURDAT2) was used as input to model Hurricane Ike. HURDAT2 does not contain estimates of the radius to maximum winds (R_{max}) in their data set. Estimates of R_{max} were retrieved from the Automated Tropical Cyclone

Forecast (Sampson & Schrader, 2000) system database. Table 6.1 provides a summary of the input used in the cyclone wind generation tool.

Table 6.1: Hurricane Ike wind field input data (V_{max} is 1-hour average)

Date (UTC)	Time (hour)	Long (°)	Lat (°)	R_{max} (km)	V_{max} (m/s)	P_c (hPa)	P_n (hPa)
09-09-2008 12:00AM	0	-80.3	21.5	27.78	25.97	965	1013
09-09-2008 06:00AM	6	-81.4	22.0	27.78	26.02	965	1013
09-09-2008 12:00PM	12	-82.4	22.4	27.78	26.36	965	1013
09-09-2008 14:00PM	14	-82.9	22.6	27.78	25.06	965	1013
09-09-2008 18:00PM	18	-83.3	22.7	27.78	25.41	966	1013
10-09-2008 12:00AM	24	-84.0	23.1	27.78	24.93	968	1013
10-09-2008 06:00AM	30	-84.6	23.4	27.78	27.34	964	1013
10-09-2008 12:00PM	36	-85.2	23.8	18.52	31.34	959	1013
10-09-2008 18:00PM	42	-85.8	24.2	18.52	33.41	958	1013
11-09-2008 12:00AM	48	-86.4	24.7	18.52	33.25	944	1013
11-09-2008 06:00AM	54	-87.1	25.1	18.52	33.22	945	1013
11-09-2008 12:00PM	60	-88.0	25.5	18.52	32.82	946	1013
11-09-2008 18:00PM	66	-88.9	25.8	111.12	32.93	952	1013
12-09-2008 12:00AM	72	-90.0	26.1	148.16	32.50	954	1013
12-09-2008 06:00AM	78	-91.1	26.4	92.6	34.57	954	1013
12-09-2008 12:00PM	84	-92.2	26.9	92.6	36.45	954	1013
12-09-2008 18:00PM	90	-93.2	27.5	92.6	36.53	954	1013
13-09-2008 12:00AM	96	-94.0	28.3	74.08	36.54	952	1013
13-09-2008 06:00AM	102	-94.6	29.1	55.56	36.83	951	1013
13-09-2008 18:00PM	103	-94.7	29.3	55.56	35.92	950	1013
13-09-2008 12:00PM	108	-95.2	30.3	55.56	31.79	959	1013
13-09-2008 18:00PM	114	-95.3	31.7	74.08	17.07	974	1013
14-09-2008 12:00AM	120	-94.9	33.5	92.6	9.76	980	1013
14-09-2008 06:00AM	126	-93.7	35.5	92.6	8.73	985	1013
14-09-2008 12:00PM	132	-91.0	37.6	92.6	8.77	987	1013
14-09-2008 18:00PM	138	-87.2	40.3	92.6	10.38	988	1013
15-09-2008 12:00AM	144	-81.5	43.3	92.6	7.30	988	1013

Several wind corrections (refer to Sections 2.3.1.1 – 2.3.1.3) were applied in the model. To convert the gradient-level winds produced by the parametric model, to surface winds (10 m elevation), a constant boundary layer wind speed correction (K_m = 0.8) was applied.

The forward motion asymmetry of the cyclone was taken into account by subtracting half (δ_{fm} = 0.5) of the cyclone forward speed from the V_{max} in the best track data. The angle to maximum wind speed (θ_{max}) was specified as 120°, based on the results of the comparisons of the measured and modelled winds.

Inflow angle was specified in the model using the equations proposed by Sobey et al. (1977)

The wind field was generated on a 500 x 500 grid with a 0.03387° x 0.025186° spacing. An example of the wind field output on 12 September 2008 at 12:00 AM UTC is shown in Figure 6.6.

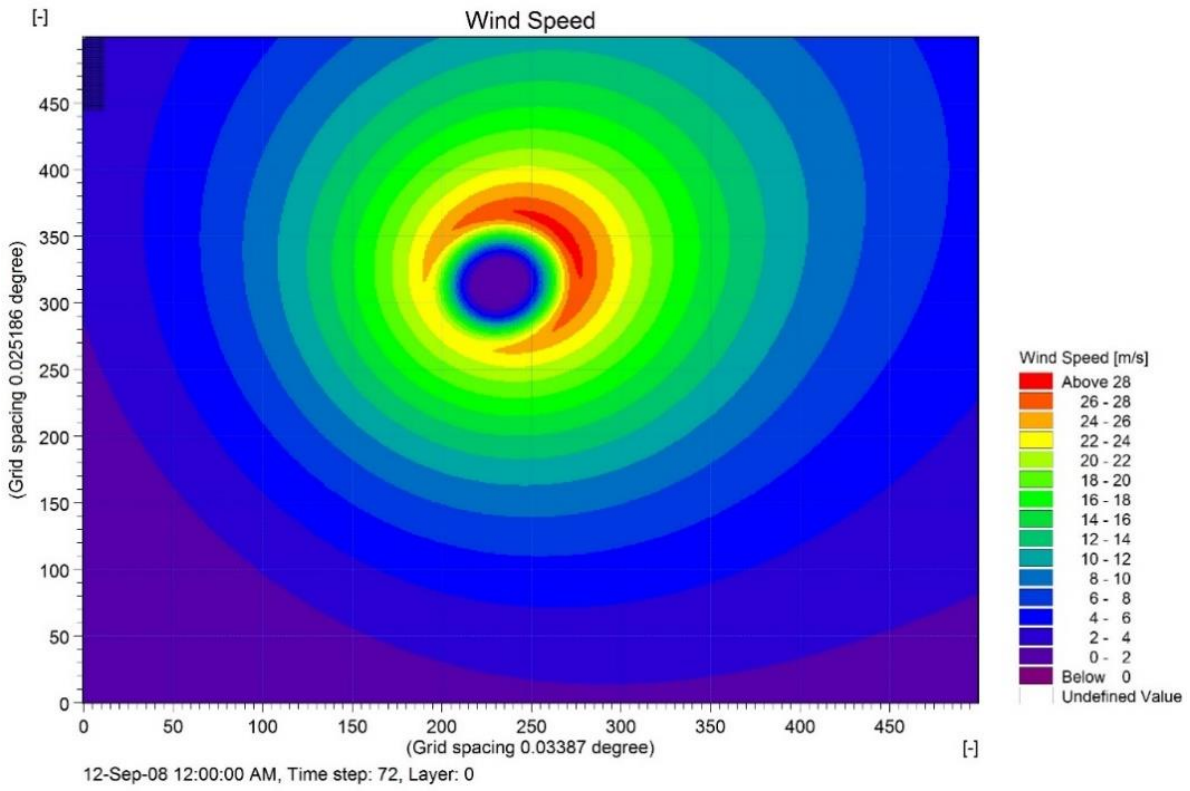

Figure 6.6: Model wind field for Hurricane

6.3. Results of Calibration Tests

6.3.1. Winds

Wind measurements during Hurricane Ike were retrieved from the National Oceanic and Atmospheric Administration (NOAA). Due to the intensity of Hurrricane Ike's wind field, several data recording stations failed when Ike made landfall. This left fewer points for comparison to the model. The wind measurement stations used for comparison are shown in Figure 6.7, where Hurricane Ike's track is plotted in red. The coordinates of the wind measurement stations can be found in Table E-1 of Appendix E.

Figure 6.7: NOAA wind recording stations (After Google Earth, 1970b)

Figures 6.8 and 6.9 provide comparisons of the measured and modelled wind speeds and directions at the 6 points shown in Figure 6.7. The direction of wind refers to the direction the winds are coming from, with respect to True North.

From the figures, it can be seen that Station 8771341 failed when Ike made landfall. An interesting occurrence at Stations 8771013 and 8771341, is the capture of the hurricane eye (very low winds) as it passes. Since the model only considered the winds of the hurricane, the initial wind speeds and directions differ slightly from the measurements, due to background winds experienced at the stations. Overall, the measured peak wind speeds compare

favourably with the modelled peaks. The modelled wind directions are also reasonably well matched to the measurements.

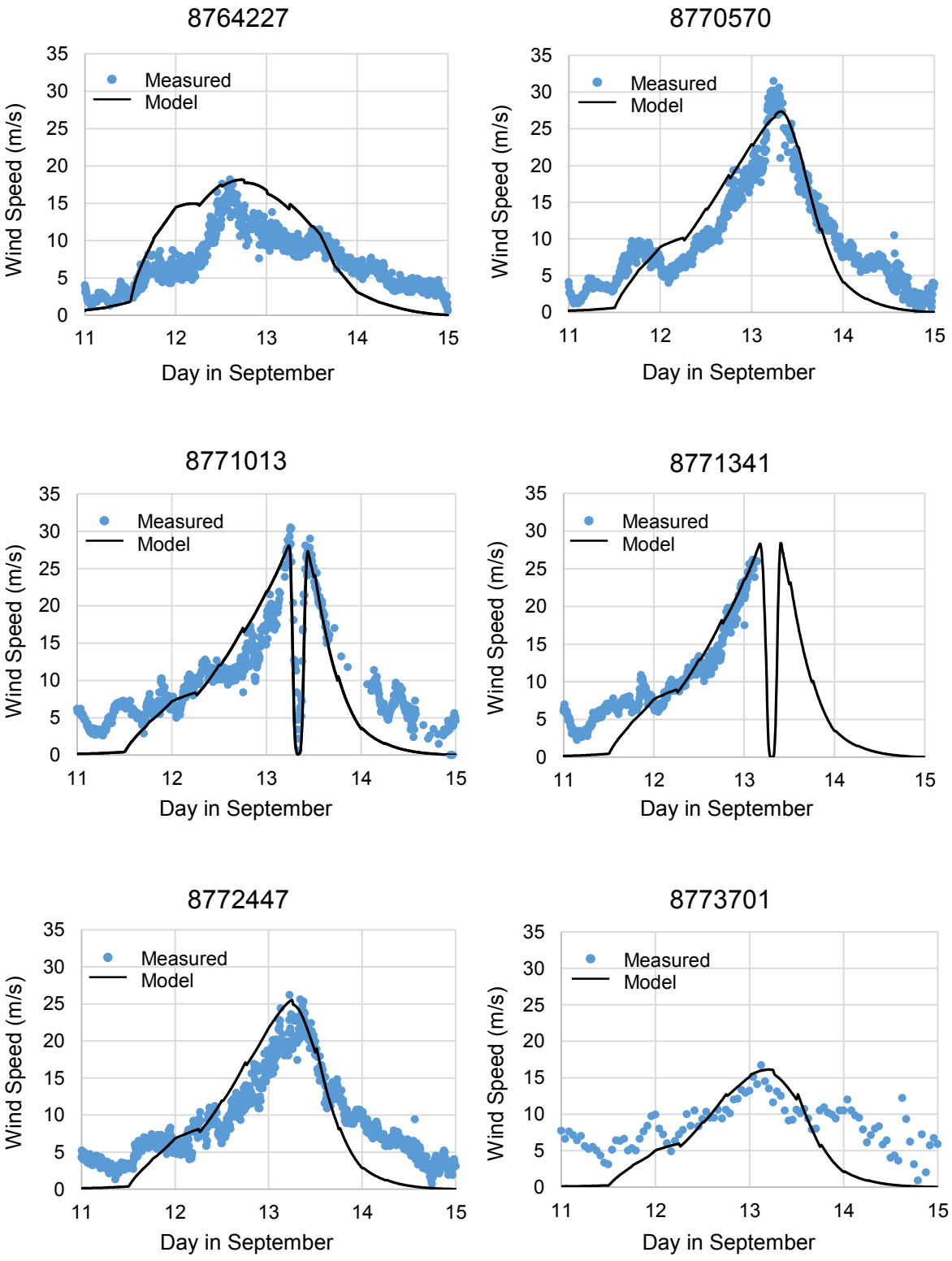

Figure 6.8: Wind speed time series (UTC) at NOAA stations during Hurricane Ike

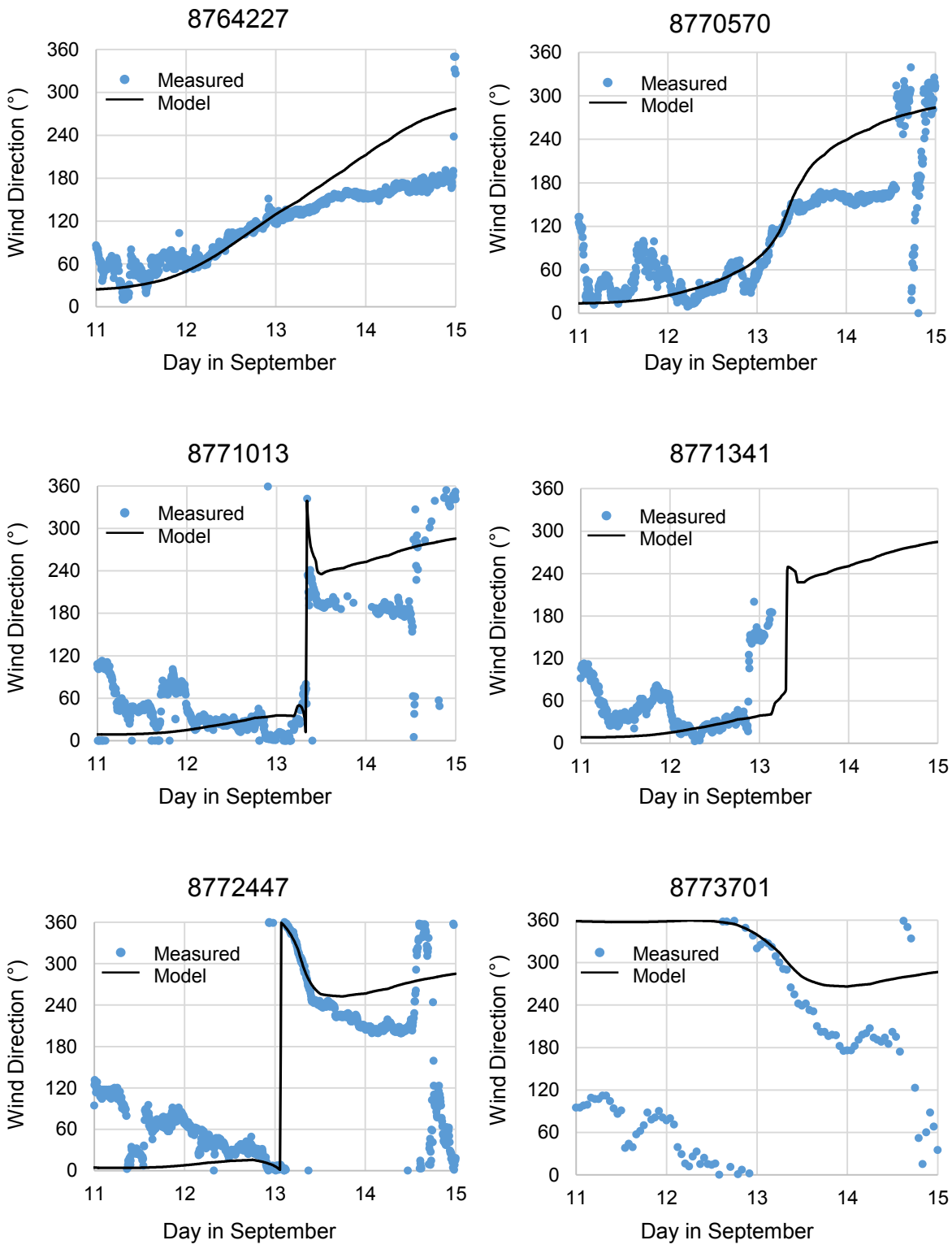

Figure 6.9: Wind direction time series (UTC) at NOAA stations during Hurricane Ike

6.3.2. Storm Surge

Figure 6.10 shows the maximum storm surge level reached during the simulation of Hurricane Ike. The maximum storm surge level reached for the simulation was 4.1 m.

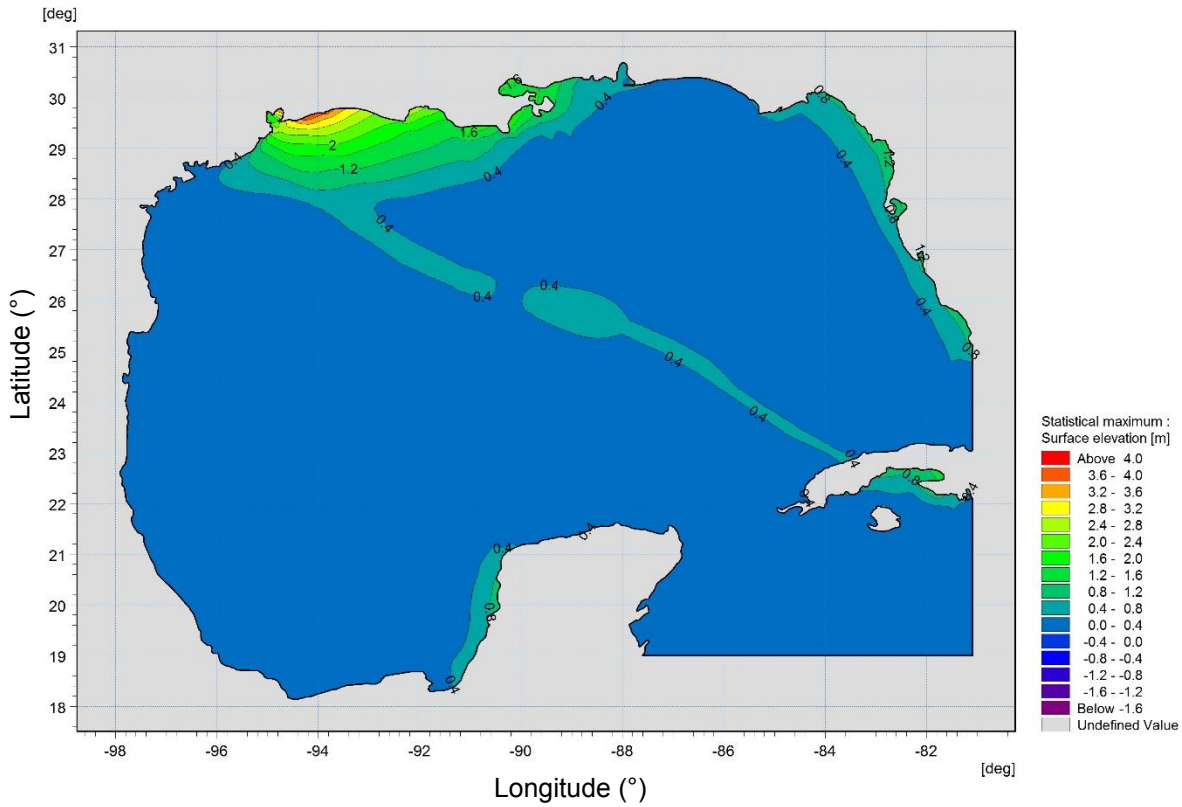

Figure 6.10: Contour plot showing the maximum storm surge level reached during the simulation of Hurricane Ike

Water level measurements during Hurricane Ike were retrieved from the National Oceanic and Atmospheric Administration (NOAA) website. The measurement stations used for comparison are shown in Figure 6.11, where Hurricane Ike's track is plotted in red. The coordinates of the measurement stations can be found in Table E-2 of Appendix E.

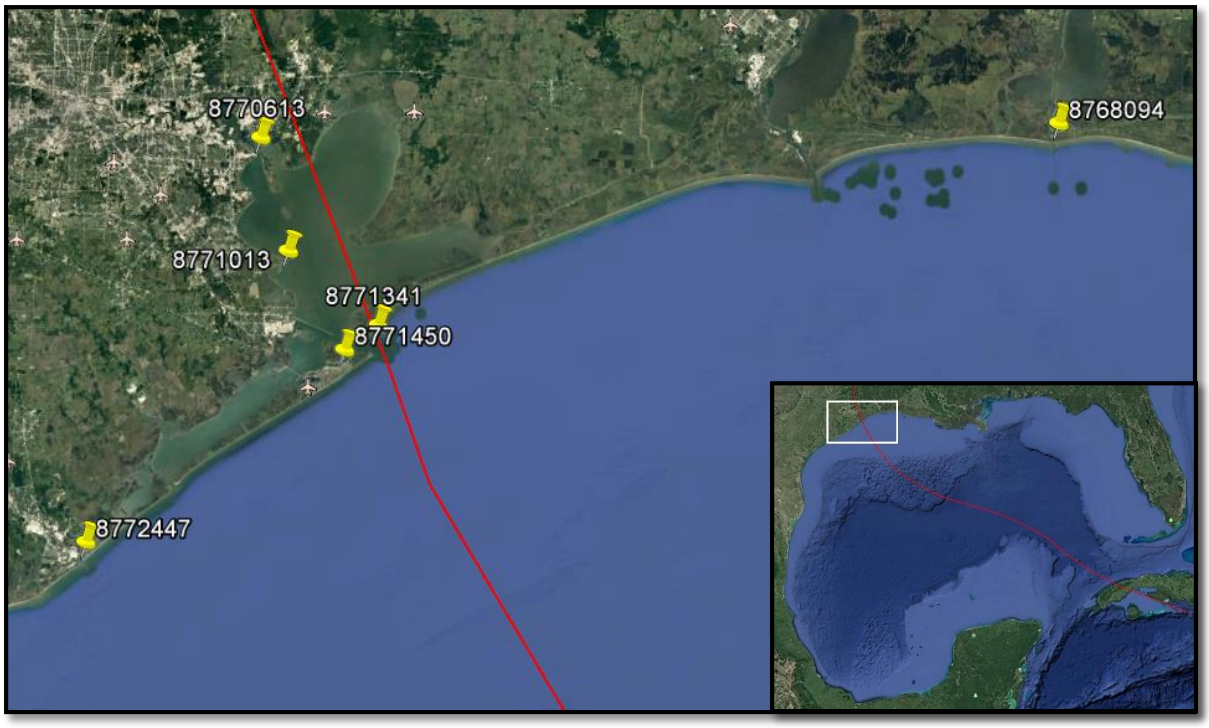

Figure 6.11: NOAA water level recording stations (After Google Earth, 1970b)

Figure 6.12 provides comparisons of the measured and modelled water surface elevations, at the 6 points shown in Figure 6.11. The graphs do not include tides, and therefore represent the storm surge levels.

The general pattern of the model fits the measured data well for all the graphs. The modelled peak surface elevation at Station 8768094, compares very favourably with the measured data. From the other graphs, it is evident that the model under-predicts the storm surge. The initial surge levels of the model differ from the measured data because of the background winds that occur, which are not modelled in the simulation.

A summary of the percentages of under-prediction at the peaks of the measured data for each station, is presented in Table 6.2. The modelled elevations in Table 6.2 are the associated model elevations corresponding to the time of the peak measured elevations. Considering all the percentages in Table 6.2, an average under-prediction value of 35.6 % is calculated. This value can be used in the application of the model test results of this study. The storm surge results would then need to be increased by 35.6 %.

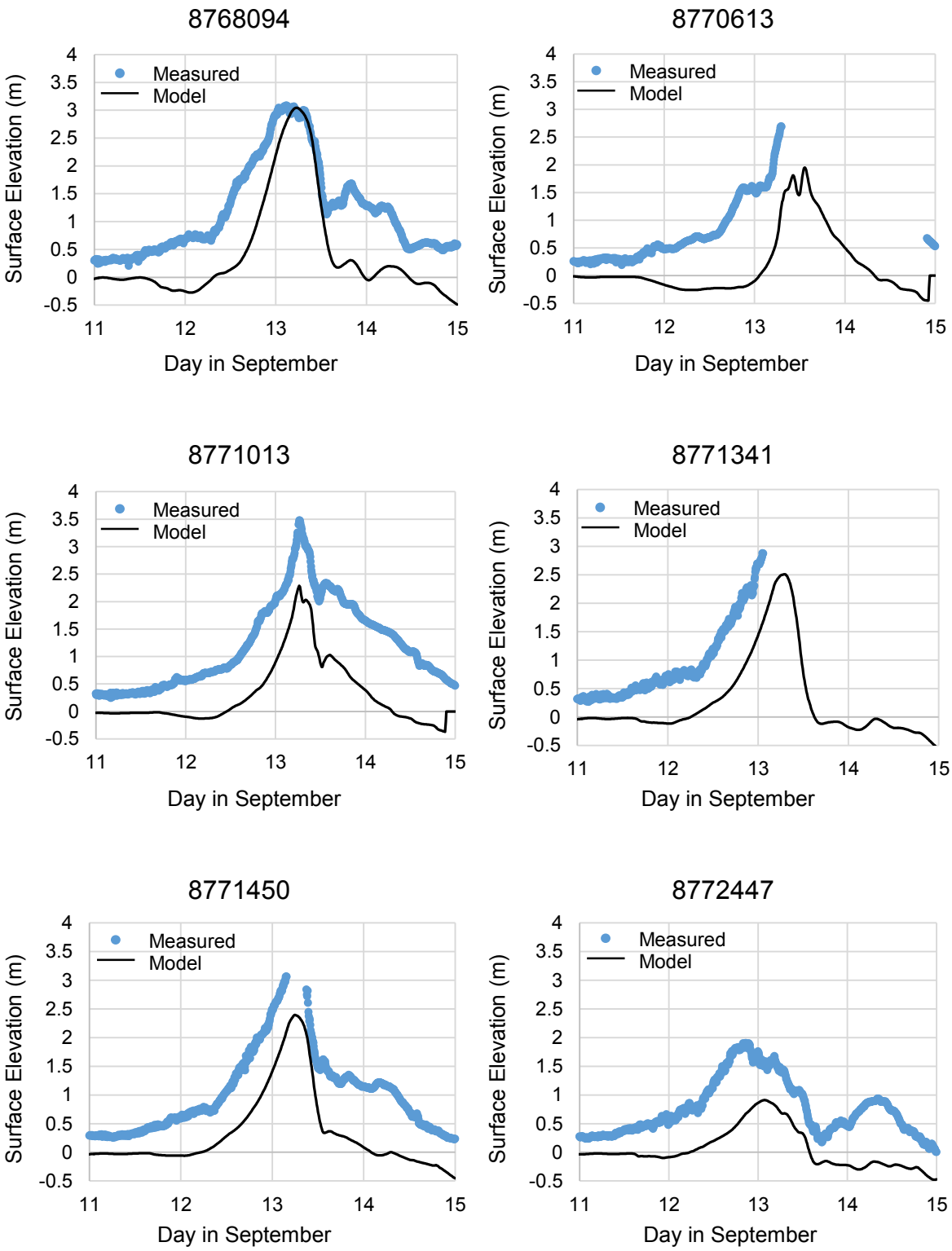

Figure 6.12: Surface elevation time series (UTC) at NOAA stations during Hurricane Ike

Table 6.2: Percentage of under-prediction at peak measured elevations for all stations

Station	Peak Measured Elevation (m)	Modelled Elevation (m)	Under-prediction (%)
8768094	3.09	3.04	1.4
8770613	2.69	1.30	51.6
8771013	3.48	2.25	35.3
8771341	2.88	1.66	42.3
8771450	3.06	2.11	31.0
8772447	1.90	0.91	52.1

6.3.3. Waves

Figure 6.13 shows the maximum significant wave height reached during the simulation of Hurricane Ike. The maximum significant wave height reached for the simulation was 15.9 m.

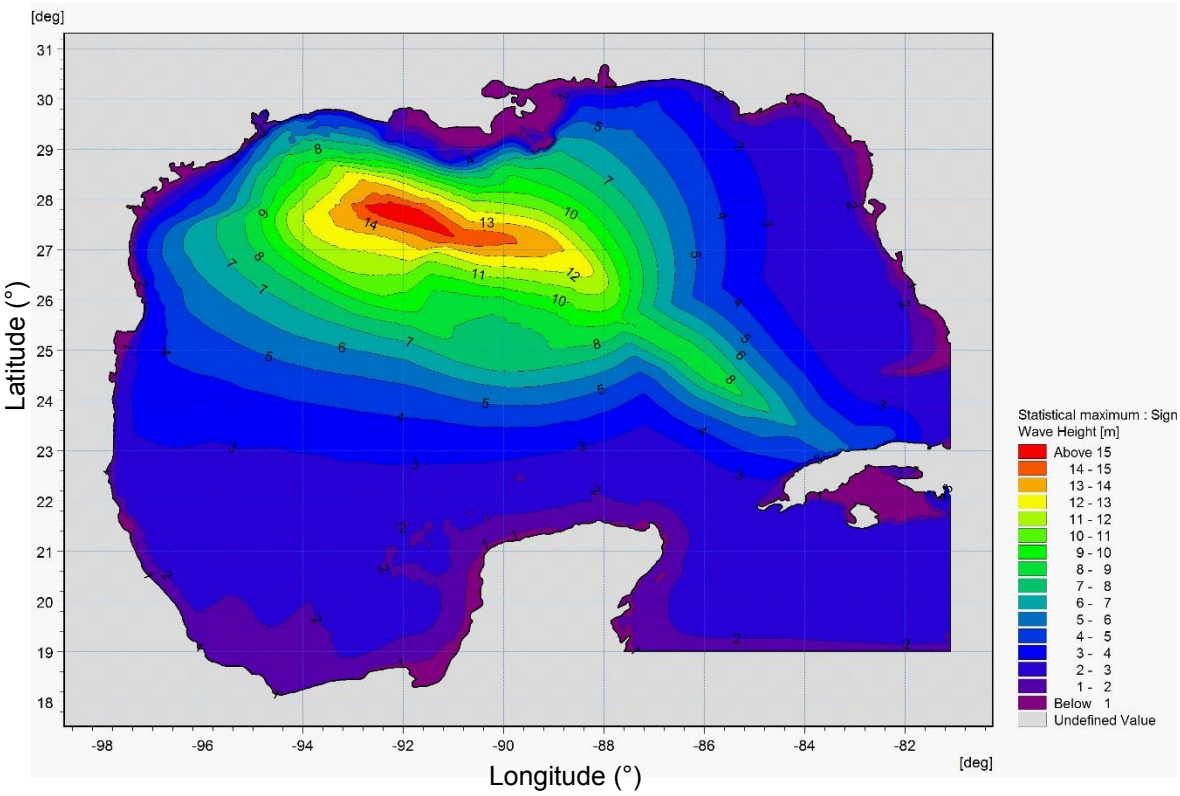

Figure 6.13: Contour plot showing the maximum significant wave height reached during the simulation of Hurricane Ike

Wave data measurements during Hurricane Ike were retrieved from the National Data Buoy Center (NDBC). The buoys used for comparison are shown in Figure 6.14, where Hurricane Ike's track is plotted in red. The coordinates of the buoys can be found in Table E-3 of Appendix E.

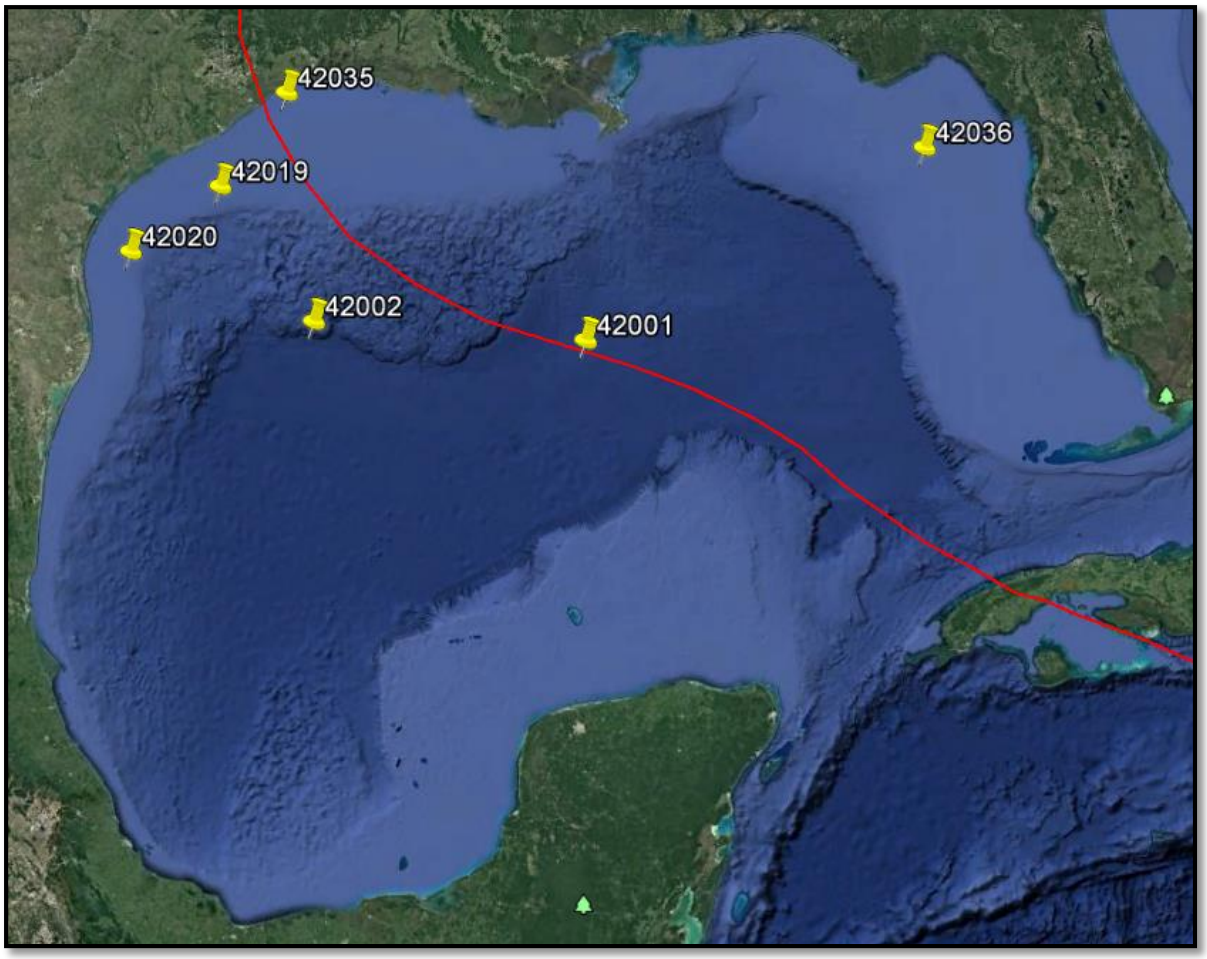

Figure 6.14: NDBC wave buoys (After Google Earth, 1970b)

Figures 6.15, 6.16 and 6.17 provide comparisons of the respective significant wave height, peak wave period, and mean wave direction, at the six buoys shown in Figure 6.14. The mean wave direction refers to the direction the waves are coming from, with respect to True North.

The significant wave height of the model matches the measured data reasonably well. It must be noted that there is a considerable initial difference between the measured and modelled heights. This is once again due to background waves caused by other meteorological conditions, which are not simulated in the numerical model. Considering that the proposed study is focused on the maximum significant wave heights, the model works reasonably well at producing these values. Proof of this is observed at Buoys 42001, 42019 and 42035, where the peak significant wave heights are matched to the measured data. It is apparent that these buoys are located very close to Ike's track. The other buoys are located further away (42036 is 450 km from Ike's track at its closest point), which could contribute to the difference in heights. An interesting occurrence at Buoys 42001 and 42035, is the capture of the hurricane eye as it passes.

The peak wave period of the model matches the measured data reasonably well. The only big difference between the measured and modelled data occurs at Buoy 42035, where the model period drops as the hurricane passes.

The mean wave direction of the model was relatively similar to the measured data. At Buoys 42002, 42019 and 42020 the model tends to produce waves from a more northerly direction compared to the measured data. There is no mean wave direction data for Buoy 42001.

6.4. Conclusions about Calibration Tests

The results of the simulation indicate that the MIKE 21/3 Coupled Model FM provide reasonably good estimates of the storm surge and wave conditions produced by Hurricane Ike. The small errors in the data are to be expected, since only the hurricane-generated waves and storm surge were simulated. It must be kept in mind that the model significantly under-predicts the storm surge. When using the storm surge results of the present study, the values can be increased by 35.6 % in order to take into account the under-prediction of storm surge in the model. This is left up to the user of the results, and will not be investigated further in this study.

Hope et al. (2013) have successfully simulated the storm surge generated by Hurricane Ike. From this study, it is evident that Hurricane Ike had a very complex wind field structure. The cyclone wind generation tool used in the present study, uses a simple parametric model to describe the wind fields. It is possible that this simple representation is not good enough to model the tropical cyclones. Hu et al. (2012) blended a parametric model with background wind fields to correct the deficiencies of a simple parametric model.

Another possible cause for the poor comparison of storm surge could lie in the Best Track data. The parametric models rely on the parameters in the Best Track data as input. If the parameters in the Best Track data were incorrect, large errors in the storm surge would be present.

Considering the positive results of the calibration tests, the modelling methodology used in the simulation of Hurricane Ike can therefore be applied to the proposed tests along the Southern African East Coast with some confidence.

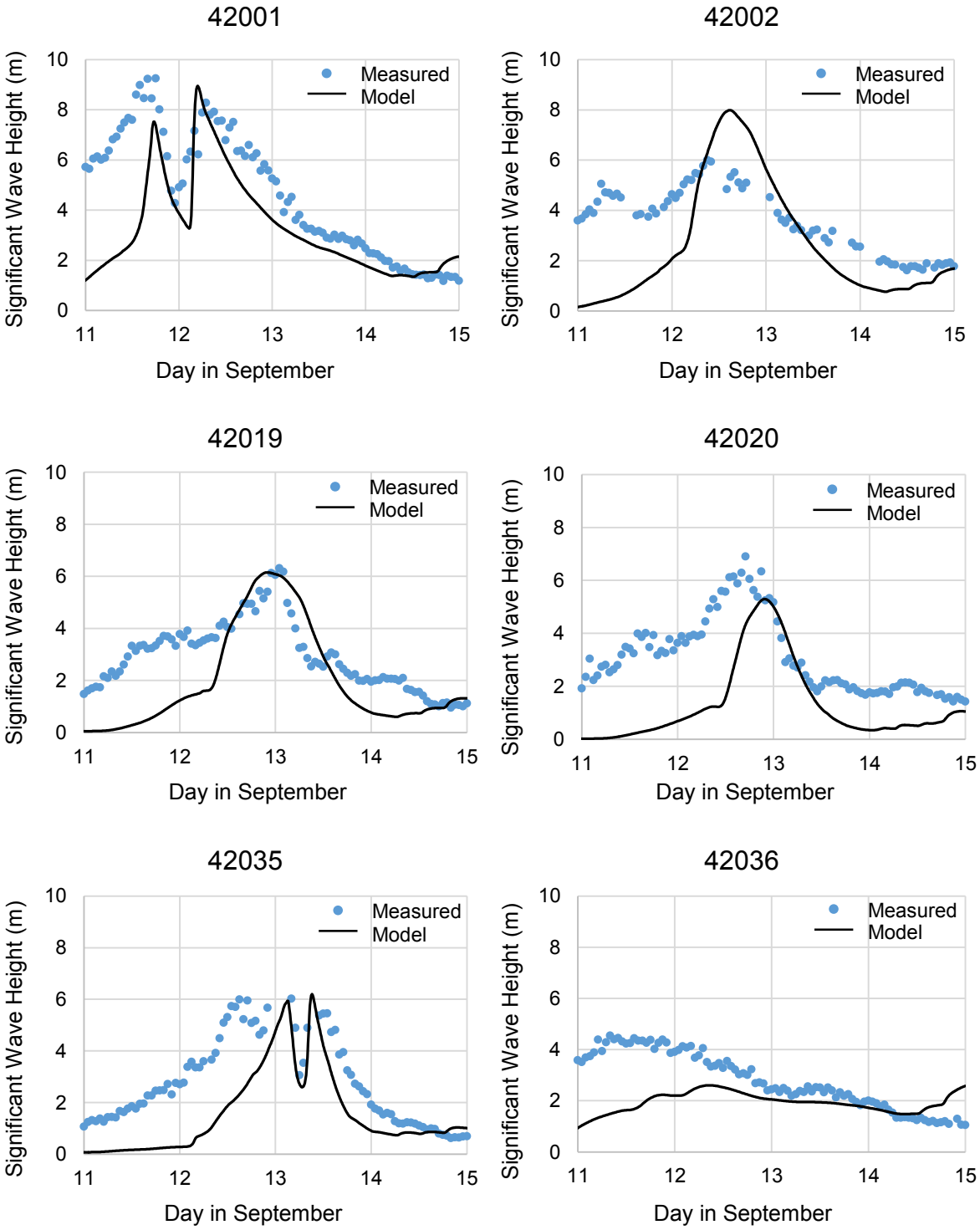

Figure 6.15: Significant wave height time series (UTC) at NDBC buoys during Hurricane Ike

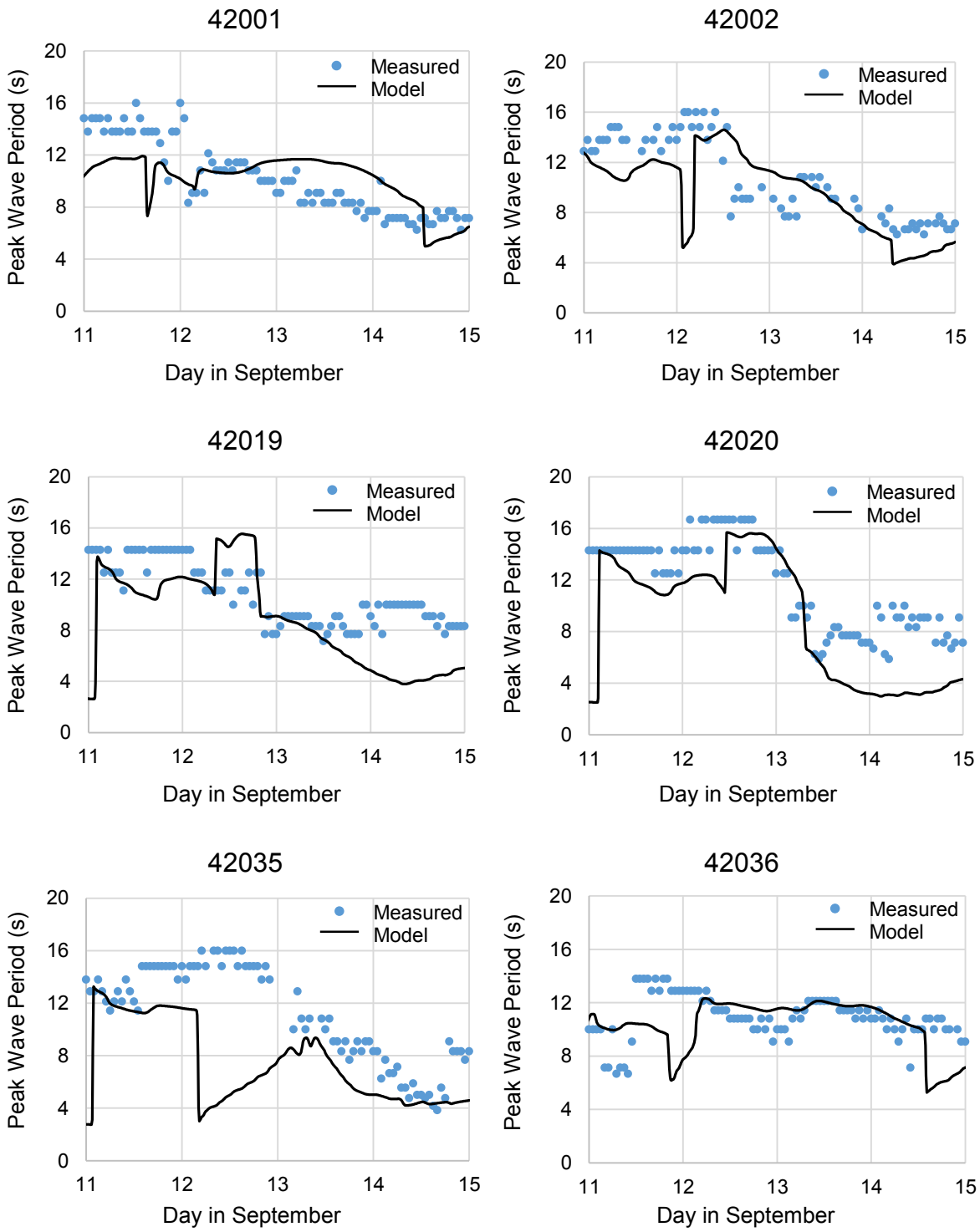

Figure 6.16: Peak wave period time series (UTC) at NDBC buoys during Hurricane Ike

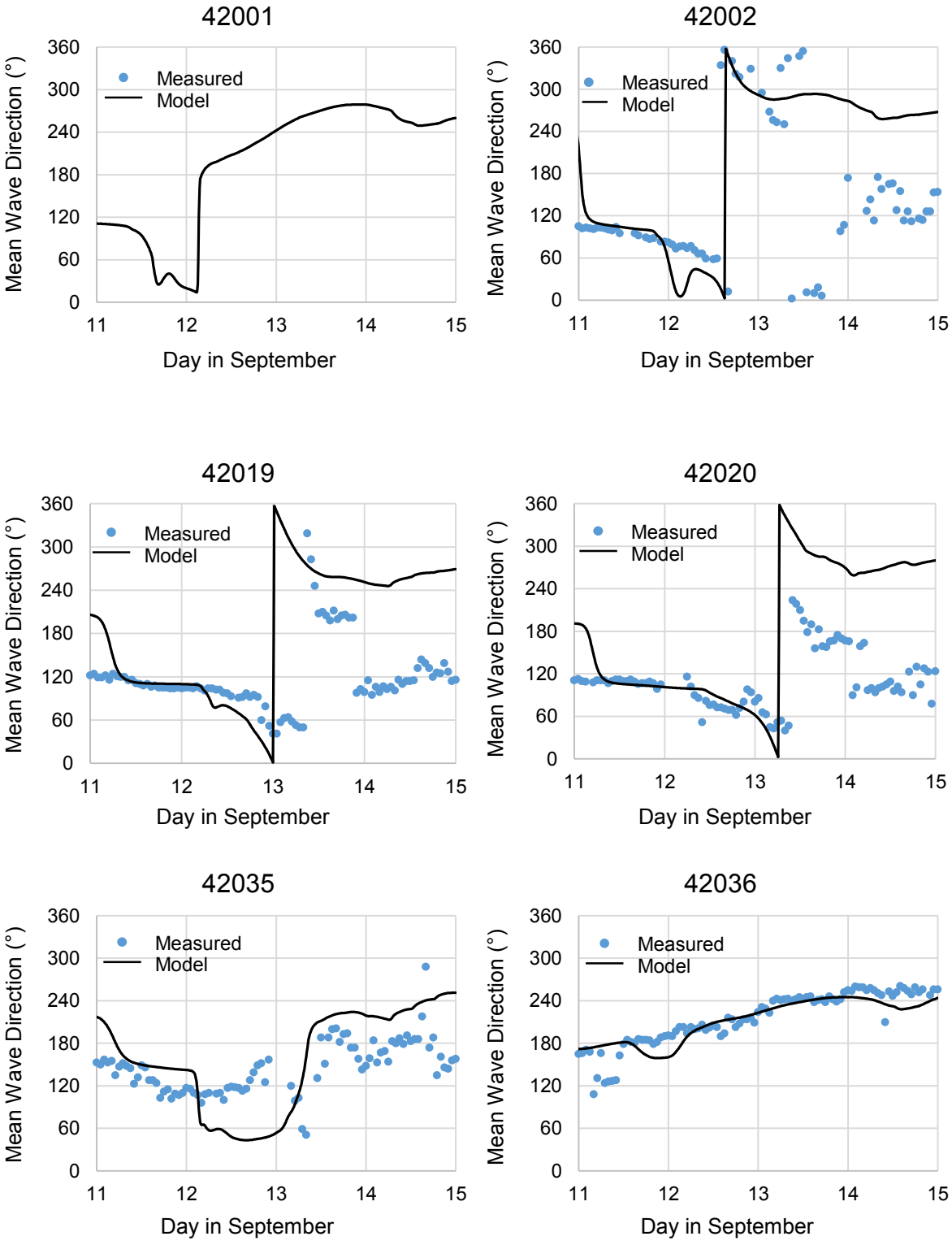

Figure 6.17: Mean wave direction time series (UTC) at NDBC buoys during Hurricane Ike

7. Results of Modelling the Southern African East Coast

7.1 Introduction

The objective of this thesis was to determine the best estimates of the 50-, 100-, 200- and 500-year significant wave height and storm surge levels expected to be produced by tropical cyclones, at four locations along the Southern African East Coast. This section presents the results of the study and how the thesis objective has been achieved.

7.2. Waves

The results of the numerical model simulations are presented in Figure 7.1. The graphs show the simulated significant wave heights over time at four return periods, for each of the four locations along the Southern African East Coast. The vertical black line represents the time of tropical cyclone landfall at a duration of 24 hours.

For the 50-year simulation, the waves are very small at Durban with a peak H_s of 0.98 m. The waves at Maputo and Pemba are similar, where Pemba has a slightly larger peak H_s value. Beira has the largest waves, peaking at 4.91 m.

For the 100-year simulation, Durban has the smallest waves where the peak H_s is 2.08 m. The waves at Maputo and Pemba are again similar, although Maputo has a slightly larger peak H_s value at this return period. Beira has the largest waves, peaking at 6.28 m.

For the 200-year simulation, the waves are again smallest at Durban with a peak H_s of 2.94 m. The difference in peak H_s values between Pemba and Maputo is quite large with H_s values of 4.76 m and 6 m respectively. Beira has the largest waves, peaking at 7.96 m.

For the 500-year simulation, the general trend is the same as that of the 200-year simulation, except that Maputo has a peak H_s value similar to Beira's peak H_s of 8.65 m. Durban has the smallest waves where the peak H_s is 4.38 m.

From Figure 7.1, it is evident that the peak H_s value for each location occurs at different times during the simulations. Beira and Maputo achieve a peak H_s value prior to the tropical cyclone making landfall. Beira peaks at approximately 4 hours prior to landfall and Maputo peaks at approximately an hour before landfall. Pemba peaks approximately an hour after landfall and Durban peaks approximately 2 hours after landfall. The differences can be attributed to the different bathymetries and wind speeds at the locations.

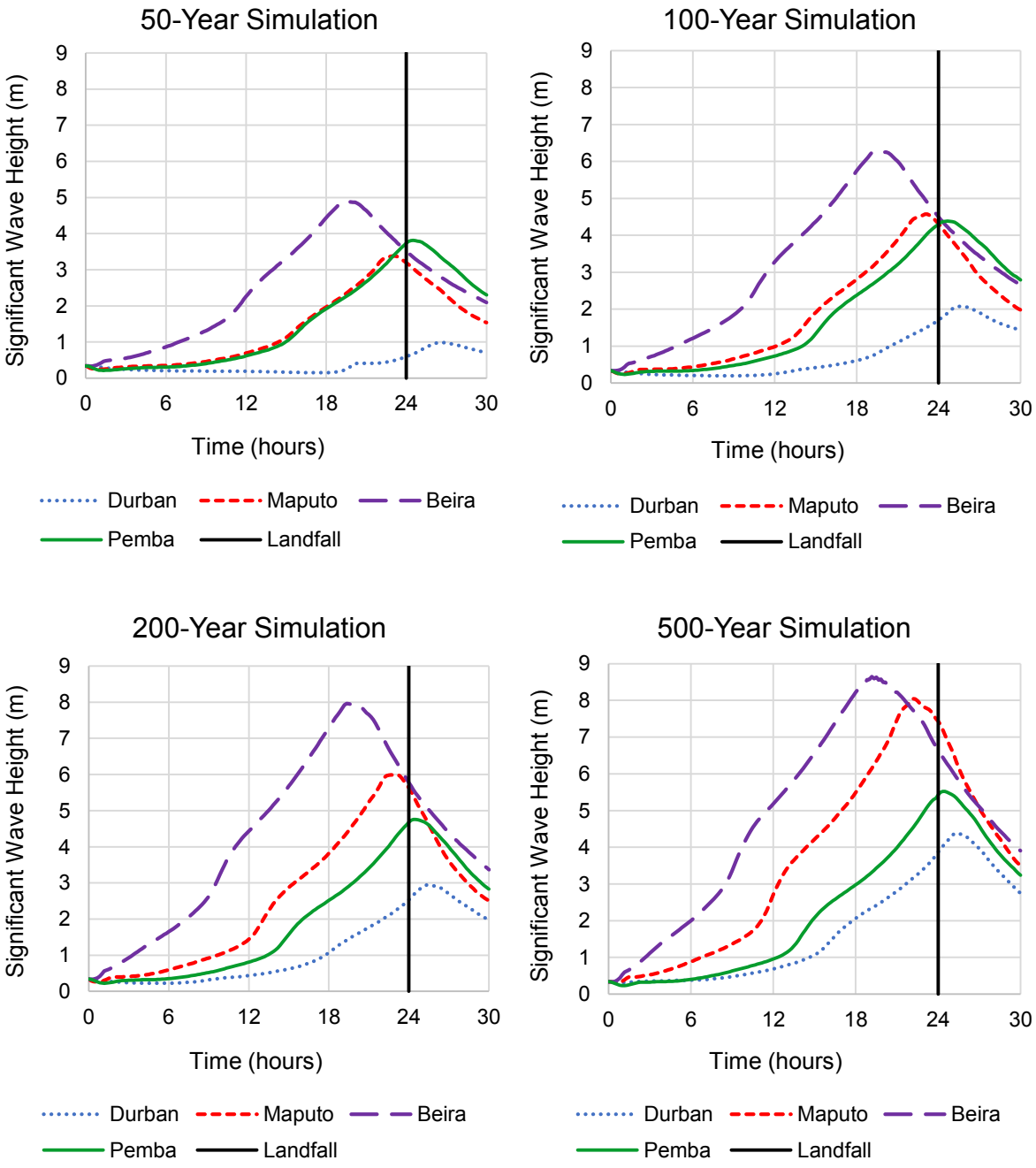

Figure 7.1: Significant wave height results of the numerical model simulations

Table 7.1 summarizes the peak significant wave heights produced in the model tests. Two areas of investigation are presented. The first is the immediate area surrounding the location, and the second is the total area where the expected maximum waves occur. Two H_s values are presented for each area in Table 7.1, the minimum and maximum H_s. These refer to the minimum and maximum H_s of the specified output points at each location. From Table 7.1, it is evident that the minimum H_s values, considering the whole area of investigation, occur in the immediate area surrounding the location. The variation between the minimum and maximum

H_s values is reasonably large in some areas, such as the 500-year simulation at Pemba where the difference is 3.74 m.

Table 7.1: Minimum and maximum H_s values for the model simulations (water depth = 20 m)

	Immediate Area		Total Area	
Location	$H_{s,min}$ (m)	$H_{s,max}$ (m)	$H_{s,min}$ (m)	$H_{s,max}$ (m)
Durban 50-Year	0.36	0.64	0.36	**0.98**
Maputo 50-Year	1.93	2.39	1.93	**3.38**
Beira 50-Year	3.62	4.37	3.62	**4.91**
Pemba 50-Year	1.25	2.82	1.25	**3.81**
Durban 100-Year	0.79	1.55	0.79	**2.08**
Maputo 100-Year	2.53	3.25	2.53	**4.57**
Beira 100-Year	4.60	5.61	4.60	**6.28**
Pemba 100-Year	1.41	3.21	1.41	**4.38**
Durban 200-Year	1.31	2.32	1.31	**2.94**
Maputo 200-Year	3.24	4.25	3.18	**6.00**
Beira 200-Year	5.71	7.10	5.71	**7.96**
Pemba 200-Year	1.55	3.50	1.55	**4.76**
Durban 500-Year	2.00	3.56	2.00	**4.38**
Maputo 500-Year	4.09	5.47	3.98	**8.05**
Beira 500-Year	6.37	7.96	6.37	**8.65**
Pemba 500-Year	1.78	4.03	1.78	**5.52**

The 100-year H_s values of Maputo and Beira in Table 7.1 are significantly less than the values obtained in the study by Theron et al. (2012). The authors used empirical methods to determine the 100-year H_s values of 7.8 m and 8.5 m at Maputo and Beira respectively, at a water depth of 14 m. The use of empirical formulas is not as advanced as employing detailed numerical models. These estimates are therefore considered less accurate. Both the results of the present study and the study by Theron et al. (2012) indicate that larger waves can be expected at Beira.

Figure 7.2 illustrates the variation of the significant wave heights experienced along the coast at each of the locations. The specified output points are plotted showing the H_s values north and south of the point where the tropical cyclone made landfall. Distances north of the landfall point are presented as positive values and southerly distances are negative. The values are the results from the 100-year simulation. The other three return periods are not shown as they exhibit the same trend, just with different magnitudes.

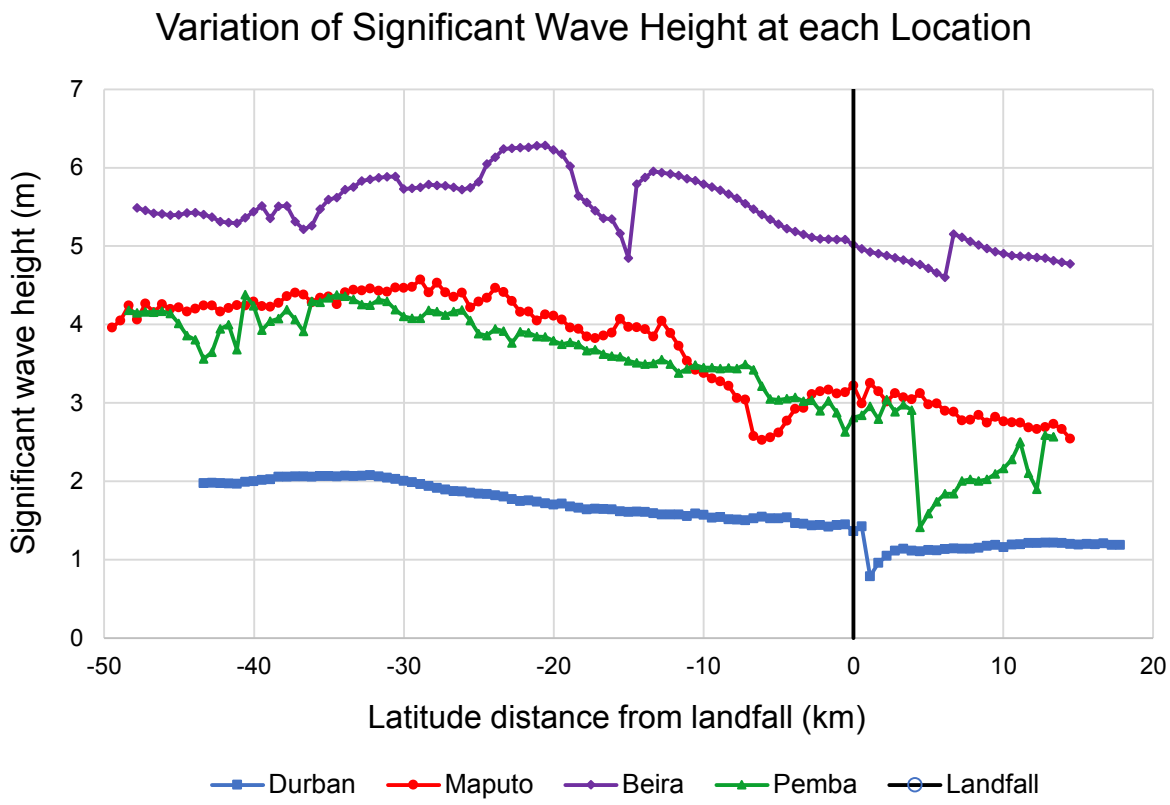

Figure 7.2: Variation of significant wave height at each of the locations

From Figure 7.2, it is clear that the largest waves occur south of the landfall point. This is due to stronger winds on the southern side of the tropical cyclone eye, caused by the forward motion asymmetry and clockwise circulation of the tropical cyclone. This is further illustrated in Figure 7.3.

From Figure 7.2, it can be seen that the waves increase in size southwards of the landfall point up to a certain point, and then start to decrease, meaning the largest waves have been captured in all the simulations. Durban has a peak H_s value at distance of approximately 33 km south of the landfall point. Maputo and Pemba peak at roughly 28 km and 41 km respectively. Beira peaks at approximately 21 km. These distances refer to this particular case.

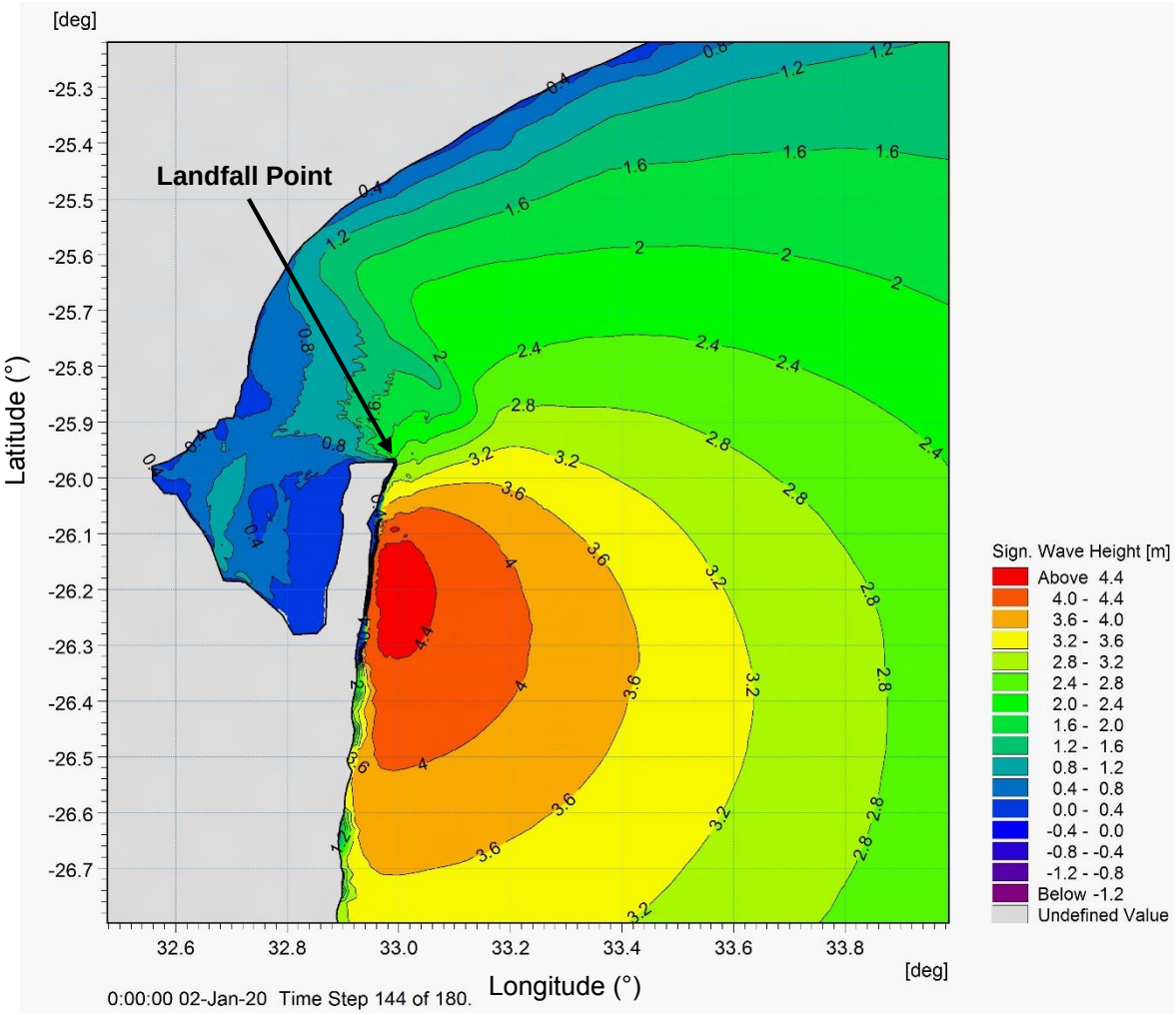

Figure 7.3: Spatial plot of the significant wave height contours at the time of landfall at Maputo, for a 100-year return period

Since the largest waves occur south of the storm centre for this test case, it is assumed that if the tropical cyclone made landfall further north, these peak waves could be experienced further north at the location. Therefore, the design wave height for each location is taken as the maximum value of the whole area instead of just at the specific location.

Table 7.2 summarizes the estimates of the significant wave heights that can be expected along the Southern African East Coast, with its associated peak wave period (T_p) and mean wave direction (θ). The mean wave direction refers to the direction the waves are coming from, with respect to True North. The wave heights are quite low in comparison to the cut-off low generated waves that occur near Durban. During the March 2007 cut-off low system that occurred along the South African Coast, a significant wave height of 8.5 m was generated. This is roughly double that of the 500-year tropical cyclone-induced wave expected to occur at Durban. The expected peak wave periods are relatively low, as these are the associated

periods corresponding to the peak significant wave heights. The expected peak wave periods range from 4.76 s to 11.6 s. The expected mean wave directions range from 94.2 ° to 103.4 °, with an average of 98.5 °.

Table 7.2: Estimates of the expected significant wave heights caused by tropical cyclones along the Southern African East Coast

Location	H_s (m)	T_p (s)	θ (°)
Durban 50-Year	0.98	4.67	94.20
Maputo 50-Year	3.38	7.77	98.15
Beira 50-Year	4.91	8.99	103.40
Pemba 50-Year	3.81	8.41	96.07
Durban 100-Year	2.08	6.33	102.21
Maputo 100-Year	4.57	8.70	96.73
Beira 100-Year	6.28	9.82	100.94
Pemba 100-Year	4.38	8.75	96.70
Durban 200-Year	2.94	7.25	101.53
Maputo 200-Year	6.00	9.68	95.25
Beira 200-Year	7.96	10.87	98.83
Pemba 200-Year	4.76	9.07	94.66
Durban 500-Year	4.38	8.55	101.06
Maputo 500-Year	8.05	11.09	100.23
Beira 500-Year	8.65	11.60	100.66
Pemba 500-Year	5.52	9.63	95.09

An example of a tropical cyclone event responsible for generating extreme waves along the South African coast is Tropical Cyclone Imboa, which formed in the Mozambique Channel in February 1984. The system tracked southwards reaching Richards Bay, where a Waverider buoy, located at a depth of roughly 25 m, recorded a peak significant wave height of approximately 8 m (Rossouw, 1989). Comparing this value to the expected estimates at Durban shown in Table 7.2, it seems the estimates are considerably low. At a return period of 500 years, Durban is expected to experience a 4.4 m wave, half of the wave height that occurred off Richards Bay.

Tropical Cyclone Lizette occurred off Beira in 1997. At one of the deployed buoys, a peak significant wave height of approximately 4 m was registered, while the buoy was at a depth of 20 m. The range of wave heights estimated for Beira in Table 7.2 (4.9 m – 8.7 m), are therefore in the order of this measurement.

7.3. Storm Surge

The results of the numerical model simulations are presented in Figure 7.4. The graphs show the simulated storm surge levels over time at four return periods, for each of the four locations along the Southern African East Coast. The vertical black line represents the time of tropical cyclone landfall at a duration of 24 hours.

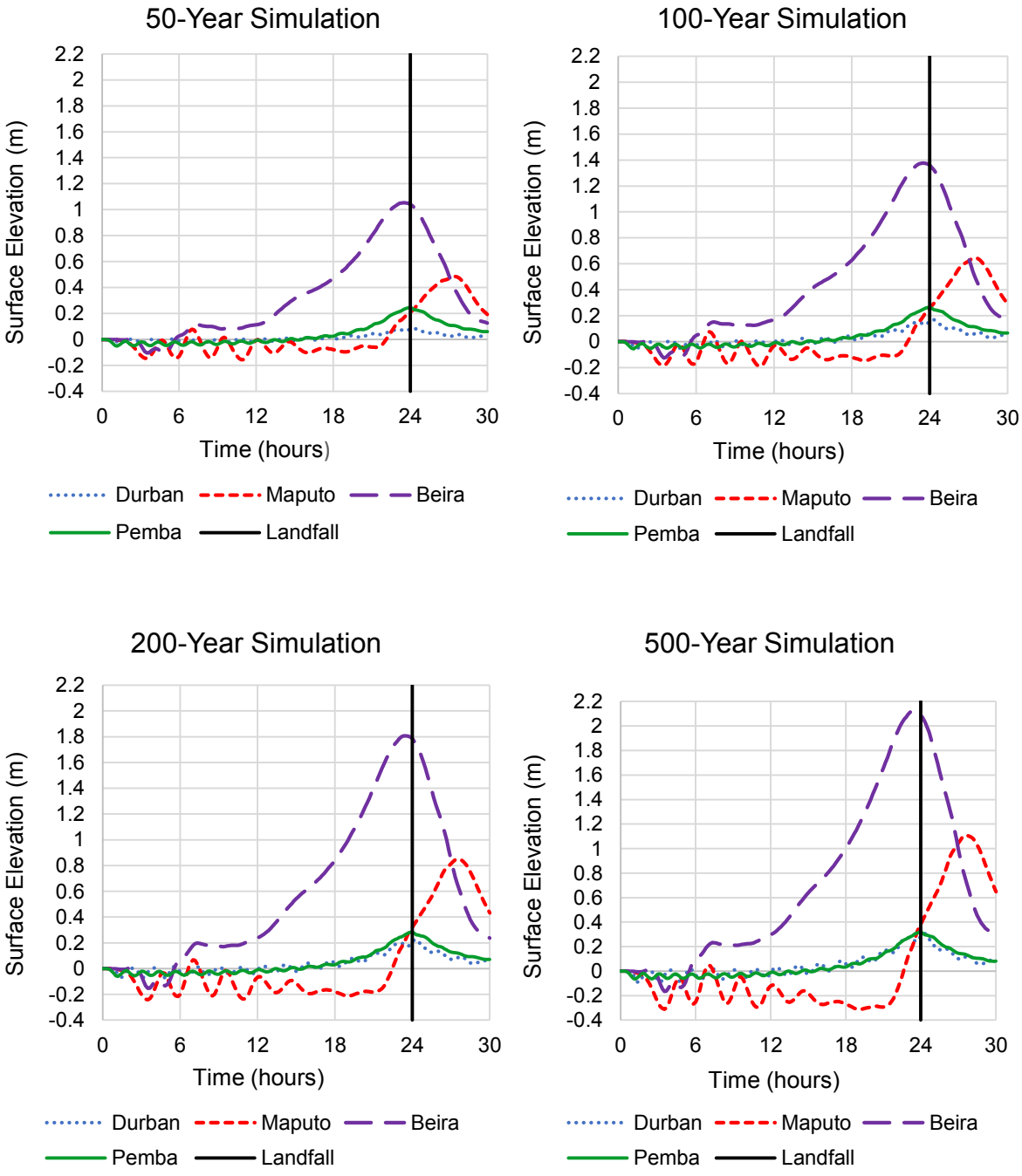

Figure 7.4: Storm Surge results of the numerical model simulations

For the 50-year simulation, the storm surge at Durban and Pemba is very small, with peaks of 0.09 m and 0.25 m respectively. The surge at Maputo is slightly larger with a peak of 0.49 m. The largest storm surge is experienced at Beira, peaking at 1.05 m.

For the 100-year simulation, the storm surge at Durban and Pemba is again very small, with peaks of 0.17 m and 0.27 m respectively. The surge at Maputo is slightly larger with a peak of 0.65 m. The largest storm surge is experienced at Beira, peaking at 1.38 m.

For the 200-year simulation, the storm surge at Durban and Pemba is again very small, with peaks of 0.22 m and 0.28 m respectively. The surge at Maputo is considerably larger with a peak of 0.85 m. The largest storm surge is experienced at Beira, peaking at 1.81 m.

For the 500-year simulation, the storm surge at Durban and Pemba is again very small, with peaks of 0.31 m and 0.32 m respectively. The surge at Maputo is considerably larger with a peak of 1.11 m. The largest storm surge is experienced at Beira, peaking at 2.12 m.

From Figure 7.4, it is evident that the peak storm surge for each location occurs when the tropical cyclone makes landfall, except for Maputo, where it peaks approximately 3.5 hours after landfall. A possible cause of this is because some of the output points are located further in the bay of Maputo, which are only reached by the tropical cyclone after it makes landfall as seen in Figure 7.5.

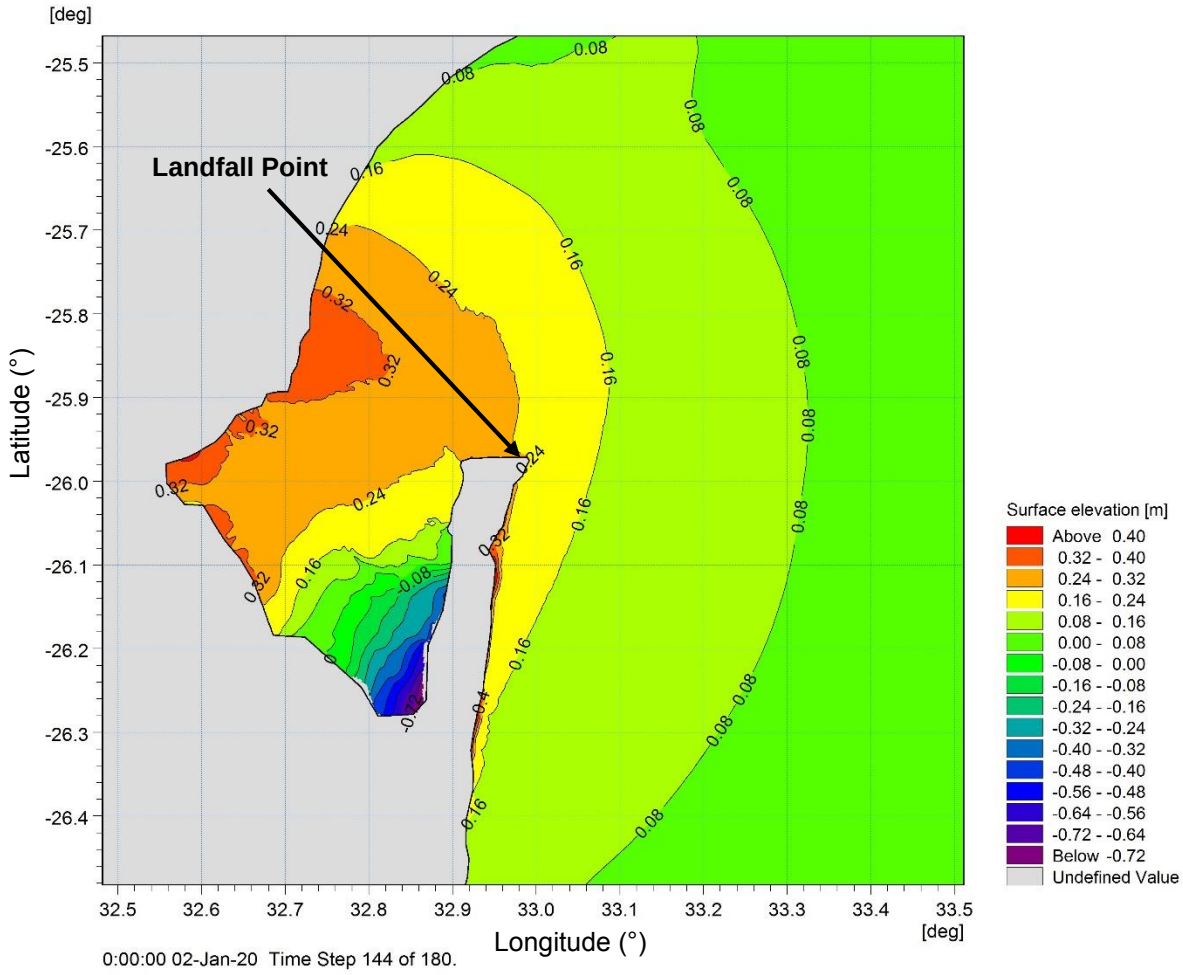

Figure 7.5: Spatial plot of the storm surge contours at the time of landfall at Maputo, for a 100-year return period

Table 7.3 summarizes the peak storm surge levels produced in the model tests. Two areas of investigation are presented. The first is the immediate area surrounding the location and the second is the total area where the expected maximum storm surge occurs. Two storm surge levels are presented for each area in Table 7.3. These refer to the minimum and maximum strom surge levels of the specified output points at each location.

Table 7.3: Minimum and maximum H_s values for the model simulations

	Immediate Area		Total Area	
Location	S_{min} (m)	S_{max} (m)	S_{min} (m)	S_{max} (m)
Durban 50-Year	0.08	0.09	0.06	**0.09**
Maputo 50-Year	0.26	0.35	0.13	**0.49**
Beira 50-Year	0.77	0.93	0.76	**1.05**
Pemba 50-Year	0.22	0.25	0.11	**0.25**
Durban 100-Year	0.16	0.17	0.12	**0.17**
Maputo 100-Year	0.31	0.45	0.16	**0.65**
Beira 100-Year	1.00	1.22	1.00	**1.38**
Pemba 100-Year	0.24	0.27	0.12	**0.27**
Durban 200-Year	0.20	0.22	0.16	**0.22**
Maputo 200-Year	0.38	0.60	0.20	**0.85**
Beira 200-Year	1.32	1.62	1.32	**1.81**
Pemba 200-Year	0.26	0.28	0.13	**0.28**
Durban 500-Year	0.28	0.31	0.23	**0.31**
Maputo 500-Year	0.45	0.78	0.26	**1.11**
Beira 500-Year	1.55	1.91	1.55	**2.12**
Pemba 500-Year	0.29	0.32	0.15	**0.32**

Figure 7.6 illustrates the variation of the storm surge levels experienced along the coast at each of the locations. The specified output points are plotted showing the surge levels north and south of the point, where the tropical cyclone made landfall. Distances north of the landfall point are presented as positive values and southerly distances are negative. The values are the results from the 100-year simulation. The other three return periods are not shown as they exhibit the same trend, just with different magnitudes.

From Figure 7.6, it is evident that the largest storm surge levels are located at different points for each location. Durban and Pemba have peak surge levels around the point of tropical cyclone landfall. Beira's peak surge is located approximately 26 km south of the landfall point. The dramatic change in surge levels at Maputo is due to the specified output points that are located in the bay of Maputo. The points follow the 10 m contour. Maputo reaches a peak surge 20 km south of the landfall point. The bathymetry plays a vital role in determining the storm surge levels. A shallow slope, such as the slopes at Maputo and Beira, generate larger storm surges compared to steep shelves at Durban and Pemba, because there is less space for the water to flow back into the ocean.

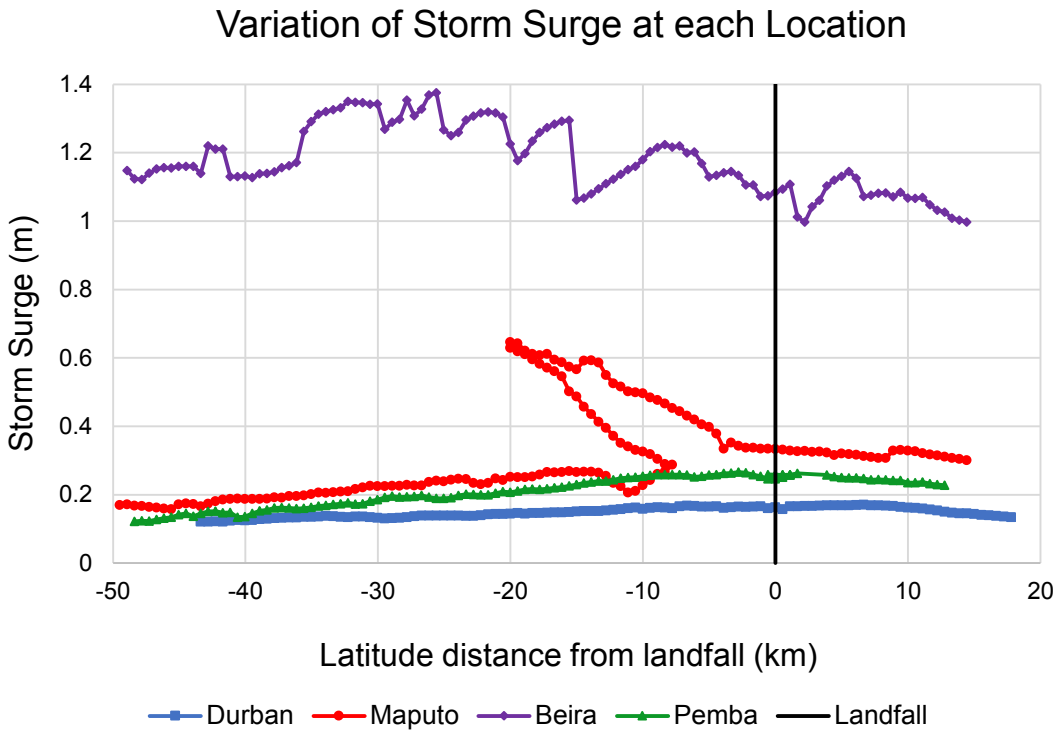

Figure 7.6: Variation of storm surge at each of the locations

The difference in locations of peak surge levels is due to the composition of the storm surge. The wind component of the storm surge is more prevalent at Beira, than at Durban and Pemba, and therefore has a peak surge located around the point of maximum winds. At Durban and Pemba, the pressure component of storm surge is more prevalent and therefore peaks around the tropical cyclone centre where the lowest pressures are observed. The bathymetry of the coast also influences the location of peak surge levels. The peak surge levels are located at shallow slopes.

As with the waves, it is assumed that if the tropical cyclone made landfall further north/south, the peak storm surge levels could be experienced further north/south at the specific location. Therefore, the design storm surge level for each location is taken as the maximum value of the whole area instead of just at the specific location. Table 7.4 summarizes the estimates of the storm surge levels at various return periods that can be expected along the Southern African East Coast. The estimated storm surge values range from 0.09 m to 2.12 m.

Table 7.4: Estimates of the expected storm surge levels caused by tropical cyclones along the Southern African East Coast

	Estimated Storm Surge (m)			
Return Period	Durban	Maputo	Beira	Pemba
50	0.09	0.49	1.05	0.25
100	0.17	0.65	1.38	0.27
200	0.22	0.85	1.81	0.28
500	0.31	1.11	2.12	0.32

7.4. Discussion of Results

7.4.1. Waves

The peak significant wave heights in Table 7.2 are plotted in Figure 7.7 for the comparison of tropical cyclone-induced waves along the Southern African East Coast.

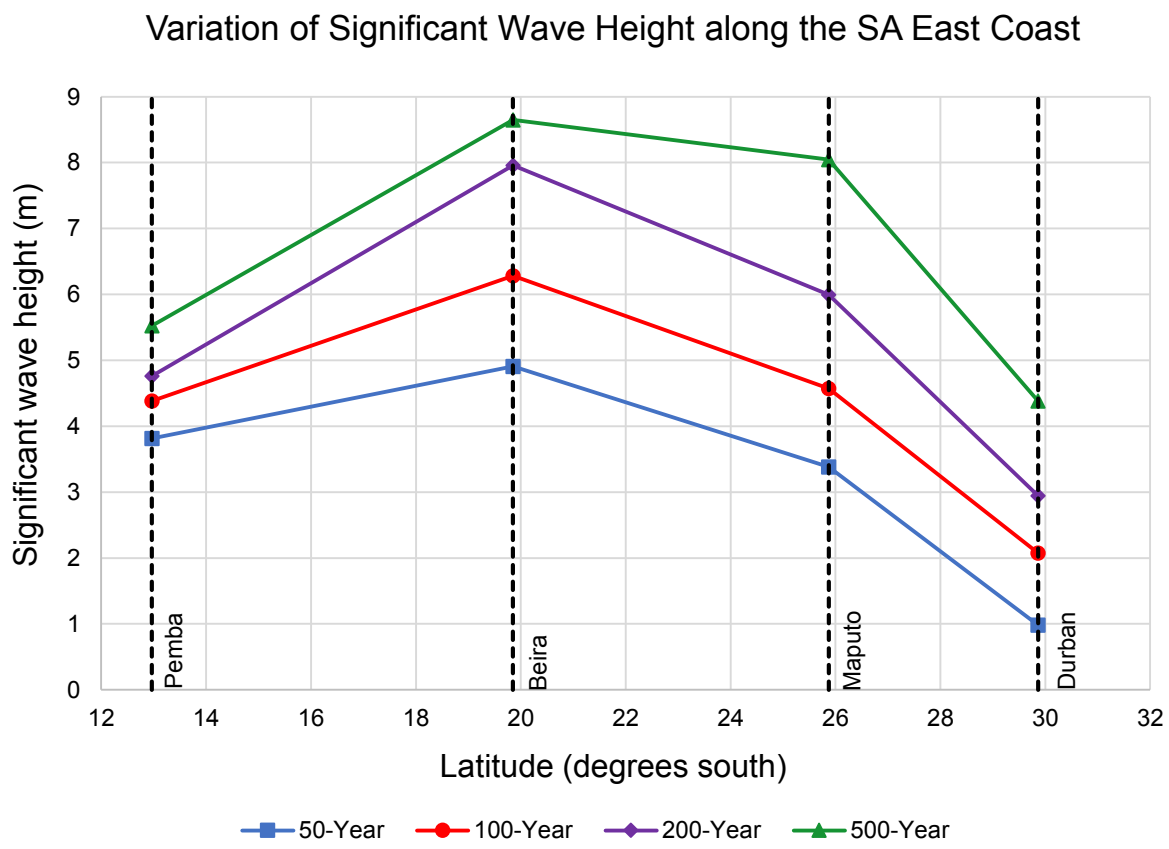

Figure 7.7: Tropical cyclone-induced wave heights along the Southern African East Coast

From Figure 7.7, it is evident that Beira experiences the largest waves out of the four locations along the coast. At the 500-year return period, a significant wave height of 8.6 m is expected

to occur at Beira. This is a very large wave, which engineers will have to take into consideration in the design of structures along this part of the coast. Due to Beira's relatively broad continental shelf, a lot of the wave energy is dissipated. This is illustrated in Figure 7.8, where the maximum significant wave height during the 500-year simulation, is plotted. The maximum offshore significant wave height caused by this 500-year tropical cyclone, is 11.9 m, meaning the wave height is reduced by 3.2 m when it arrives at the 20 m contour in Beira.

Durban experiences the smallest waves out of the four locations. Two reasons exist for the small waves. The first is due to the limited number of tropical cyclones that move so far south. From Table 2.2 (Section 2.4.1) of Rossouw's (1999) study, Durban is expected to experience 1.5 tropical cyclones over a period of 100 years. The second reason is due to the reduced wind speeds from Fearon's (2014) study (Figure 2.16) that are expected to occur at Durban. Cut-off low pressure systems pose more of a threat in terms of the expected waves at Durban. Pemba and Maputo experience similar wave heights at the 50 and 100-year return periods, although at the 200 and 500-year return period, considerably larger waves are expected to occur at Maputo.

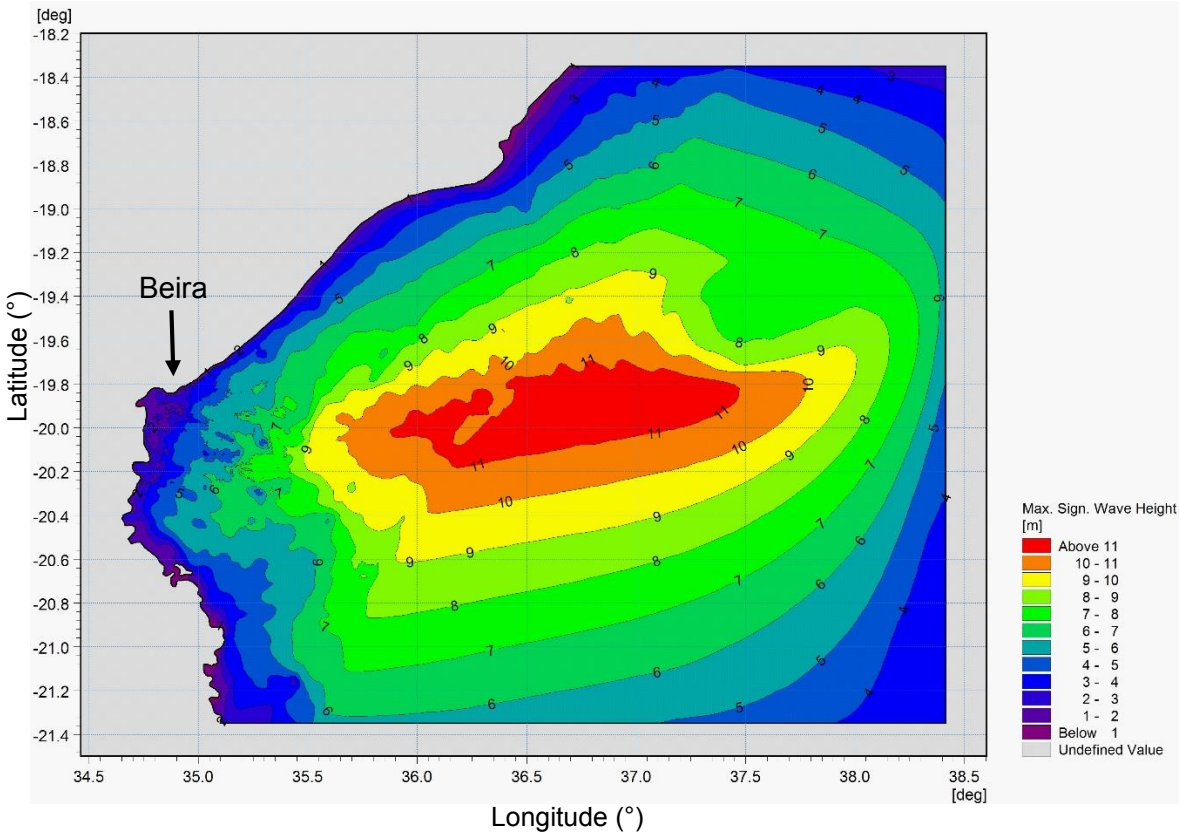

Figure 7.8: Contour plot showing the maximum significant wave height reached during the 500-year simulation at Beira

7.4.2. Storm Surge

The peak storm surge levels in Table 7.4 are plotted in Figure 7.9 for the comparison of tropical cyclone-induced storm surge along the Southern African East Coast.

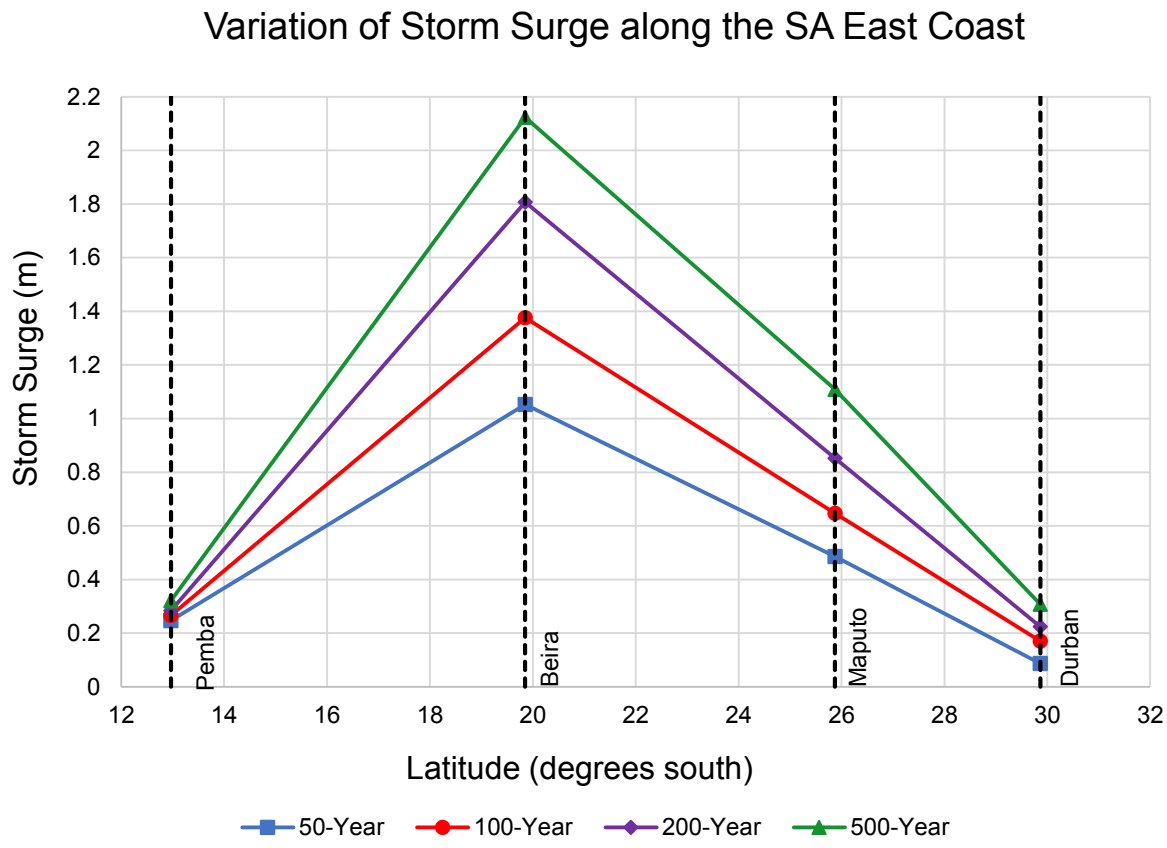

Figure 7.9: Tropical cyclone-induced storm surge levels along the Southern African East Coast

From Figure 7.9, it is evident that Beira experiences the largest storm surge out of the four locations along the coast. At the 500-year return period, a storm surge of 2.1 m is expected to occur at Beira. This is illustrated in Figure 7.10, where the maximum storm surge level during the 500-year simulation, is plotted. Two reasons exist for the high storm surge levels experienced at Beira. The first is due to the high wind speeds expected to be produced by tropical cyclones at Beira, from Fearon's (2014) study (Figure 2.16). The second reason is due to the relatively flat and shallow continental shelf in the region surrounding Beira. A shallow slope has a larger storm surge because there is less room for the water to flow back into the ocean. In addition, Beira has a converging coastline, which creates a funnel effect as the sea moves into the bay.

The storm surge at Maputo is also considerable, with storm surge levels ranging from 0.5 m to 1.1 m. This can be attributed to the broad continental shelf at Maputo. Storm surge caused

by tropical cyclones at Pemba and Durban, is of not much concern, with maximum storm surge levels of roughly 0.3 m at the 500-year return period. Two reasons exist for the low surge levels. The first is due to low intensity tropical cyclones that reach the locations. The second reason is due to the relatively narrow continental shelf at the two locations. Tropical Cyclone Eline, which made landfall 80 km south of Beira in February 2000, generated an estimated storm surge of over 4 m (INGC, 2009). The 2.1 m storm surge estimated for Beira, at a return period of 500 years, is therefore slightly low. This is further confirmation that the model tends to under-predict the storm surge, as discussed in Section 6.4.

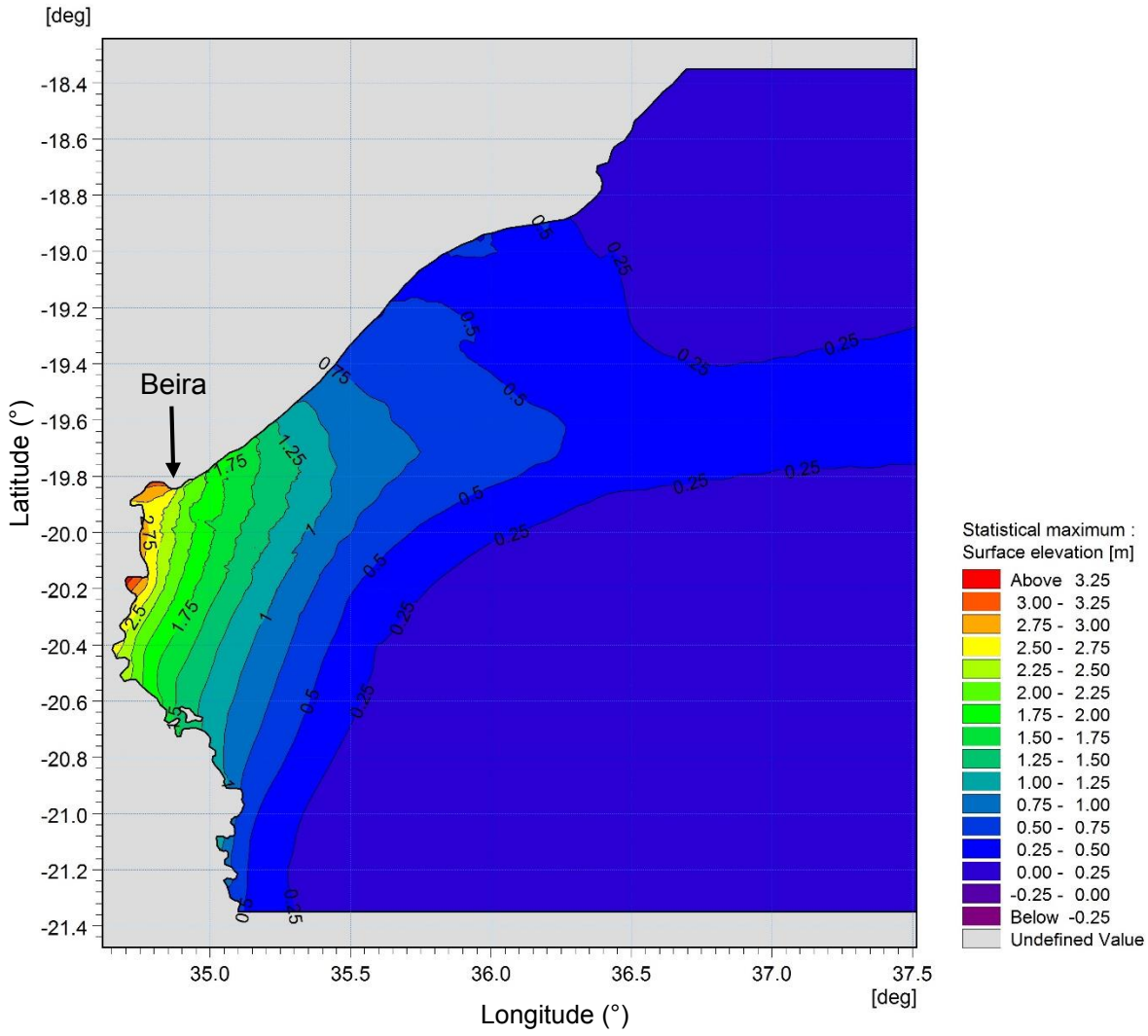

Figure 7.10: Contour plot showing the maximum storm surge level reached during the 500-year simulation at Beira

8. Conclusions and Recommendations

8.1. Conclusions

In the planning and design of infrastructure along a coast, the risk exposure to tropical cyclone-induced threats is of utmost importance in areas susceptible to these storms. Considerable research into the risk presented by tropical cyclones, has been conducted using numerical models, although very little has been done for the South-West Indian Ocean. The objective of this thesis is to determine best estimates of the 50-, 100-, 200- and 500-year significant wave height and storm surge levels expected to be produced by tropical cyclones, at four locations along the Southern African East Coast. This objective has been achieved by generating these parameters using numerical modelling techniques at each of the four locations.

The waves and storm surge levels were investigated by applying third-generation numerical models at each of the four locations, namely; Durban, Maputo, Beira and Pemba. Extreme wind speed estimates resulting from a previous study by Fearon (2014), were used as wind input into the numerical models. Various methods were employed to determine the remaining input parameters. Historical tropical cyclone data from the best track data, as well as the results of other studies, were used as input. Sensitivity tests using these parameters were conducted in order to see how each parameter influences the model results. The results of the sensitivity tests were used to determine the design storm parameters for the proposed numerical model tests.

The model tests comprised of the numerical modelling of a tropical cyclone varying in time and space, resulting in estimates of the significant wave height and storm surge levels at the location of interest. A total of four return periods were simulated for each of the four locations, resulting in a total of 16 simulations. The output of the simulations were specified at points along the 20 m contour for the waves and the 10 m contour for storm surge. The maximum significant wave height and storm surge level reached, considering all the points, was taken as the design estimate.

The numerical model was calibrated by simulating Hurricane Ike, which occurred over the Gulf of Mexico in September 2008. The model produced reasonably good results when compared to the measured data, although the model did under-estimate the storm surge. It is advisable to take this into account when using the estimates of the expected storm surge levels.

The results of the model tests indicate that the expected waves produced by tropical cyclones along the Southern African East Coast, do pose a major threat and need to be taken into consideration in the planning and design of coastal infrastructure. The largest waves are

expected to occur at Beira and the smallest at Durban. At the 100-year return period, Durban, Maputo, Beira and Pemba have expected significant wave heights of 2.1 m, 4.6 m, 6.3 m and 4.4 m respectively. Estimates of the expected tropical cyclone-induced storm surge indicate that Durban and Pemba are not at risk of flooding, with maximum expected storm surge levels of roughly 0.3 m at the 500-year return period. Beira and Maputo on the other hand, are at risk with maximum storm surge levels of 2.1 m and 1.1 m respectively, at the 500-year return period.

8.2. Recommendations

Due to time constraints, a limited number of locations along the Southern African East Coast were investigated. In Figures 7.7 and 7.9, there is a large gap between the locations, leaving a large portion of coast unknown in terms of the expected waves and storm surge. In the application of the results of this study, it is not recommended that the user interpolate the values between the locations in Figures 7.7 and 7.9 for detailed studies. However, as a first approximation, interpolating between the locations would provide reasonably good estimates. It is therefore recommended that the tests be extended to include more locations for investigation. This would allow for a better representation of the expected waves and storm surge along the Southern African East Coast.

In addition to waves and storm surge, tropical cyclones can be destructive to a coast by means of currents generated by waves, and sediment transport. Quantification of the risk exposure to tropical cyclone-induced currents and sediment transport would be of great value to a coast and its infrastructure. It is recommended that the present research be extended to include the expected estimates of currents and sediment transport rates caused by tropical cyclones, at various return periods of interest.

The methodology used for this study was based on a deterministic approach, where the design storm parameters were developed from various sources. In this approach, constant design parameters were used in the simulations. In reality, this is not the case, as storms tend to build up and decay over time. In order to overcome this problem, a probabilistic approach can be adopted for the present study. In this approach, the 5000 years of synthetic tropical cyclone tracks resulting from Fearon's (2014) study are used. Using a coupled spectral wave and hydrodynamic model, each synthetic track is simulated. For each simulation, the significant wave height and storm surge level is determined at the site of interest, allowing extreme values to be derived. The shortcoming of this approach is the large number of simulations required, which is why the deterministic approach was adopted for the present study.

The ocean temperature has risen due to the effects of climate change. As a result, the minimum sea-surface temperature required for the generation of tropical cyclones has moved further south, and hence the storms are also moving south. This means that the South African coastline will be increasingly affected by tropical cyclones in the future. By considering climate change, a study of tropical cyclone-induced waves and storm surge at more southerly locations in South Africa, such as East London and Mossel Bay, could be investigated using the methods of the present study.

References

Berg, R. 2009. Tropical Cyclone Report Hurricane Ike (AL092008) 1 - 14 September 2008. National Hurricane Center.

Chadwick, A., Morfett, J. & Borthwick, M. 2004. Hydraulics in Civil and Environmental Engineering 4th ed., Abingdon: Spon Press.

Conner, W.C., Kraft, R.H. & Harris, D.L. 1957. Empirical methods for forecasting the maximum storm tides due to hurricanes and other tropical storms. *Monthly Weather Rev*. 85: 113-116

Dean, R.G. &. Dalrymple, R.A. 2002. Coastal processes with engineering applications. Cambridge: Cambridge University Press

Depperman, C. 1947. Notes on the Origin and Structure of Philippine Typhoons. *Bulletin of the American Meteorological Society, 28*: 399 - 404.

DHI, 2014a. Mike 21/3 Coupled Model FM – User Guide. Copenhagen, Denmark: Danish Hydraulic Institute.

DHI, 2014b. Mike 21 Flow Model FM, Hydrodynamic Module – User Guide. Copenhagen, Denmark: Danish Hydraulic Institute.

DHI, 2014c. Mike 21 SW, Spectral Waves FM Module – User Guide. Copenhagen, Denmark: Danish Hydraulic Institute.

DHI, 2014d. Mike 21, Cyclone Wind Generation Tool – Scientific Documentation. Copenhagen, Denmark: Danish Hydraulic Institute.

Dima, I., & Desflots, M. 2010. Wind Profiles in Parametric Hurricane Models. [Online]. Available: http://www.air-worldwide.com/Publications/AIR-Currents/attachments/AIRCurrents--Wind-Profiles-in-Parametric-Hurricane-Models/ [2016, July 18].

Emanuel, K., Vivant, S., & Risi, C. 2006. A Statistical Deterministic Approach to Hurricane Risk Assessment. *American Meteorological Society, 87*, 299 - 314.

Fearon, G. 2014. Extreme Wind Speeds for the South-West Indian Ocean using Synthetic Tropical Cyclone Tracks. Thesis prepared for Master's degree in Civil Engineering. University of Stellenbosch

GEBCO. 2014. General Bathymetric Chart of the Oceans. [Online]. Available: http:// http://www.gebco.net. [2016, June 14].

Google Earth V 7.1.7.2600. 1970a. Southern African East Coast. 19.8497° S, 34.8904° E. AfriGIS (Pty) Ltd, 2016. Available: https://www.google.co.za/earth/ [2016, June 26].

Google Earth V 7.1.7.2600. 1970b. Gulf Of Mexico. 29.4304° N, 94.7499° W. INEGI, 2016. Available: https://www.google.co.za/earth/ [2016, September 21].

Gourlay, M.R. 1992. Wave set-up, wave run-up and beach water table: Interaction between surf zone hydraulics and groundwater hydraulics. *Coastal Engineering,* 17.1-2: 93 - 144

Graf, M., & Nishijima, K. 2009. A Probabilistic Typhoon Model for the Northwest Pacific Region. Taipei, Taiwan: Paper Presented at the Seventh Asia-Pacific Conference on Wind Engineering.

Graham, S. & Riebeek, H. 2006. *Hurricanes: The Greatest Storms on Earth*. [Online]. Available: http://earthobservatory.nasa.gov/Features/Hurricanes/hurricanes_1.php. [2016, February 16].

Gray, W.M. 1968. A global view of the origin of tropical disturbances and storms. *Monthly Weather Review*, 96.10: 669-700.

Gray, W.M. 1979. Hurricanes: Their formation, structure and likely role in the tropical circulation. In D. B. Shaw (ed.) *Meteorology over the Tropical Oceans*, Royal Meteorological Society, James Glaisher House, Grenville Place, Bracknell.155-218

Hanslow, d. & Nielsen, P. 1993. Shoreline Set-up on Natural Beaches. *Journal of Coastal Research,* 15: 1-10.

Harper, B., Hardy, T., Mason, L. & Astorquia, A. 2004. Queensland Climate Change and Community Vulnerability to Tropical Cyclones, Ocean Hazards Assessment. Stage 2. Tropical Cyclone Induced Water Levels and Waves: Hervey Bay and Sunshine Coast. Queensland Government.

Harper, B., Hardy, T., Mason, L., Bode, L., Young, I., & Nielsen, P. 2001. Queensland Climate Change and Community Vulnerability to Tropical Cyclones, Ocean Hazards Assessment - Stage 1. Brisbane, Queensland, Australia: Department of Natural Resources and Mines.

Holland, G. 1980. An Analytical Model of the Wind and Pressure Profiles in Hurricanes. *Monthly Weather Review*, 108: 1212 – 1218.

Holland, G.J. 1993. Ready Reckoner - Chapter 9. *Global Guide to Tropical Cyclone Forecasting*. WMO/TC-No. 560, Report No. TCP-31. Geneva, Switzerland: World Meteorological Organization.

Holthuijsen, L.H. 2007. Waves in Oceanic and Coastal Waters, New York: Cambridge University Press.

Hope, M.E., Westerink, J.J., Kennedy, A.B., Kerr, P.C., Dietrich, J.C., Dawson, C., Bender, C.J., Smith, J.M., Jensen, R.E., Zijlema, M., Holthuijsen, L.H., Luettich Jr., R.A., Powell, M.D., Cardone, V.J., Cox, A.T., Pourtaheri, H., Roberts, H.J., Atkinson, J.H., Tanaka, S., Westerink, H.J., & Westerink, L.G. 2013. Hindcast and validation of Hurricane Ike (2008) waves, forerunner, and storm surge. *Journal of Geophysical Research: Oceans*, 118: 1-37

Horikawa, K. 1978. Coastal engineering: an introduction to ocean engineering. Tokyo: University of Tokyo Press.

Hu, K., Chen, Q., & Fitzpatrick, P. 2012. Assessment of a Parametric Hurricane Surface Wind Model for Tropical Cyclones in the Gulf of Mexico. INTECH.

INGC. 2009. *Sea Level Rise and Cyclone Analysis, INGC Climate Change Report.* Mozambique: National Institute for Disaster Management.

Knaff, J., DeMaria, M., Marchok, T., Gross, J., & McAdie, C. 2007. Statistical Tropical Cyclone Wind Radii Prediction Using Climatology and Persistence. *American Meteorological Society, 22*: 781-791.

Kuleshov, Y., Chane Ming, F., Qi, L., Chouaibou, I., Hoareau, C. & Roux, F. 2009. Tropical cyclone genesis in the Southern Hemisphere and its relationship with the ENSO. *Annales Geophysicae*, 27: 2523 – 2538.

Landsea, C. 2014. *Frequently Asked Questions*. [Online]. Available: http: //www.aoml.noaa.gov/hrd/tcfaq/F1.html. [2016, February 18].

Matyas, C.J. 2014. Tropical cyclone formation and motion in the Mozambique Channel. *International Journal of Climatology*, 35: 375 – 390.

Meza-Padilla, R., Appendini, C.M. & Pedrozo-Acuna, A. 2015. Hurricane-induced waves and storm surge modelling for the Mexican coast. *Ocean Dynamics,* 65: 1199–1211.

Neumann, C.J. 1987. The national hurricane center risk analysis program (HURISK), NOAA Technical Memorandum NWS NHC 38.

NGDC. 2001. U.S. Coastal Relief Model. National Geophysical Data Center, NOAA. [Online]. Available: http://www.ngdc.noaa.gov/mgg/coastal/crm.html [2016, August 16].

NOAA, [S.a.]. Comprehensive Large Array-Data Stewardship System (CLASS). [Online]. Available: http://www.class.noaa.gov/. [2016, February 15].

Raubenheimer, B., Guza, R.T. & Elgar, S. 2001. Field observations of wave-driven setdown and setup. *Journal of Geophysical Research*, 106.C3: 4629 – 4638.

Rhome, J.R. & Raman, S. 2006. Environmental Influences on Tropical Cyclone Structure and Intensity: A Review of Past and Present Literature. *Indian Journal of Marine Sciences, 35*.2: 61 - 74.

Rossouw, C. 1999. The Probability of Occurrence and the Intensity of Tropical Cyclones along the Southern African East Coast. Thesis prepared for Master's degree in Civil Engineering. University of Stellenbosch

Rossouw, J. 1989. Design waves for the South African Coastline. PhD Thesis prepared for the degree of Doctor of Philosophy. University of Stellenbosch

Sampson, C. R. & Schrader, A. J. 2000. The Automated Tropical Cyclone Forecasting System (Version 3.2). *Bulletin of the American Meteorological Society.* 81, 1231-1240.

Smith, J.M. 2013. Wave and Storm Surge Modeling. 6th SCACR – International Short Course/Conference on Applied Coastal Research.

Sobey, R.J., Harper, B.A. & Stark, K.P. 1977. Numerical simulation of tropical cyclone storm surge. Research Bulletin CS-14, Dept Civil and Systems Engineering, James Cook University.

Theron, A.K., Barwell, L., Maherry, A., Luck-Vogel, M., Robberts, W., Rossouw, M., Terblanche, L., de Wet, P., Rafael, J. & Araujo, F. 2012. Responding to climate change in Mozambique: Theme 2: Coastal planning and adaptation to mitigate climate change impacts. Stellenbosch: CSIR.

USACE, 1984. Shore protection manual (SPM). Department of the Army, U S Army Corps of Engineers, CERC, Vicksburg, Mississippi. Vol. 1

USACE, 2006. Coastal Engineering Manual, Part II. Morang, ed., Mississippi: US Army Corps of Engineers

Willoughby, H. E., & Rahn, M. E. 2004. Parametric Representation of the Primary Hurricane Vortex. Part I: Observations and Evaluation of the Holland (1980) Model. *Monthly Weather Review, 132*: 3033-3048.

Willoughby, H. E., Darling, R., & Rahn, M. E. 2006. Parametric Representation of the Primary Hurricane Vortex. Part II: A New Family of Sectionally Continuous Profiles. *Monthly Weather Review*, 134: 1102 – 1120.

WMO. [S.a.]. *Tropical Cyclones: Questions and Answers.* [Online]. Available: http://www.wmo.int/pages/mediacentre/factsheet/tropicalcyclones.html. [2016, February 11].

Yin, J., Welch, M., Yashiro, H., & Shinohara, M. 2009. Basin wide Typhoon Risk Modelling and Simulation for Western North Pacific Basin. Taipei, Taiwan: Paper Presented at The Seventh Asia-Pacific Conference on Wind Engineering (APCWE7).

Young, I.R. & Sobey, R.J. 1981. The numerical prediction of tropical cyclone wind-waves, James Cook University of North Queensland, Townville, Dept. of Civil & Systems Eng., Research Bulletin No. CS20

Appendix A: Sensitivity Test Data

Météo France La Réunion (MFR) provide R_{max} estimates of tropical cyclones over the South-West Indian Ocean during the years 2004 to 2014. Using this data, a comparison of the historically measured values to empirically formulated values of R_{max} found in the literature was made. Only R_{max} values of tropical cyclones that entered the Mozambique Channel (defined as area of ocean between Mozambique and 45°E line of longitude) were taken into consideration, as this is the area of interest for the present study. A list of these tropical cyclones can be found in Table A-1.

Table A-1: Tropical Cyclones entering the Mozambique Channel during the years 2004 - 2014

Number	Year	Name
1	2004	Cela
2	2004	Elita
3	2004	Gafilo
4	2005	Ernest
5	2006	Boloetse
6	2007	Anita
7	2007	Bondo
8	2007	Favio
9	2008	Elnus
10	2008	Fame
11	2008	Jokwe
12	2009	Fanele
13	2009	Izilda
14	2010	Joel
15	2012	Funso
16	2012	Giovanna
17	2012	Irina
18	2013	Haruna
19	2014	Guito
20	2014	Hellen

The Joint Typhoon Warning Centre (JTWC) provides information on historical tropical cyclones. The JTWC also provides historical tropical cyclone tracks that can be viewed in Google Earth, from 1982 to 2014. These tracks were used with Google Earth to determine three track directions to be used in the sensitivity tests. From the 33 years of historical tracks, only the tropical cyclones making landfall on the Southern African East Coast were taken into consideration. A list of the 21 tropical cyclones and their calculated track directions are presented in Table A-2.

Table A-2: Tropical cyclones making landfall during the years 1982 – 2014.

Number	Year	Name	Track Direction (°)
1	1982	Benedicte	291
2	1982	Electre	287
3	1984	Domoina	237
4	1986	Berobia	295
5	1988	02S	206
6	1988	Filao	305
7	1994	Nadia	260
8	1995	Fodah	26
9	1996	Bonita	255
10	1997	Lizette	294
11	1998	13S	180
12	2000	Eline	282
13	2000	Hudah	353
14	2003	Atang	270
15	2003	Delfina	282
16	2003	Japhet	306
17	2007	Favio	313
18	2008	Jokwe	232
19	2009	Izilda	289
20	2013	Haruna	345
21	2014	Hellen	224

Appendix B: Numerical Model Wind Field Input

Table B-1: Durban's 100-year simulation wind field input

Time (hours)	Longitude (°)	Latitude (°)	R_{max} (km)	V_{max} (m/s)	P_c (hPa)	P_n (hPa)
0	34.5811	-29.4389	31	12.8731	996	1013
24	31.0447	-29.8641	31	12.8731	996	1013
30	30.1562	-29.9556	31	12.8731	996	1013

Table B-2: Durban's 200-year simulation wind field input

Time (hours)	Longitude (°)	Latitude (°)	R_{max} (km)	V_{max} (m/s)	P_c (hPa)	P_n (hPa)
0	34.5811	-29.4389	31	16.0889	991	1013
24	31.0447	-29.8641	31	16.0889	991	1013
30	30.1562	-29.9556	31	16.0889	991	1013

Table B-3: Durban's 500-year simulation wind field input

Time (hours)	Longitude (°)	Latitude (°)	R_{max} (km)	V_{max} (m/s)	P_c (hPa)	P_n (hPa)
0	34.5811	-29.4389	31	20.5106	983	1013
24	31.0447	-29.8641	31	20.5106	983	1013
30	30.1562	-29.9556	31	20.5106	983	1013

Table B-4: Maputo's 100-year simulation wind field input

Time (hours)	Longitude (°)	Latitude (°)	R_{max} (km)	V_{max} (m/s)	P_c (hPa)	P_n (hPa)
0	36.1630	-25.4541	31	21.3146	982	1013
24	32.7517	-25.8721	31	21.3146	982	1013
30	31.8953	-25.9642	31	21.3146	982	1013

Table B-5: Maputo's 200-year simulation wind field input

Time (hours)	Longitude (°)	Latitude (°)	R_{max} (km)	V_{max} (m/s)	P_c (hPa)	P_n (hPa)
0	36.1630	-25.4541	31	25.3344	974	1013
24	32.7517	-25.8721	31	25.3344	974	1013
30	31.8953	-25.9642	31	25.3344	974	1013

Table B-6: Maputo's 500-year simulation wind field input

Time (hours)	Longitude (°)	Latitude (°)	R_{max} (km)	V_{max} (m/s)	P_c (hPa)	P_n (hPa)
0	36.1630	-25.4541	31	30.1581	965	1013
24	32.7517	-25.8721	31	30.1581	965	1013
30	31.8953	-25.9642	31	30.1581	965	1013

Table B-7: Beira's 100-year simulation wind field input

Time (hours)	Longitude (°)	Latitude (°)	R_{max} (km)	V_{max} (m/s)	P_c (hPa)	P_n (hPa)
0	38.1560	-19.4380	31	28.1482	969	1013
24	34.8905	-19.8497	31	28.1482	969	1013
30	34.0712	-19.9424	31	28.1482	969	1013

Table B-8: Beira's 200-year simulation wind field input

Time (hours)	Longitude (°)	Latitude (°)	R_{max} (km)	V_{max} (m/s)	P_c (hPa)	P_n (hPa)
0	38.1560	-19.4380	31	33.3739	958	1013
24	34.8905	-19.8497	31	33.3739	958	1013
30	34.0712	-19.9424	31	33.3739	958	1013

Table B-9: Beira's 500-year simulation wind field input

Time (hours)	Longitude (°)	Latitude (°)	R_{max} (km)	V_{max} (m/s)	P_c (hPa)	P_n (hPa)
0	38.1560	-19.4380	31	36.9917	952	1013
24	34.8905	-19.8497	31	36.9917	952	1013
30	34.0712	-19.9424	31	36.9917	952	1013

Table B-10: Pemba's 100-year simulation wind field input

Time (hours)	Longitude (°)	Latitude (°)	R_{max} (km)	V_{max} (m/s)	P_c (hPa)	P_n (hPa)
0	43.7423	-12.5689	31	20.9126	983	1013
24	40.5848	-12.9666	31	20.9126	983	1013
36	39.0027	-13.1508	31	20.9126	983	1013

Table B-11: Pemba's 200-year simulation wind field input

Time (hours)	Longitude (°)	Latitude (°)	R_{max} (km)	V_{max} (m/s)	P_c (hPa)	P_n (hPa)
0	43.7423	-12.5689	31	22.1185	981	1013
24	40.5848	-12.9666	31	22.1185	981	1013
36	39.0027	-13.1508	31	22.1185	981	1013

Table B-12: Pemba's 500-year simulation wind field input

Time (hours)	Longitude (°)	Latitude (°)	R_{max} (km)	V_{max} (m/s)	P_c (hPa)	P_n (hPa)
0	43.7423	-12.5689	31	24.1284	977	1013
24	40.5848	-12.9666	31	24.1284	977	1013
36	39.0027	-13.1508	31	24.1284	977	1013

Appendix C: Model Output Points

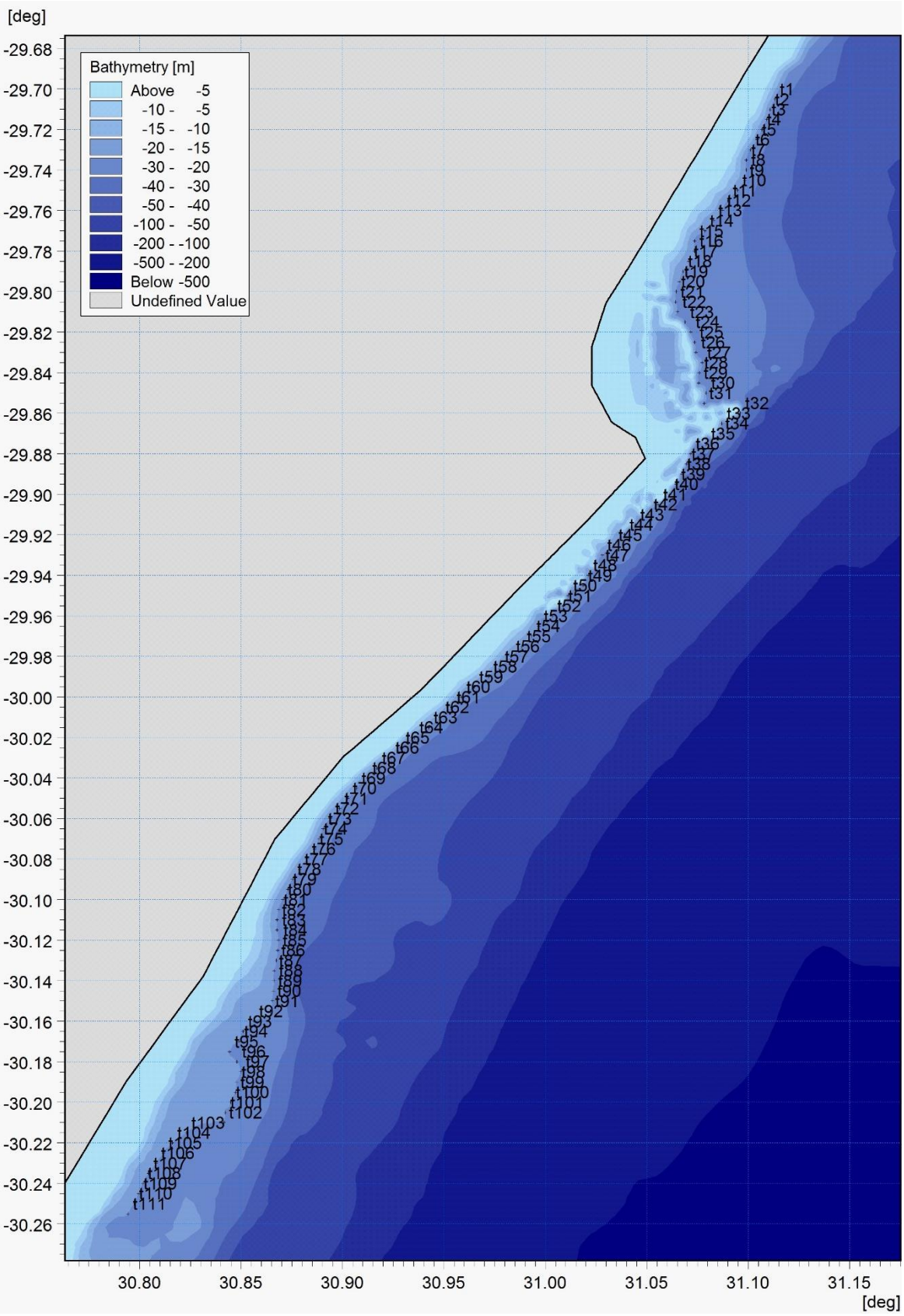

Figure C-1: Durban wave output points

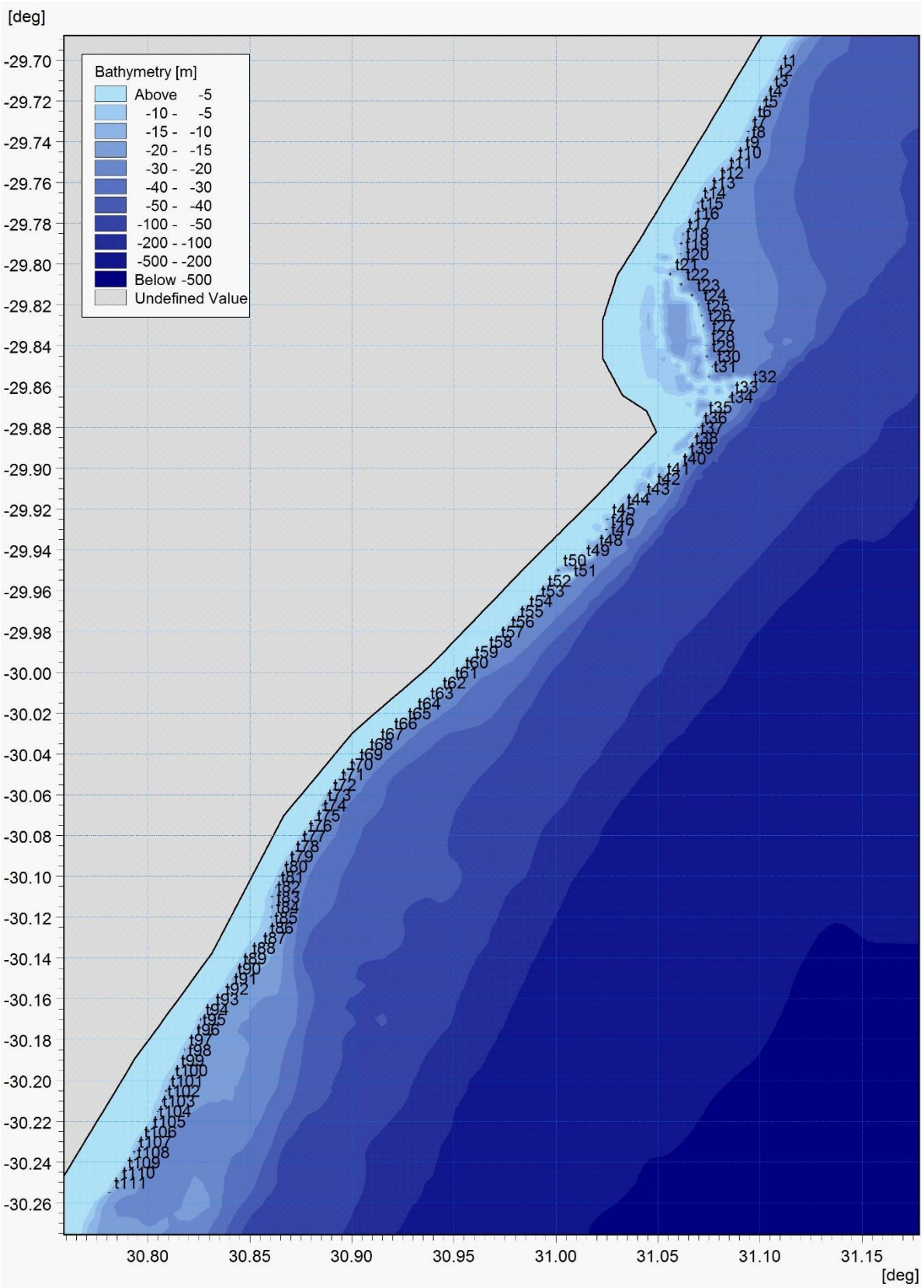

Figure C-2: Durban storm surge output points

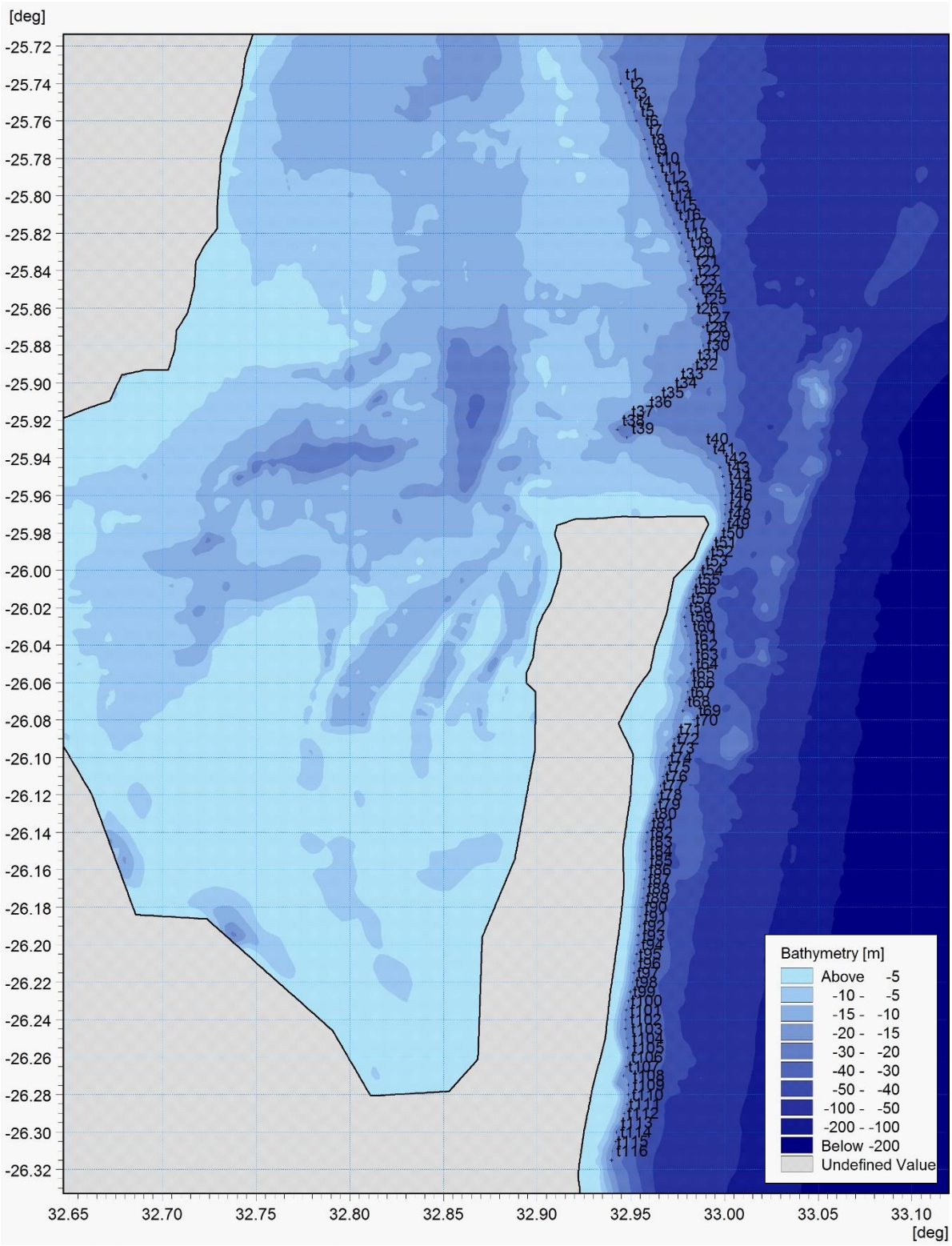

Figure C-3: Maputo wave output points

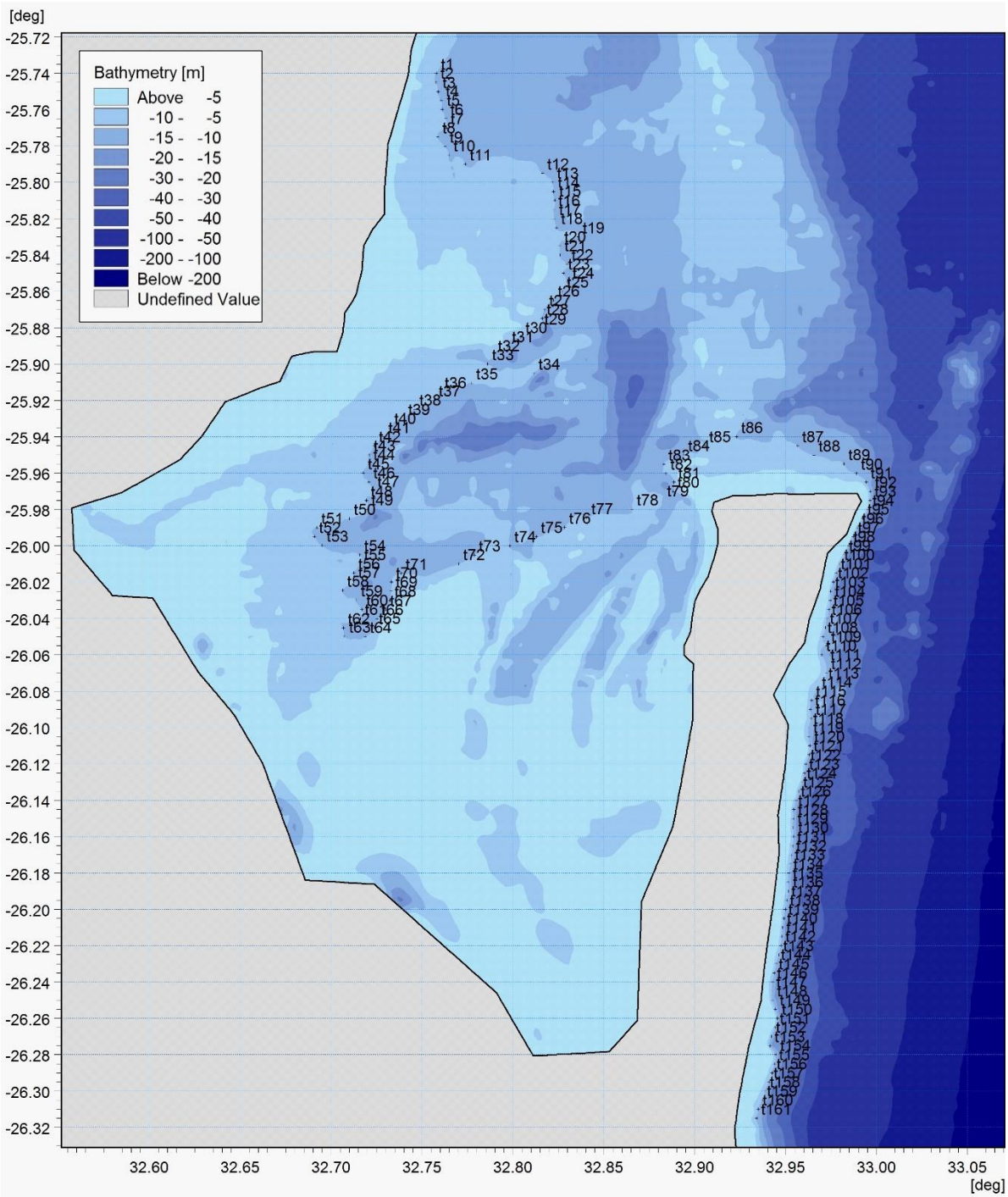

Figure C-4: Maputo storm surge output points

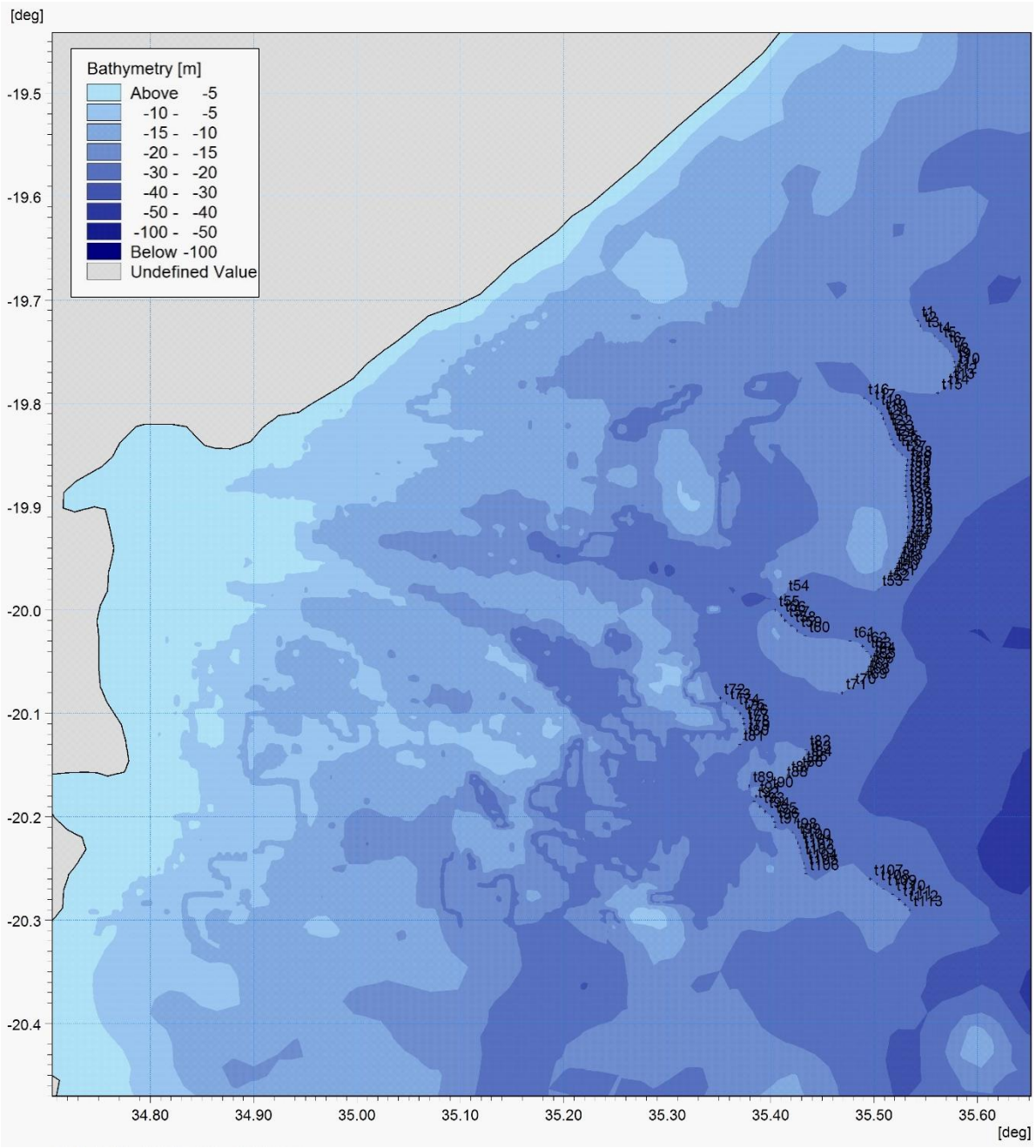

Figure C-5: Beira wave output points

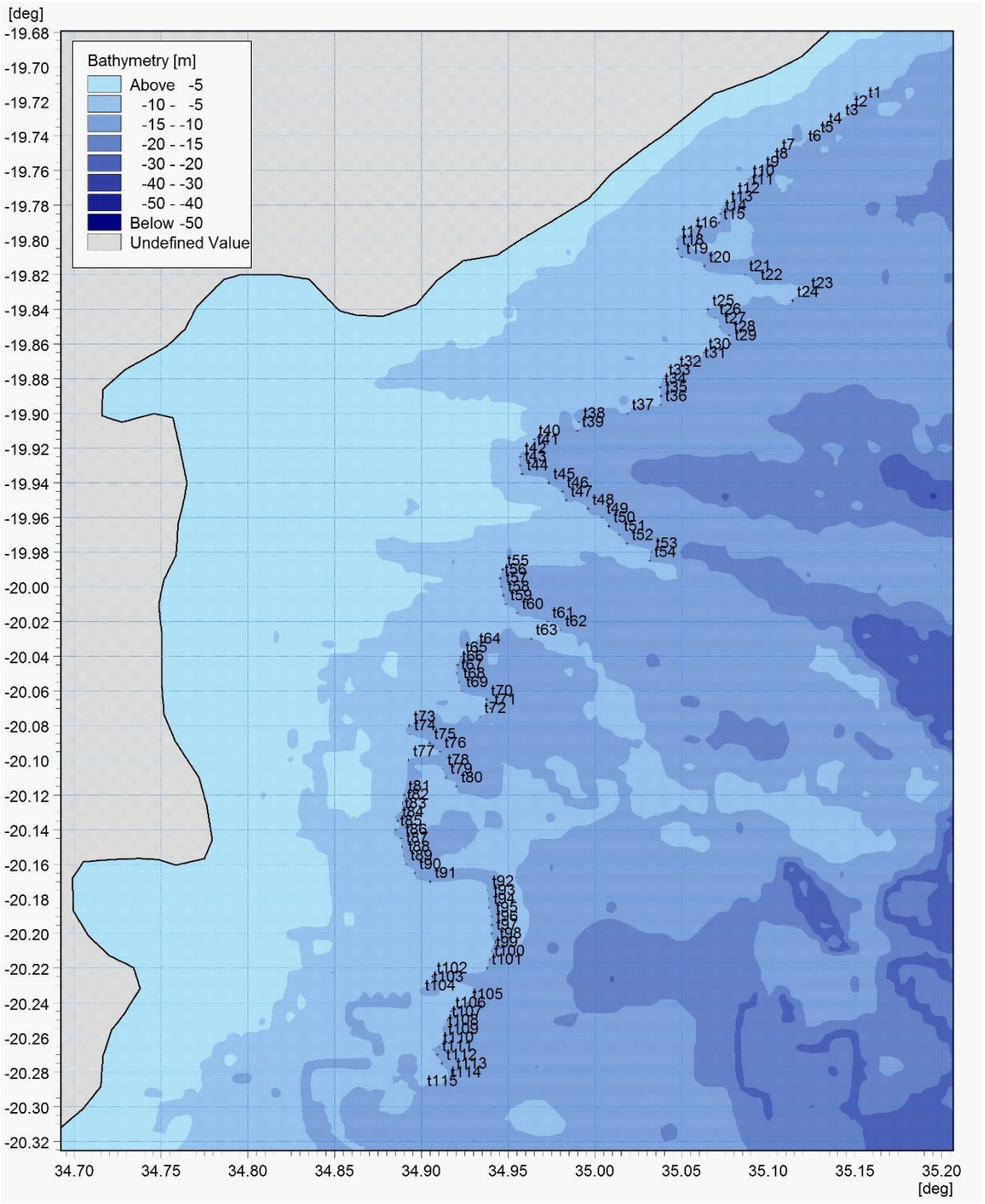

Figure C-6: Beira storm surge output points

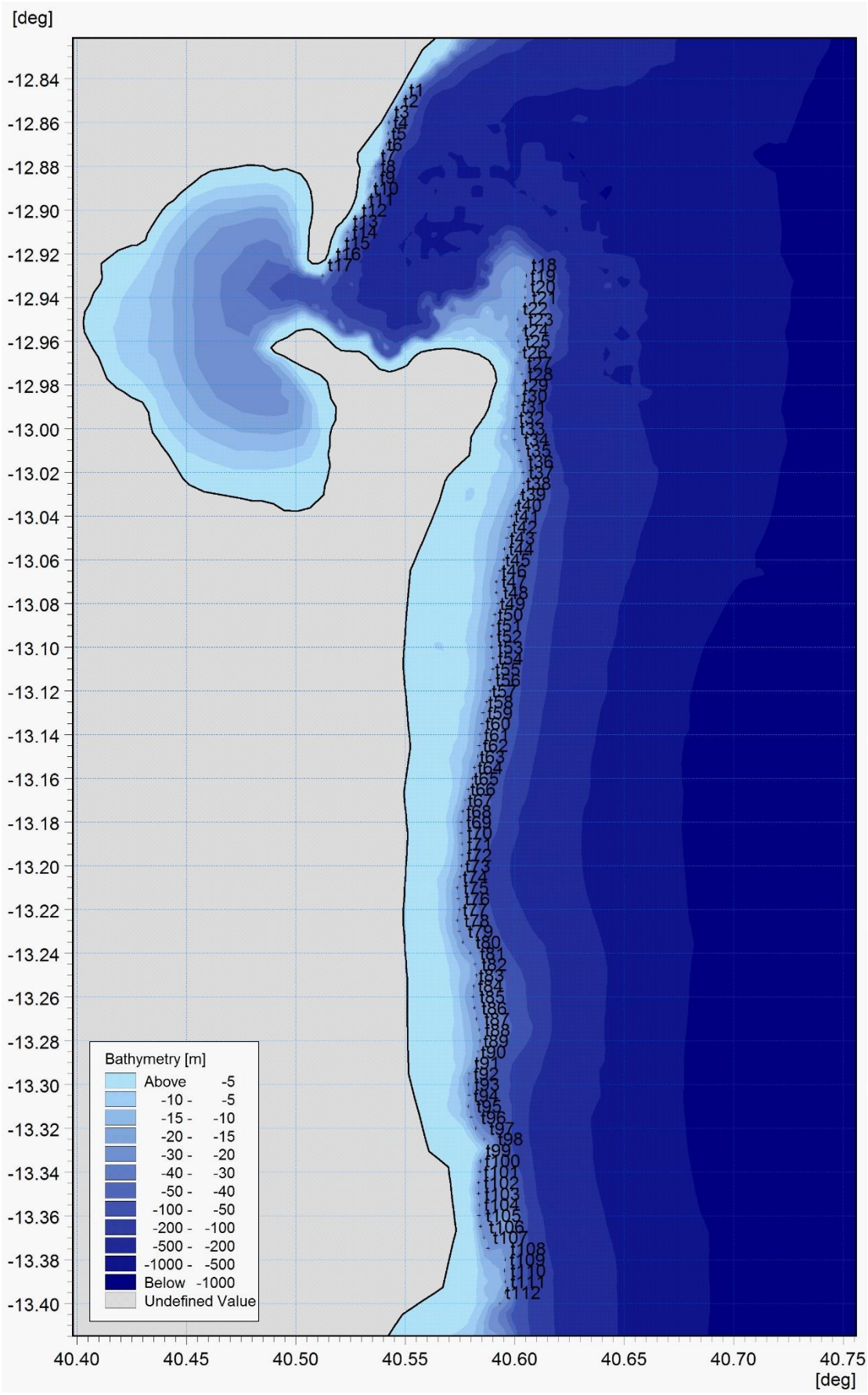

Figure C-7: Pemba wave output points

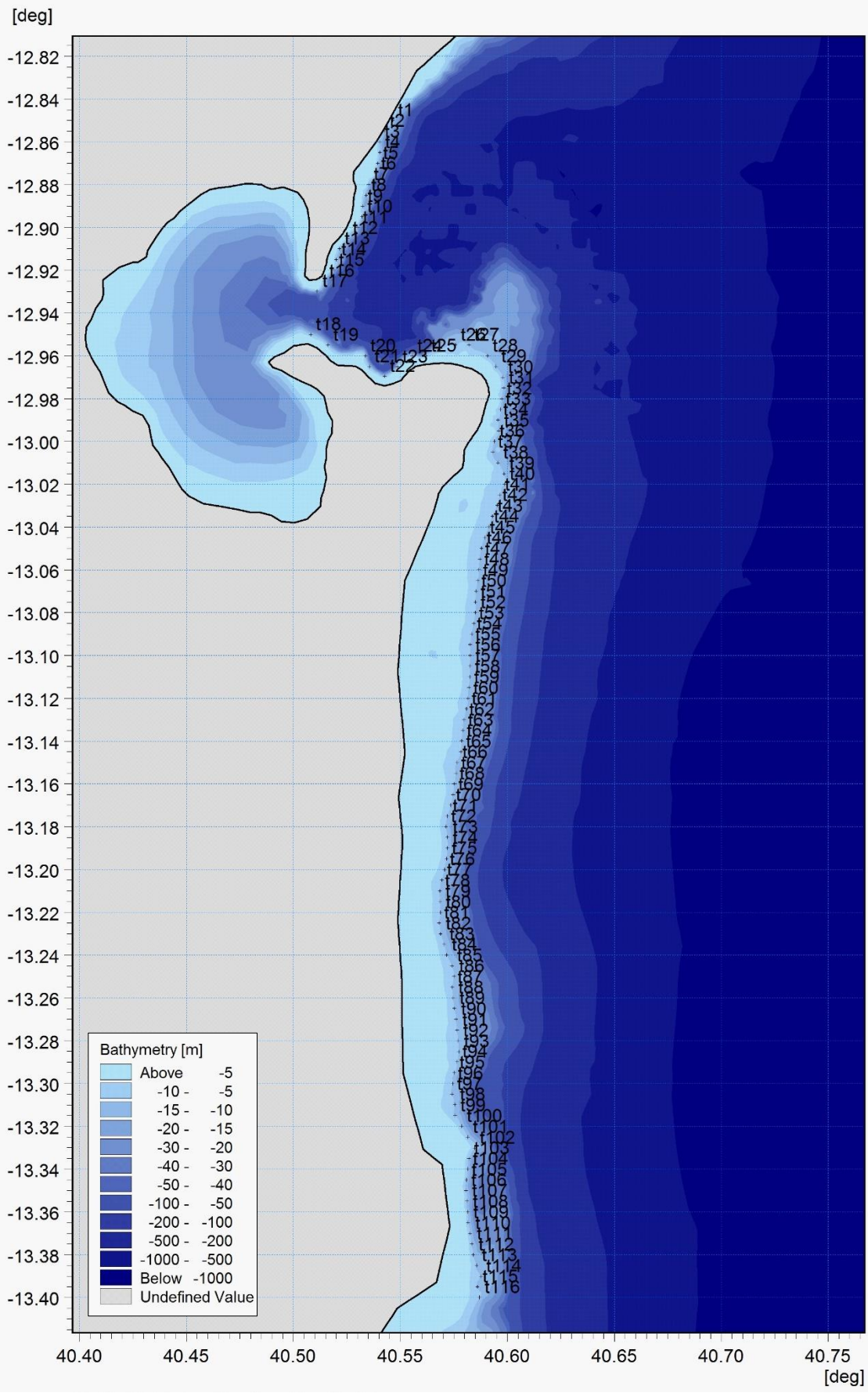

Figure C-8: Pemba storm surge output points

Appendix D: Model Output Coordinates

Table D-1: Durban model output coordinates

	Waves (20 m contour)		Storm surge (10 m contour)	
Point	Longitude (°)	Latitude (°)	Longitude (°)	Latitude (°)
1	31.11322367	-29.70498692	31.10892085	-29.70502102
2	31.11080942	-29.7100744	31.10702231	-29.70993083
3	31.1090758	-29.71511766	31.10473202	-29.7149547
4	31.10679057	-29.71992452	31.10185068	-29.71990468
5	31.10429884	-29.72498083	31.09970815	-29.72515019
6	31.10104082	-29.72998984	31.09660048	-29.7299601
7	31.09899648	-29.73497366	31.0941079	-29.73500844
8	31.09896713	-29.73998782	31.09355373	-29.73992666
9	31.09823238	-29.74498884	31.09050582	-29.74498342
10	31.09478415	-29.74998629	31.08697302	-29.75004018
11	31.08998096	-29.75498901	31.08253321	-29.75497496
12	31.08717846	-29.7600011	31.07809989	-29.75996245
13	31.08286019	-29.76494183	31.07422073	-29.76494994
14	31.07875135	-29.76997665	31.06978741	-29.76993743
15	31.07351948	-29.77502615	31.06826345	-29.77506346
16	31.07358981	-29.78000816	31.0662546	-29.77998168
17	31.07082513	-29.78496491	31.06229217	-29.78500397
18	31.06799018	-29.79001153	31.06132126	-29.78992786
19	31.06610021	-29.79501794	31.06111321	-29.79492111
20	31.06445945	-29.79997963	31.06139061	-29.79998371
21	31.06410871	-29.80499298	31.05598126	-29.80490761
22	31.0650696	-29.81002365	31.06139754	-29.8098353
23	31.06879251	-29.81496306	31.06667533	-29.81509989
24	31.07173459	-29.81999587	31.06989943	-29.82002787
25	31.07348686	-29.82498348	31.07146645	-29.82501341
26	31.07438754	-29.82997775	31.07236799	-29.82997186
27	31.07725079	-29.83500431	31.07415872	-29.83496151
28	31.07582236	-29.84001776	31.07373849	-29.83997428
29	31.07564009	-29.84499845	31.07390452	-29.84503865
30	31.07919209	-29.85000443	31.07677359	-29.84997869
31	31.07828169	-29.85498514	31.07496436	-29.85494186
32	31.09593891	-29.86000275	31.09435252	-29.85997839
33	31.08701237	-29.86498137	31.08530634	-29.86496601
34	31.08620009	-29.87000232	31.08288588	-29.86997808
35	31.0791549	-29.87498231	31.07256834	-29.87494126
36	31.07162354	-29.87996261	31.07009898	-29.88005113
37	31.06953542	-29.8850061	31.06843644	-29.8849654
38	31.06734868	-29.88996701	31.06579593	-29.89000192
39	31.0645855	-29.89496856	31.06325322	-29.8949651

40	31.06138054	-29.90003641	31.05985479	-29.90002607
41	31.0556915	-29.90496718	31.05193327	-29.90498924
42	31.05096419	-29.90999496	31.04711679	-29.90997687
43	31.04441875	-29.91498136	31.04200692	-29.91494004
44	31.03906161	-29.91999403	31.03230061	-29.92000101
45	31.03353306	-29.92498175	31.02516147	-29.92496419
46	31.02816475	-29.93002956	31.02472138	-29.93000071
47	31.02706189	-29.93501777	31.02464803	-29.93496388
48	31.02103256	-29.94000548	31.01902473	-29.93997596
49	31.01864887	-29.9449932	31.01247237	-29.94501248
50	31.01129749	-29.94998092	31.00117686	-29.9499512
51	31.00893384	-29.9550087	31.00628673	-29.95496328
52	31.00338571	-29.95999855	30.99359763	-29.95997535
53	30.99671539	-29.96498626	30.99030409	-29.96503293
54	30.99327006	-29.96999401	30.98471901	-29.96997838
55	30.98846262	-29.97500176	30.98007368	-29.97494155
56	30.9829541	-29.97996945	30.97567283	-29.97995362
57	30.97754573	-29.9849772	30.97066795	-29.98495961
58	30.97183689	-29.99000498	30.96478089	-29.99001556
59	30.9649262	-29.99501273	30.95792418	-29.994933
60	30.95871659	-30.00000045	30.95304509	-30.00007331
61	30.95370884	-30.00496813	30.94820251	-30.00491589
62	30.9483205	-30.00997588	30.94204552	-30.00989683
63	30.94245142	-30.01498363	30.93602688	-30.01501613
64	30.93545151	-30.02001467	30.92984943	-30.02011482
65	30.92864097	-30.02498236	30.92512343	-30.02496973
66	30.92359316	-30.02999011	30.91822118	-30.02990322
67	30.91688928	-30.03499589	30.91159687	-30.035022
68	30.91217068	-30.03993122	30.90631595	-30.04000181
69	30.90694259	-30.04499906	30.90133614	-30.04498163
70	30.90263593	-30.05000681	30.89654162	-30.0499846
71	30.89851459	-30.05499358	30.89232616	-30.05494125
72	30.89389093	-30.05997243	30.88838863	-30.06001371
73	30.89044621	-30.06501629	30.88584082	-30.06499352
74	30.88832244	-30.06999563	30.88368676	-30.0699965
75	30.88630171	-30.07493943	30.88049041	-30.07499947
76	30.88253886	-30.0799735	30.87639076	-30.08000245
77	30.87887772	-30.08500758	30.87351868	-30.08502858
78	30.87530418	-30.09001306	30.87029917	-30.08998523
79	30.87302389	-30.0949038	30.86721864	-30.09498821
80	30.87049499	-30.0999091	30.86460134	-30.09999118
81	30.86846161	-30.1049716	30.86270206	-30.10501732
82	30.86773466	-30.10999143	30.86084911	-30.10995081
83	30.86781094	-30.11500008	30.86066381	-30.11497694
84	30.86841217	-30.11995183	30.860548	-30.11997992

85	30.86804017	-30.12501979	30.8595752	-30.12500605
86	30.8673537	-30.13000301	30.85753695	-30.13000903
87	30.86631129	-30.13496081	30.85415531	-30.13496568
88	30.86613332	-30.13996946	30.84878175	-30.14001498
89	30.86585365	-30.14497811	30.84435782	-30.14499479
90	30.86539489	-30.14996627	30.84167104	-30.14999776
91	30.86435248	-30.15497492	30.83977176	-30.15495441
92	30.8563469	-30.15998057	30.83550997	-30.15998055
93	30.85097089	-30.16499935	30.83083126	-30.16498352
94	30.84896821	-30.17000506	30.82592094	-30.1699865
95	30.84443065	-30.17494384	30.82446173	-30.17496631
96	30.84787748	-30.17999858	30.82142752	-30.17999245
97	30.84971962	-30.1849146	30.8179764	-30.1849491
98	30.84771107	-30.1899741	30.81732786	-30.18995207
99	30.84707546	-30.19498275	30.81380725	-30.19500137
100	30.84486352	-30.19996598	30.81093517	-30.19993486
101	30.84234404	-30.20500428	30.80887376	-30.20498416
102	30.84145418	-30.20993665	30.80711346	-30.21001029
103	30.82297049	-30.21497073	30.8047741	-30.21496694
104	30.8160653	-30.21997477	30.80294431	-30.21996992
105	30.81177934	-30.2249693	30.80016488	-30.22501922
106	30.80809277	-30.23000337	30.79576412	-30.22999903
107	30.80427908	-30.23503744	30.79316998	-30.23495568
108	30.80152089	-30.23996389	30.79222034	-30.24002814
109	30.79947259	-30.24500674	30.78768061	-30.24500795
110	30.79726065	-30.24998997	30.78504015	-30.24998776
111	30.79415885	-30.25502404	30.78100998	-30.25496758

Table D-2: Maputo model output coordinates

	Waves (20 m contour)		Storm surge (10 m contour)	
Point	Longitude (°)	Latitude (°)	Longitude (°)	Latitude (°)
1	32.94466116	-25.74007219	32.75780212	-25.74003604
2	32.94733865	-25.74500442	32.75765051	-25.74496349
3	32.94895924	-25.75007756	32.75878761	-25.75004256
4	32.95156627	-25.75486887	32.76045536	-25.7548942
5	32.95283456	-25.75994201	32.76121343	-25.75997327
6	32.95523021	-25.76501516	32.76295699	-25.76497652
7	32.9572031	-25.76994738	32.76318441	-25.76997978
8	32.95861231	-25.77502053	32.75856019	-25.77513465
9	32.95981072	-25.77997572	32.76260425	-25.78014693
10	32.96136085	-25.78490794	32.76472489	-25.78506984
11	32.96305189	-25.78998109	32.77373759	-25.78999274
12	32.96516571	-25.79498378	32.81638766	-25.79500131
13	32.96699767	-25.799916	32.8216496	-25.79996639
14	32.96847734	-25.80505961	32.82225606	-25.80504545
15	32.97087299	-25.81013275	32.82301413	-25.8099729
16	32.97292519	-25.81493973	32.82248348	-25.81505197
17	32.97588453	-25.82008334	32.82281783	-25.82007935
18	32.97701189	-25.82501556	32.82395388	-25.825078
19	32.97919616	-25.82987733	32.83592033	-25.83007664
20	32.98046445	-25.83495047	32.82562009	-25.83507528
21	32.98222596	-25.83981224	32.82592304	-25.83999819
22	32.9832124	-25.84495584	32.82978563	-25.84499683
23	32.98138043	-25.84995853	32.82774073	-25.84999547
24	32.98497612	-25.85492315	32.83024005	-25.85491837
25	32.98666717	-25.86006676	32.82717966	-25.85996024
26	32.98236909	-25.86506944	32.82225221	-25.86496349
27	32.98864006	-25.87000167	32.81747637	-25.87011836
28	32.98721036	-25.87504027	32.81614255	-25.87491665
29	32.9886914	-25.87990652	32.81484365	-25.8801558
30	32.98805667	-25.8848433	32.80451492	-25.88493372
31	32.98319041	-25.88999166	32.79699673	-25.88999269
32	32.98192096	-25.89492843	32.78933801	-25.89505166
33	32.97430421	-25.90000626	32.78593827	-25.89998475
34	32.97106004	-25.90487252	32.81159395	-25.9051466
35	32.96380425	-25.91000233	32.7772868	-25.91040844
36	32.95745697	-25.91508016	32.76002799	-25.91524932
37	32.94786551	-25.92008746	32.75672066	-25.91994397
38	32.94285821	-25.92502424	32.74597661	-25.92489466
39	32.94790624	-25.92920509	32.73976191	-25.92995068
40	32.98757763	-25.93491394	32.73228321	-25.9350067
41	32.99139667	-25.93999534	32.72891253	-25.94006273

42	32.99745626	-25.94499803	32.72375117	-25.94501342
43	32.99900639	-25.94993025	32.72090716	-25.94996411
44	32.99978145	-25.9550034	32.72069649	-25.9549148
45	33.00048606	-25.96000608	32.71763909	-25.95994468
46	33.00034513	-25.96493831	32.72069377	-25.96489537
47	33.00013375	-25.97001145	32.72290578	-25.96974073
48	32.99971099	-25.9750846	32.71942977	-25.97511275
49	32.99879364	-25.97997317	32.7195351	-25.97985277
50	32.99590477	-25.98497585	32.70991785	-25.98503687
51	32.99195899	-25.990049	32.69223809	-25.98998299
52	32.99018768	-25.9949676	32.69087001	-25.99503435
53	32.98724254	-25.99999465	32.69497424	-25.99987524
54	32.98493212	-26.0050217	32.71564144	-26.00489725
55	32.98315781	-26.00996586	32.71574677	-26.00995328
56	32.98120285	-26.01499291	32.71248143	-26.01490397
57	32.97978105	-26.01996919	32.71248143	-26.01974932
58	32.97851457	-26.02503793	32.70637206	-26.02459468
59	32.97930163	-26.02996342	32.71374154	-26.0299359
60	32.98053282	-26.0349507	32.71690156	-26.03499192
61	32.98175038	-26.04004921	32.71616422	-26.03994261
62	32.98185617	-26.04494691	32.70668418	-26.04510397
63	32.98226202	-26.04999469	32.70721085	-26.04973866
64	32.98216056	-26.05499174	32.71880405	-26.04996676
65	32.98006476	-26.05992466	32.72372076	-26.04498081
66	32.98034404	-26.06505326	32.72531349	-26.04013336
67	32.97942008	-26.07003881	32.72988395	-26.03514741
68	32.97772057	-26.07503586	32.73244617	-26.03009221
69	32.98351998	-26.08002623	32.73293092	-26.02496775
70	32.98204891	-26.08504961	32.73313866	-26.0199818
71	32.97316271	-26.09002588	32.73854011	-26.01513435
72	32.97197162	-26.09494339	32.77004856	-26.00994065
73	32.96942326	-26.09997957	32.77874472	-26.00506571
74	32.96828181	-26.10500199	32.79832089	-25.99992939
75	32.96711316	-26.11005522	32.81279793	-25.99502677
76	32.9658956	-26.11502691	32.82829996	-25.98989161
77	32.96434829	-26.11999859	32.8405964	-25.9846632
78	32.96284986	-26.12502897	32.86547973	-25.97991891
79	32.96196206	-26.13002602	32.88218055	-25.97494941
80	32.9599306	-26.13507946	32.8880582	-25.97013216
81	32.95858622	-26.14002578	32.88847722	-25.96487962
82	32.95795208	-26.14504819	32.88412326	-25.96011005
83	32.95762197	-26.15000051	32.88303654	-25.95512927
84	32.95772343	-26.15502292	32.89390372	-25.9498768
85	32.95772479	-26.16002355	32.90540481	-25.94498657
86	32.95711602	-26.1650206	32.92297341	-25.94009634

87	32.95665943	-26.16994155	32.95648054	-25.94489601
88	32.95627703	-26.17505048	32.96559745	-25.95020407
89	32.95564288	-26.17994607	32.98209524	-25.95500837
90	32.95483118	-26.18494312	32.98887534	-25.96007151
91	32.95470135	-26.19004964	32.99423259	-25.96497552
92	32.95378819	-26.19497059	32.99657465	-25.97004651
93	32.95358526	-26.20001837	32.99641872	-25.97503634
94	32.95305052	-26.2050257	32.99529601	-25.98002617
95	32.95170614	-26.21002275	32.99254898	-25.98492978
96	32.95160467	-26.2150198	32.98943034	-25.99007554
97	32.95069247	-26.21999593	32.98712254	-25.99503418
98	32.94980467	-26.22496761	32.98479115	-26.00001305
99	32.94868857	-26.23001539	32.98225316	-26.00495526
100	32.94753679	-26.234924	32.97969587	-26.00997627
101	32.94705439	-26.24000183	32.97782426	-26.01497504
102	32.94715586	-26.24502363	32.97620257	-26.01999605
103	32.94761286	-26.25005069	32.97480981	-26.02506788
104	32.94819681	-26.25507774	32.97459129	-26.03000009
105	32.94842421	-26.26004455	32.9738632	-26.03500533
106	32.94758637	-26.26497004	32.97289642	-26.03996397
107	32.9461138	-26.27004787	32.97183608	-26.0449538
108	32.94857699	-26.27496662	32.97057032	-26.05005242
109	32.94857699	-26.27999367	32.97253696	-26.05495341
110	32.94804033	-26.28504239	32.96969626	-26.06001049
111	32.94649159	-26.29001866	32.97200715	-26.06499623
112	32.94545064	-26.29502032	32.97250662	-26.06995965
113	32.94224294	-26.30000163	32.971024	-26.07499912
114	32.94193855	-26.30504941	32.96756231	-26.07998895
115	32.93984053	-26.31003796	32.9642265	-26.08509271
116	32.9396628	-26.31501423	32.96360217	-26.08999371
117	-	-	32.96398156	-26.09498293
118	-	-	32.9627329	-26.10000879
119	-	-	32.96269283	-26.10495377
120	-	-	32.96320114	-26.10993005
121	-	-	32.96284885	-26.11500299
122	-	-	32.96107833	-26.12007328
123	-	-	32.96029792	-26.12500549
124	-	-	32.95901804	-26.13006257
125	-	-	32.95717079	-26.13503099
126	-	-	32.95586911	-26.13998283
127	-	-	32.95448511	-26.14495445
128	-	-	32.95426681	-26.15013139
129	-	-	32.95406268	-26.15501153
130	-	-	32.95440606	-26.15997495
131	-	-	32.9539066	-26.16506325

132	-	-	32.95326881	-26.17003492
133	-	-	32.9526139	-26.17499356
134	-	-	32.95167632	-26.17999462
135	-	-	32.95145801	-26.18501563
136	-	-	32.9514892	-26.19006783
137	-	-	32.95070746	-26.19506483
138	-	-	32.94989661	-26.19996109
139	-	-	32.94911695	-26.20507567
140	-	-	32.94839774	-26.21004171
141	-	-	32.94792994	-26.21503154
142	-	-	32.94743096	-26.21999018
143	-	-	32.94623435	-26.22503058
144	-	-	32.94489203	-26.22996279
145	-	-	32.94370581	-26.23501987
146	-	-	32.94278394	-26.24008017
147	-	-	32.94228496	-26.24507
148	-	-	32.94273945	-26.25004998
149	-	-	32.94433149	-26.25504462
150	-	-	32.94537272	-26.26004541
151	-	-	32.94437475	-26.26500405
152	-	-	32.94212933	-26.27002506
153	-	-	32.94134873	-26.27508503
154	-	-	32.944405	-26.2799813
155	-	-	32.94390602	-26.28506469
156	-	-	32.9425389	-26.29003073
157	-	-	32.94088602	-26.29495819
158	-	-	32.9386406	-26.30004157
159	-	-	32.93711036	-26.30507412
160	-	-	32.93489612	-26.31000157
161	-	-	32.93396053	-26.31502259

Table D-3: Beira model output coordinates

	Waves (20 m contour)		Storm surge (10 m contour)	
Point	Longitude (°)	Latitude (°)	Longitude (°)	Latitude (°)
1	35.5423125	-19.7200608	35.1549819	-19.7199195
2	35.5449327	-19.7249522	35.1469514	-19.7249702
3	35.5476146	-19.7297797	35.1416298	-19.7299170
4	35.5584496	-19.7349290	35.1322609	-19.7350138
5	35.5635989	-19.7398638	35.1274640	-19.7401105
6	35.5686504	-19.7450452	35.1203436	-19.7450573
7	35.5729415	-19.7498727	35.1052870	-19.7500071
8	35.5760526	-19.7547002	35.1011709	-19.7550962
9	35.5776617	-19.7597422	35.0960070	-19.7600356
10	35.5784127	-19.7649988	35.0883734	-19.7649750
11	35.5773399	-19.7699335	35.0878496	-19.7699892
12	35.5758380	-19.7748683	35.0799166	-19.7749285
13	35.5733706	-19.7799103	35.0758005	-19.7800176
14	35.5683183	-19.7847601	35.0723579	-19.7848821
15	35.5615598	-19.7899094	35.0713850	-19.7900460
16	35.4906338	-19.7950349	35.0555611	-19.7949891
17	35.4970367	-19.8000080	35.0473409	-19.7999737
18	35.5029369	-19.8049427	35.0476033	-19.8047834
19	35.5072280	-19.8099847	35.0499644	-19.8100303
20	35.5089444	-19.8147049	35.0629952	-19.8150386
21	35.5107681	-19.8197470	35.0863439	-19.8201106
22	35.5126991	-19.8250035	35.0928332	-19.8249270
23	35.5147374	-19.8300456	35.1221285	-19.8299990
24	35.5165755	-19.8349042	35.1138208	-19.8348961
25	35.5187210	-19.8400535	35.0651631	-19.8400039
26	35.5223684	-19.8449883	35.0692349	-19.8450012
27	35.5268741	-19.8499230	35.0719187	-19.8498134
28	35.5322379	-19.8549650	35.0774781	-19.8549715
29	35.5315177	-19.8599257	35.0780334	-19.8600614
30	35.5312305	-19.8648079	35.0628565	-19.8650586
31	35.5310390	-19.8699773	35.0605429	-19.8699634
32	35.5305604	-19.8750510	35.0461837	-19.8748898
33	35.5306561	-19.8800289	35.0399003	-19.8799720
34	35.5306561	-19.8849111	35.0374054	-19.8849618
35	35.5307518	-19.8897933	35.0380522	-19.8900439
36	35.5320921	-19.8949627	35.0379598	-19.8951261
37	35.5324424	-19.8999540	35.0187400	-19.8999310
38	35.5327267	-19.9047874	34.9906495	-19.9049208
39	35.5330111	-19.9099051	34.9899103	-19.9099106
40	35.5328215	-19.9148333	34.9649475	-19.9149986
41	35.5324424	-19.9198562	34.9640235	-19.9198959

42	35.5325372	-19.9249739	34.9567237	-19.9250705
43	35.5324424	-19.9299020	34.9568161	-19.9299679
44	35.5308313	-19.9351145	34.9581097	-19.9348652
45	35.5287463	-19.9399479	34.9734486	-19.9399474
46	35.5268509	-19.9448760	34.9812136	-19.9450022
47	35.5246711	-19.9498042	34.9833682	-19.9500808
48	35.5231547	-19.9549219	34.9959109	-19.9550825
49	35.5210698	-19.9598500	35.0039906	-19.9600073
50	35.5188900	-19.9649677	35.0080689	-19.9649321
51	35.5166155	-19.9698959	35.0141642	-19.9699514
52	35.5103605	-19.9749188	35.0185503	-19.9750300
53	35.5039160	-19.9799417	35.0324012	-19.9800317
54	35.4133845	-19.9849212	35.0317087	-19.9849565
55	35.4040118	-19.9999823	34.9468177	-19.9898436
56	35.4101843	-20.0049623	34.9453364	-19.9949864
57	35.4139018	-20.0100126	34.9458983	-19.9999639
58	35.4198639	-20.0150628	34.9471026	-20.0050217
59	35.4255454	-20.0199727	34.9486280	-20.0099993
60	35.4333311	-20.0250229	34.9552915	-20.0149768
61	35.4768891	-20.0298627	34.9727269	-20.0200568
62	35.4888834	-20.0349830	34.9801130	-20.0251146
63	35.4930217	-20.0399631	34.9633632	-20.0299006
64	35.4971601	-20.0449432	34.9306845	-20.0348932
65	35.4970900	-20.0498531	34.9228175	-20.0400371
66	35.4951260	-20.0548331	34.9207750	-20.0450296
67	35.4930919	-20.0598834	34.9203968	-20.0500978
68	35.4911279	-20.0649336	34.9214559	-20.0549391
69	35.4888132	-20.0698435	34.9231200	-20.0600073
70	35.4782920	-20.0750340	34.9374926	-20.0649999
71	35.4692437	-20.0800140	34.9393837	-20.0699925
72	35.3512007	-20.0848444	34.9336347	-20.0749094
73	35.3568573	-20.0899789	34.8928621	-20.0799776
74	35.3652988	-20.0948523	34.8930133	-20.0849702
75	35.3706074	-20.0998998	34.9045870	-20.0899627
76	35.3734792	-20.1048603	34.9107143	-20.0949553
77	35.3740884	-20.1098207	34.8924838	-20.1000235
78	35.3750457	-20.1149552	34.9122272	-20.1050161
79	35.3750457	-20.1199157	34.9140426	-20.1100087
80	35.3745235	-20.1248761	34.9201699	-20.1149256
81	35.3700852	-20.1299236	34.8899318	-20.1200388
82	35.4341095	-20.1350888	34.8890661	-20.1249444
83	35.4348467	-20.1396960	34.8876955	-20.1299942
84	35.4353995	-20.1448561	34.8863248	-20.1351163
85	35.4311609	-20.1498320	34.8849541	-20.1400219
86	35.4267379	-20.1546235	34.8880562	-20.1450718

87	35.4161412	-20.1599679	34.8887054	-20.1499052
88	35.4119026	-20.1649437	34.8896363	-20.1548244
89	35.3792833	-20.1701039	34.8910791	-20.1600186
90	35.3979887	-20.1749875	34.8961290	-20.1649242
91	35.3858256	-20.1797791	34.9050024	-20.1700462
92	35.3840748	-20.1849392	34.9381152	-20.1750961
93	35.3897878	-20.1898229	34.9389087	-20.1800017
94	35.3947636	-20.1948908	34.9388366	-20.1848352
95	35.4015823	-20.1998667	34.9402794	-20.1898851
96	35.4038860	-20.2051189	34.9405680	-20.1948628
97	35.4046231	-20.2100026	34.9404958	-20.1999127
98	35.4210249	-20.2150706	34.9424437	-20.2050347
99	35.4243421	-20.2198621	34.9403516	-20.2100125
100	35.4262772	-20.2249301	34.9392694	-20.2149902
101	35.4283044	-20.2298138	34.9378988	-20.2199680
102	35.4290415	-20.2348817	34.9062288	-20.2249457
103	35.4298708	-20.2398576	34.9039555	-20.2300317
104	35.4323587	-20.2450177	34.8992585	-20.2348732
105	35.4332802	-20.2499935	34.9268650	-20.2398865
106	35.4339252	-20.2548772	34.9168615	-20.2449003
107	35.4963560	-20.2598739	34.9148787	-20.2497754
108	35.5026012	-20.2648560	34.9126424	-20.2549696
109	35.5092674	-20.2697680	34.9125702	-20.2599473
110	35.5178984	-20.2749606	34.9097977	-20.2650341
111	35.5241436	-20.2798725	34.9091473	-20.2700924
112	35.5298976	-20.2849248	34.9117487	-20.2749339
113	35.5345288	-20.2899771	34.9175297	-20.2799922
114	-	-	34.9143039	-20.2848599
115	-	-	34.9005249	-20.2898376

Table D-4: Pemba model output coordinates

	Waves (20 m contour)		Storm surge (10 m contour)	
Point	Longitude (°)	Latitude (°)	Longitude (°)	Latitude (°)
1	40.54911859	-12.84998526	40.54637618	-12.84998345
2	40.5465752	-12.85498533	40.5424607	-12.854978
3	40.54229768	-12.86001431	40.54011758	-12.86000338
4	40.54195085	-12.86501439	40.54045671	-12.86499794
5	40.54108379	-12.86995666	40.53947014	-12.86999249
6	40.53911844	-12.87495674	40.5384219	-12.87495621
7	40.53616265	-12.87997507	40.53518469	-12.87995076
8	40.5362545	-12.88501686	40.53395146	-12.88497615
9	40.53585424	-12.89001731	40.53231744	-12.89000153
10	40.53290762	-12.89500495	40.53216329	-12.89499608
11	40.53087869	-12.89996641	40.53000515	-12.90002146
12	40.52749854	-12.9049816	40.52525724	-12.90495435
13	40.52349114	-12.90999263	40.52152675	-12.90997974
14	40.52322745	-12.91500309	40.52004688	-12.91500512
15	40.51973869	-12.91999238	40.51875199	-12.91993801
16	40.51559044	-12.92500569	40.51434322	-12.92496339
17	40.51199368	-12.92996944	40.51116767	-12.9297113
18	40.60511886	-12.92997293	40.50809597	-12.94998794
19	40.6046572	-12.93496587	40.51624489	-12.95496969
20	40.6046572	-12.93997131	40.53366438	-12.95999053
21	40.60540063	-12.94497318	40.5354785	-12.96499258
22	40.60097275	-12.95003363	40.54259754	-12.9694656
23	40.60366798	-12.95498406	40.54848808	-12.96505558
24	40.60148221	-12.96002567	40.55548862	-12.96004147
25	40.60216909	-12.96494372	40.56203805	-12.95999646
26	40.60079481	-12.96997492	40.57578781	-12.95497392
27	40.60315767	-12.97500288	40.58197935	-12.95497818
28	40.60337748	-12.97997588	40.59065635	-12.95997505
29	40.60118126	-12.98498295	40.59464035	-12.96497192
30	40.60096146	-12.99001091	40.5978478	-12.97003632
31	40.60024711	-12.99501139	40.59825295	-12.9749319
32	40.59939538	-13.00001187	40.5973076	-12.9799963
33	40.5997757	-13.00499839	40.59680116	-12.98492564
34	40.60153411	-13.00999887	40.59568699	-12.98999004
35	40.60252321	-13.01497187	40.59595709	-12.99495315
36	40.60362222	-13.01997235	40.59399886	-12.99995002
37	40.60383711	-13.02502053	40.59315479	-13.00494689
38	40.602517	-13.02997096	40.59555194	-13.01001129
39	40.60015179	-13.0349764	40.598388	-13.01507569
40	40.59830913	-13.03998184	40.5986581	-13.01997127
41	40.59721037	-13.04500966	40.59646353	-13.02496814

42	40.59627528	-13.04996009	40.59514679	-13.02989749
43	40.59517519	-13.05499304	40.59288469	-13.03496189
44	40.59481766	-13.05997097	40.59119656	-13.03992499
45	40.59314208	-13.06497014	40.58930585	-13.04495563
46	40.59140943	-13.06994808	40.58788782	-13.0499525
47	40.59140943	-13.07498102	40.58711128	-13.05498314
48	40.59215199	-13.07995896	40.58667236	-13.05998001
49	40.59075174	-13.08495903	40.58613216	-13.06497688
50	40.58976165	-13.08999197	40.58535562	-13.06997375
51	40.5891841	-13.09496991	40.58501799	-13.07497062
52	40.58929411	-13.10000285	40.58505175	-13.08000126
53	40.58968046	-13.10499902	40.58417393	-13.08499813
54	40.58981797	-13.10997696	40.5832961	-13.08992748
55	40.58847035	-13.1150099	40.58258708	-13.09495811
56	40.58869037	-13.11998784	40.58258708	-13.09995498
57	40.58701378	-13.1249836	40.58255332	-13.10495185
58	40.58536364	-13.12996154	40.58245203	-13.10998249
59	40.5848961	-13.13496698	40.58197935	-13.11497936
60	40.58401602	-13.13991741	40.5815742	-13.11997623
61	40.58347183	-13.1449931	40.58079766	-13.12500687
62	40.58294929	-13.14994353	40.57968349	-13.12996997
63	40.58140915	-13.15505898	40.57914329	-13.13500061
64	40.58041906	-13.15995441	40.57856933	-13.13996372
65	40.57872501	-13.16496944	40.57816417	-13.14492683
66	40.57724135	-13.16991497	40.57647604	-13.14995746
67	40.57605992	-13.17499788	40.57593584	-13.15492057
68	40.57534556	-13.17997088	40.57522682	-13.1599512
69	40.57533583	-13.18496552	40.57458533	-13.1650156
70	40.57563836	-13.18994346	40.57353869	-13.16997871
71	40.57563836	-13.1949764	40.57201937	-13.17497558
72	40.57552835	-13.19995434	40.57131036	-13.18000622
73	40.57471132	-13.20496779	40.57188432	-13.18493556
74	40.57369474	-13.20999575	40.57201937	-13.18999996
75	40.57410687	-13.21496875	40.5715467	-13.19492931
76	40.57451899	-13.21999671	40.57056758	-13.1999937
77	40.5737136	-13.22495913	40.56931836	-13.20492305
78	40.57445617	-13.22996457	40.56847429	-13.20995368
79	40.57605131	-13.23494251	40.56854182	-13.21495056
80	40.57959912	-13.23994795	40.56871063	-13.22004872
81	40.58161911	-13.24504222	40.56803538	-13.2249443
82	40.58238842	-13.25001522	40.56881192	-13.2300087
83	40.58104213	-13.25498823	40.57050005	-13.23497181
84	40.58071061	-13.25994226	40.57164798	-13.24000244
85	40.58134254	-13.26494274	40.57404513	-13.24503308
86	40.58241407	-13.26997069	40.57505801	-13.24992866

87	40.58365045	-13.27497117	40.57418018	-13.25495929
88	40.58381519	-13.28000695	40.57458533	-13.25998993
89	40.58318326	-13.28497995	40.5751593	-13.26495304
90	40.58204386	-13.29003146	40.5759696	-13.26998367
91	40.57899284	-13.29500252	40.57647604	-13.27508183
92	40.5785803	-13.29998046	40.57698248	-13.27994365
93	40.57907534	-13.3049584	40.57732011	-13.28507557
94	40.57871781	-13.30999134	40.57654357	-13.2899374
95	40.57996905	-13.31494913	40.57526059	-13.29500179
96	40.58194726	-13.31997709	40.57441652	-13.29999866
97	40.58593116	-13.32500504	40.57407889	-13.30499554
98	40.58975021	-13.32995057	40.5754294	-13.30995865
99	40.58420238	-13.33498907	40.57559821	-13.31492175
100	40.58387268	-13.33990713	40.57863685	-13.31995239
101	40.58324075	-13.34496256	40.58150668	-13.32494926
102	40.58321327	-13.34993556	40.58468037	-13.33004742
103	40.58358432	-13.3550126	40.58197935	-13.33497677
104	40.58352932	-13.35996304	40.58133786	-13.33997364
105	40.58424438	-13.36496848	40.58089895	-13.34500427
106	40.58575701	-13.36997392	40.58066261	-13.34996738
107	40.58762789	-13.37491626	40.581034	-13.35496425
108	40.59554858	-13.3799767	40.58150668	-13.35999489
109	40.59513594	-13.38503068	40.58170925	-13.364958
110	40.59557598	-13.38998112	40.58262084	-13.36995487
111	40.59546597	-13.39501406	40.58326233	-13.37491798
112	40.59307388	-13.39999047	40.58414016	-13.38001614
113	-	-	40.58565948	-13.38497925
114	-	-	40.58765148	-13.39000988
115	-	-	40.58596335	-13.39497299
116	-	-	40.58684117	-13.40000362

Appendix E: Coordinates of Calibration Measurements

Table E-1: Coordinates of Wind Measurement Stations in the Gulf of Mexico

Station	Longitude (°)	Latitude(°)
8764227	-91.33833	29.44833
8770570	-93.87000	29.72833
8771013	-94.91667	29.48167
8771341	-94.72500	29.35667
8772447	-95.30167	28.94333
8773701	-96.38833	28.45167

Table E-2: Coordinates of Water Level Measurement Stations in the Gulf of Mexico

Station	Longitude (°)	Latitude (°)
8768094	-93.34333	29.76833
8770613	-94.98500	29.68167
8771013	-94.91667	29.48167
8771341	-94.72500	29.35667
8771450	-94.79167	29.31000
8772447	-95.30167	28.94333

Table E-3: Coordinates of Wave Buoys in the Gulf of Mexico

Buoy	Longitude (°)	Latitude (°)
42001	-89.668	25.897
42002	-93.758	26.091
42019	-95.352	27.907
42020	-96.694	26.968
42035	-94.413	29.232
42036	-84.517	28.500